

Effect of bioinspired surface microstructures
on hemodynamics and platelet adhesion

DISSERTATION

To Fulfill the
Requirements for the Degree of
Doctor of Engineering (Dr.Eng.)

Submitted to the Council of
the Faculty of Physics and Astronomy
the Friedrich Schiller University Jena

by M.Eng. Tam Thanh Pham
born on 23th April 1982 in Vung Tau, Vietnam

Statement of Authorship

Except where reference is made in the text of the thesis, this thesis contains no material published elsewhere or extracted in whole or in part from a thesis submitted for the award of any other degree or diploma.

In the selection and evaluation of the following material I have the following persons listed free of charge for help:

1. Mr. Stefan Wiedemeier (Institute for Bioprocessing and Analytical Measurement Techniques, Rosenhof 1, D-37308 Heilbad Heiligenstadt, Germany) for the experiment with flow channel.
2. Mr. S. Wächter and Mr. J. Giesecke (Günter Köhler Institute of Joining Technology and Materials Testing GmbH, Jena, Germany) for the fabrication of the microstructured glass.
3. Mr. Stephan Lotze (Department of General, Visceral and Vascular Surgery, Friedrich Schiller University Jena) and Dr. Harald Schubert (Institute of Laboratory Animals Science Jena) for their help during the pig operations and blood flow measurements.
4. Mr. Jens Schumacher (Institute of Mathematics, Friedrich Schiller University Jena, Ernst Abbe Platz 2, D-07743 Jena) for CCD using.

No other person's work has been used without due acknowledgement in the main text of the thesis.

This thesis has not been submitted for award of any other degree or diploma in any other tertiary institution.

Jena, 30 June 2016

Tam Thanh Pham

Acknowledgements

I sincerely thank my supervisors, Prof. Klaus D. Jandt and Prof. Utz Settmacher, for their patient guidance and continuous support throughout my PhD's time. I also owe my deepest gratitude to Dr. Jörg Bossert and Dr. Jürgen Zanow. This thesis would not have been completed without their practical guidance, valuable support, and considerable encouragement from the initial to the final step of my PhD thesis.

I am grateful to all my colleagues in the Otto Schott Institute of Materials Research (OSIM), Friedrich-Schiller-University Jena, for the research cooperation, continuous support and their friendship. Their boundless support and kindness has given me the strength to continue my research.

I would like to thank DAAD (German Academic Exchange Service) and IZKF (Interdisciplinary Center for Clinical Research), Friedrich-Schiller-University Jena, Germany for providing me the scholarships in the years of my PhD candidature.

Finally, I am forever indebted to my family and my friends for their continuous support and encouragement. Thinking of them makes me feel more confident and happy, and it is the motivation for me to finish my research.

Tam Thanh Pham

Abstract

Occlusion by thrombosis due to the absence of the endothelial cell (EC) layer is one of the most frequent causes of failure of artificial vascular grafts. Bioinspired surface structures may have a potential to reduce the adhesion of platelets contributing to hemostasis. The aim of this PhD research was to design a suitable microstructured surface mimicking the EC morphology for synthetic vascular grafts that inhibits the platelet adhesion and aggregation, the main cause of thrombosis.

Platelet adhesion as a function of the microstructure dimensions was investigated under flow conditions on polydimethylsiloxane (PDMS) surfaces by a combined experimental and theoretical approach. Platelet adhesion was statistically significantly reduced (by up to 78 %; $p \leq 0.05$) on the microstructured PDMS surfaces compared to that on the unstructured control surface. Finite element method (FEM) simulations of blood flow dynamic revealed that on the surfaces with the highest differences of the shear stress between the top of the microstructures and the ground areas, platelet adhesion was reduced most.

The relationships between EC geometrical parameters in different natural blood vessels and shear stress were statistically investigated and found to be exponential. By using FEM simulations of different EC computational models created based on the real EC found in the previous step, the pyramid model with suggested geometrical parameters was found the most suitable model for bioinspired microstructured surface of vascular grafts inducing the highest shear difference between top and ground of the microstructures which may, thereby, reduce platelet adhesion.

These findings provide new insight into the fundamental mechanisms of reducing platelet adhesion on bioinspired microstructured surfaces.

Zusammenfassung

Thrombotische Okklusion, induziert durch das Fehlen der Endothelzellen (EZ), ist eine der häufigsten Ursachen für das Versagen von künstlichen Blutgefäßen. Eine potentielle Möglichkeit die Ablagerung von Thrombozyten zu reduzieren, ist die Verwendung von bioinspirierten Oberflächenstrukturen. Ziel dieser Doktorarbeit war es eine mikrostrukturierte Oberfläche, welche die EZ-Morphologie nachahmt, zu entwickeln, um in künstlichen Blutgefäßen die Blutplättchen-Adhäsion und Aggregation zu verringern, welche die Hauptursache der Thrombose ist.

Die Thrombozytenablagerung wurde als Funktion der Mikrostrukturdimensionen unter Strömungsbedingungen auf Polydimethylsiloxan (PDMS)-Oberflächen mittels einer Kombination aus experimentellen und theoretischen Ansätzen untersucht. Dabei wurde die Thrombozytenablagerung auf mikrostrukturierten PDMS Oberflächen im Vergleich zur unstrukturierten Kontrolloberfläche statistisch signifikant verringert (bis zu 78 %; $p \leq 0.05$). Die Simulation des Blutflusses mittels der Finite-Elemente-Methode (FEM) auf verschiedenen Oberflächenstrukturen ergab, dass auf Oberflächen mit den höchsten Schubspannungsunterschieden zwischen Spitze und Boden der Mikrostrukturen die Thrombozytenablagerung am stärksten reduziert war.

Die Beziehung zwischen den geometrischen Parametern der EZ verschiedener natürlicher Blutgefäße und der Scherspannung wurde statistisch untersucht. Dabei wurde eine exponentielle Abhängigkeit beider Faktoren aufgezeigt. Durch FEM-Simulationen des Blutflusses auf verschiedene EZ-Computermodelle, welche auf den realen EZ des vorherigen Schrittes basieren, wurde das Pyramidenmodell mit den vorgeschlagenen geometrischen Parametern als das geeignetste Modell für bioinspirierte und mikrostrukturierte Oberflächen von Blutgefäßen nachgewiesen. Dieses Modell führt zu den höchsten Schubspannungsunterschieden zwischen der Spitze und dem Boden der Mikrostrukturen, welche die Blutplättchen-Adhäsion reduzieren.

Diese Ergebnisse liefern neue Einblicke in die grundlegenden Mechanismen der reduzierten Thrombozytenablagerung auf bioinspirierten und mikrostrukturierten Oberflächen.

Contents

Statement of Authorship	ii
Acknowledgments	iii
Abstract	iv
List of Figures	x
List of Tables	xv
List of Abbreviations	xvi
1 Introduction	1
2 Background	3
2.1 Platelets	3
2.2 Mechanisms of thrombosis formation on biomaterial surfaces . . .	5
2.3 Effect of hemodynamic factors on thrombosis formation	7
3 Literature review	10
3.1 Endothelialization approaches for the inner surface of vascular grafts	10
3.1.1 Biofunctionalization of biomaterials for accelerated in situ endothelialization	12
3.1.2 Physical modification of inner graft surfaces for EPCs ad- hesion and proliferation	13
3.2 Coating with anticoagulants	14
3.3 Bioinspired nano- and microstructured surface approach	15
3.3.1 Hierarchical structure of the inner surface of a natural blood vessels	15
3.3.2 Nano- and microstructured surface mimicking inner topog- raphy of natural blood vessels	17
3.4 Summary	19

4	Aims and Objectives of the PhD research	21
4.1	Open questions	21
4.2	Aims and Objectives	22
4.3	Hypotheses	23
4.4	Contributions	24
4.5	Related publications	24
4.6	Thesis Outline	25
 5	 Hemodynamic aspects of reduced platelet adhesion on bioinspired microstructured surfaces	 27
5.1	Introduction	28
5.2	Materials and methods	29
5.2.1	Design and fabrication of microstructured PDMS surfaces	29
5.2.2	Flow cell and platelet adhesion experiments	31
5.2.3	Contact angle measurement	32
5.2.4	Preparation of blood and platelet labelling	32
5.2.5	Simulation of blood flow	33
5.2.6	Statistical analysis	33
5.3	Results	34
5.3.1	Characterization of microstructured surfaces with microscopy	34
5.3.2	Platelet adhesion on the microstructured and unstructured surfaces	35
5.3.3	Contact angle and pressure drop	36
5.3.4	Hemodynamic simulation of blood flow	38
5.4	Discussion	40
5.4.1	Water contact angle	40
5.4.2	Surface resistant to flow	41
5.4.3	Shear stress	41
5.5	Conclusion	44
 6	 Quantitative characterization of endothelial cell morphologies depending on shear stresses in different blood vessels of domestic pigs	 45
6.1	Introduction	45

CONTENTS

6.2	Materials and Methods	46
6.2.1	Blood flow measurement	46
6.2.2	Fixation of pigs' blood vessels	48
6.2.3	Measurements of the blood vessel diameter, EC length, width, aspect ratio, area and perimeter	49
6.2.4	Characterization of EC height	50
6.2.5	Calculation of wall shear stress	50
6.2.6	Statistical analysis	52
6.3	Results	52
6.4	Discussion	56
6.5	Conclusion	60
7	Optimizing the inhibition of platelet adhesion on bioinspired mi- crostructured surfaces - a Finite Element Method (FEM) ap- proach	61
7.1	Introduction	62
7.2	Materials and methods	63
7.2.1	Blood flow measurement and endothelial cell characterization	63
7.2.2	Wall shear stress and oscillatory shear index	63
7.2.3	Simulation of blood flow	64
7.2.4	Finding the optimal geometrical parameters, distance and pattern for vascular grafts	65
7.3	Results	66
7.3.1	Hemodynamic simulations of three EC models	66
7.3.2	Optimal geometrical parameters and distance	69
7.4	Discussion	73
7.4.1	Hemodynamic simulations of three EC models	74
7.4.2	Optimal geometrical parameters and distance	75
7.5	Conclusion	77
8	Summary	78
	References	82

CONTENTS

Curriculum Vitae	102
------------------	-----

List of Figures

2.1	Platelet adhesion and aggregation on subendothelium to create blood clotting [19]	4
2.2	Schematic representation of platelet adhesion to an artificial surface under flow conditions through interaction with surface adsorbed adhesion molecules like fibrinogen, von Willebrand factor, vitronectin and fibronectin [25]	6
2.3	Schematic diagram of a vascular graft connected with a natural artery. Smooth muscle cells migrate from the media to the intima of the adjacent artery and extend over and proliferate on the graft surface. This smooth muscle cell layer is covered by endothelial cells [8]	7
3.1	Biofunctional of the implant surface to to catch EPCs from the blood flow to enhance in situ endothelialization [51].	11
3.2	Structure of natural blood vessels [101].	16
3.3	Inner layer structure of a natural blood vessel of the domestic pig: (a) SEM picture of inner surface with groove structures (magnification of 50 X) (b) SEM picture of inner surface with microstructure of endothelial cells (magnification of 500 X).	17

LIST OF FIGURES

5.1	Set-up of the experimental flow cell and design of microstructured surfaces used in this study: a) schematical illustration of the microstructured surfaces with hemispherical microstructures arranged in regular arrays; b) sketch of the experimental flow cell with the multilayer plate construction: PTFE top plate with inlet and outlet, PTFE middle plate with the flow channel (height: 0.5 mm, largest width: 4 mm, length: 17.2 mm), PDMS sample containing the microstructured area (1 × 1 cm) and a microscope slide as a base plate, all plates had a size of 76 × 26 mm; c) sketch of the flow cell with case; d) photograph of the flow cell with inlet and outlet connected to silicon tubes; e) photograph of the flow cell from the bottom-side with the flow channel visible in the middle part.	30
5.2	Characterization of the microstructured PDMS surfaces using SEM exemplarily illustrated for the surface structure type 1: a) SEM-2D micrograph of the hemispherical microstructured surface; b) SEM-3D image of the hemispherical microstructures acquired by using a 4 quadrant detector; c) profile of the microstructure illustrated in b) (yellow line; see for comparison also Table 5.1).	34
5.3	Platelet adhesion to microstructured and unstructured PDMS surfaces illustrated by overlapping of the representative fluorescence images and the corresponding light microscopy images: a) unstructured surface; b) structure type 1; c) structure type 2; d) structure type 3.	35
5.4	Coverage of the microstructured and unstructured PDMS surfaces with platelets. * $p \leq 0.05$ vs. unstructured surface, # $p \leq 0.05$ vs. structure type 1, \$ $p \leq 0.05$ vs. structure type 2.	36

LIST OF FIGURES

5.5	Hemodynamic simulations of blood flow on microstructured surfaces. Simulation plots showing wall shear stress distribution caused by the blood flow on the microstructured surfaces: a) structure type 1; b) structure type 2; c) structure type 3. Red indicates the highest (3.0 Pa) and blue the lowest value (0 Pa) of the wall shear stress (a-c). Simulation plots showing blood velocity close to the surface of structure type 2: d) on the unstructured area; e) on top of the microstructures; f) inbetween the microstructures. Red indicates the highest (0.0035 m/s) and blue the lowest value (0 m/s) of the blood velocity. The size of the arrows also demonstrates the magnitude of the velocity vectors (d-f).	39
5.6	Proposed model of reduced platelet adhesion on microstructured surfaces.	42
6.1	Operation to measure blood flow rates in different blood vessels of three domestic pigs: (a) Exposed blood vessel of a domestic pig; (b) blood flow measurement carried out with QuickFit sensor and VeriQ system; (c) pulsatile blood flow measured by VeriQ.	47
6.2	Characterization of endothelial cell dimensions and blood vessel diameter: (a) SEM picture of common carotid artery cross section; (b) lumen perimeter of common carotid artery marked with GIMP; (c) endothelium of common carotid artery with a magnification of 500x; (d) perimeters of endothelial cells marked with GIMP.	49
6.3	FIB-SEM images of endothelial cell layer in common carotid artery: (a) Endothelial cell (indicated with the arrow) before cross sectioning at a view angle of 54° to the surface; (b) endothelial cell (arrow) after cross sectioning at its highest point for determination of the cell height; (c) endothelial cell layer sectioned at different points to measure the cell heights (view direction perpendicular to the surface).	51

LIST OF FIGURES

6.4	SEM images of endothelial cell layers obtained from four different blood vessels of pigs with a magnification 500x: (a) hepatic artery; (b) renal artery; (c) iliac artery; (d) carotid artery. The endothelial cells in hepatic and renal arteries had a longer and narrower shape compared to those in carotid and iliac arteries.	53
6.5	Correlations of endothelial cell geometry parameters with shear stress fitted with an exponential function of Equation 6.2. The data are shown as mean values and according standard deviation(for each type of blood vessel of each pig). (a) Correlation of endothelial cell aspect ratio with shear stress, $a = -2.95$; $b = 18.18$ and $y_0 = 4.15$. (b) Correlation of endothelial cell length with shear stress, $a = -5.95$; $b = 34.53$ and $y_0 = 18.24$. (c) Correlation of endothelial cell width with shear stress, $a = 3.64$; $b = 8.64$ and $y_0 = 4.38$. (d) Correlation of endothelial cell height with shear stress, $a = 1.44$; $b = 25.47$ and $y_0 = 2.85$	55
7.1	Rebuilt diagram of pulsatile blood flow in one cardiac cycle (0.52 s) in a natural porcine common carotid artery measured by VeriQ Flowmeter system (Medistim ASA, Norway) with average blood flow rate of 36.5 ml/min, i.e. average blood velocity of 0.46 m/s. .	65
7.2	Illustration of the Central Composite Design (CCD) and the search strategy: a) three-dimensional CCD consisting of the corners of a cube (black) complemented by star design points (red); b) the response variable is simulated at the points of an initial Central Composite Design; c) based on these values the unknown response surface is approximated by a quadratic surface. The direction of steepest ascent (black dots) suggests points for further simulations.	66
7.3	Simulation plots show the time-averaged WSS distributions on the three models during one cardiac cycle: a) cuboid; b) ellipsoid; c) pyramid, with red being the highest value (36 Pa) and blue being the lowest value of WSS (0 Pa).	67

LIST OF FIGURES

7.4	The WSS difference between top and ground areas of the microstructures for the whole cardiac cycle of 0.52 s of three models: cuboid, ellipsoid and pyramid.	68
7.5	Velocity vectors and OSI distribution in three different models. Simulation plots showing velocity vectors at the chosen time step $t = 0.114$ s: a) cuboid model; b) ellipsoid model; c) pyramid model. The size and color of vectors in all the images show the magnitude of velocity, with red being the highest value (0.07 m/s) and blue being the lowest value (0 m/s). Simulation plots showing OSI values for one cardiac cycle in three models: d) cuboid model; e) ellipsoid model; f) pyramid model with red being the highest OSI value ($5e^{-4}$) and blue being the lowest value of WSS (0).	70
7.6	Contour plots for the approximated response surface for shear difference (between top and ground of the microstructures) in the common carotid artery resulting from the final Central Composite Design (CCD).	71

List of Tables

5.1	Dimensions, average static contact angle (mean \pm standard deviation based on $n = 5$) and pressure drop (mean standard deviation based on $n = 3$) of the microstructured and unstructured surfaces.	37
6.1	Endothelial cells characterization of four natural blood vessel types using FIB-SEM images. The average values of all endothelial cell geometry parameters were obtained together with blood vessel diameters and blood flow rates in those arteries. The average wall shear stress in each blood vessel type was then calculated based on vessel diameter and blood flow rate.	54
7.1	Results of the best combination of geometrical parameters and distance for the endothelial cell pyramid model in two different patterns for the carotid and iliac artery. (*The parameters were calculated based on the blood flow rate and vessel diameter investigated in chapter 6 [123]. **The information was investigated in chapter 6 [123].)	72

List of Abbreviations

CCA	Common Carotid Artery
CCD	Central Composite Design
EC	Endothelial Cell
ECM	Extra Cellular Matrix
EPC	Endothelial Progenitor Cell
ePTFE	expanded Polytetrafluoroethylene
FEM	Finite Element Method
FIB	Focused Ion Beam
IA	Iliac Artery
OSI	Oscillatory Shear Index
PAD	Peripheral Artery Disease
PDMS	Polydimethylsiloxane
PU	Polyurethane
SEM	Scanning Electron Microscopy
vWF	von Willebrand factor
WSS	Wall Shear Stress

1

Introduction

Peripheral arterial disease (PAD) is a very common disease in western countries [1]. Stenoses and occlusion of peripheral arteries due to atherosclerosis may cause typical symptom of claudication and necrosis of affected leg. To treat this symptom and to prevent amputation, it is necessary to revascularize the ischemic tissue. Surgically created long vascular conduit (bypasses) can bring the blood to the arteries distally to the occluded segment. During last 20 years minimal-invasive endovascular methods have developed rapidly to treat arterial stenose and occlusion. Less invasively endovascular revascularization represents a major benefit in the treatment of the often multimorbid patients. Nevertheless of the rapid development of endovascular skills and technique, the results for long-distant arterial occlusion are unsatisfactory and bypass surgery represents the best option for these lesion and after failure of endovascular treatment.

Autogenous vein grafts have been widely used in the field of reconstructive arterial surgery [2, 3]. They seem to be an ideal substitute for occluded arteries due to atherosclerosis. Nevertheless, long-term observation have revealed several disadvantages of using autologous vein grafts, such as size discrepancy, intimal thickening, intimal hyperplasia, thickening of the venous valves, and aneurysmal dilatation. However, the major drawback of autogenous vein grafts for arterial reconstruction is that in 30-50% of these patients these superficial veins for grafting are inadequate or unavailable [4, 5, 6]. That results in the need for alternative vascular grafts [7].

Nowadays, artificial vascular grafts are used as bypasses for long-distant arteries occluded due to atherosclerosis in the case of the unavailability of a suitable autologous vein graft [8, 9, 10, 11]. The materials which are largely used for vascular grafts are *expanded polytetrafluoroethylene (ePTFE)* or *polyethylene terephthalate (Dacron)* and *polyurethane (PU)*. These materials possess remarkable properties, such as biocompatibility, high flexibility, elasticity and a low coefficient of friction [12]. In the last two decades, many researchers have attempted to fabricate small-diameter synthetic vascular grafts for arterial substitutes. However, thrombosis and the formation of anastomosis stenosis due to intimal hyperplasia are still major failures of synthetic vascular grafts, especially for bypasses to distal arteries with a small diameter ($< 6\text{ mm}$) [11, 13]. For this case, saphenous vein has shown better performance as a vascular substitute [5, 12, 14, 15]. So far, some clinical studies have demonstrated that synthetic vascular grafts with diameters greater than 6 mm perform well in high flow with 5-10 year patency rates of 90%. In contrast, synthetic vascular grafts with diameters smaller than 6 mm to distal popliteal or crural arteries have a significant more worse and come compared to equivalent vein bypasses with a 5 year a patency less than 30% [8, 11, 16, 17, 18].

The poor patency rate of synthetic vascular grafts due to thrombosis is the main motivation for further investigations of mimicking the biological and physical functions of natural vasculature to improve the performance of vascular grafts. The state-of-the-art approaches against thrombosis formation on vascular graft inner wall are *endothelialization*, *coating with anticoagulants* and *nano- and micro-structured surfaces* of the inner surface of vascular grafts.

2

Background

This chapter gives an introduction about the characteristics of platelets and an overview about the mechanisms of thrombosis formation on biomaterial. The effect of hemodynamic factors on thrombosis formation are also discussed in this chapter.

2.1 Platelets

Platelets, also called *thrombocytes*, are blood cells whose main function is to contribute to hemostasis. They are designed to initially arrest bleeding through formation of platelet plugs and stabilize the initial platelet plugs by catalyzing coagulation reactions leading to the formation of fibrin. In mammals platelets are nonnucleated, disk-shaped cells which having a diameter of $2\mu m - 4\mu m$ and an average volume of $10 \times 10^{-9} mm^3$. Platelets originate from the cytoplasm of bone marrow and circulate at an average concentration of about 250,000 cells per microliter of whole blood [8].

The external platelet membrane surface consists of membrane-bound receptors (e.g. glycoproteins Ib and IIb/IIIa) which play a key role in hemostasis. They mediate the contact reactions of adhesion (platelet-surface interactions) and aggregation (platelet-platelet interactions) [8].

Platelets are extremely sensitive cells that may respond to minimal stimulations. Activation causes platelets to become sticky and change in shape to

2.1 Platelets

irregular spheres with spiny pseudopods. Platelet activation is initiated by the interaction of an extracellular stimulus with the platelet receptors on the platelet plasma membrane surface. Activation of platelets leads to the internal contraction and extrusion of storage granule contents into the extracellular environment which stimulate other platelets, leading to irreversible platelet aggregation and the formation of platelet thrombus [8].

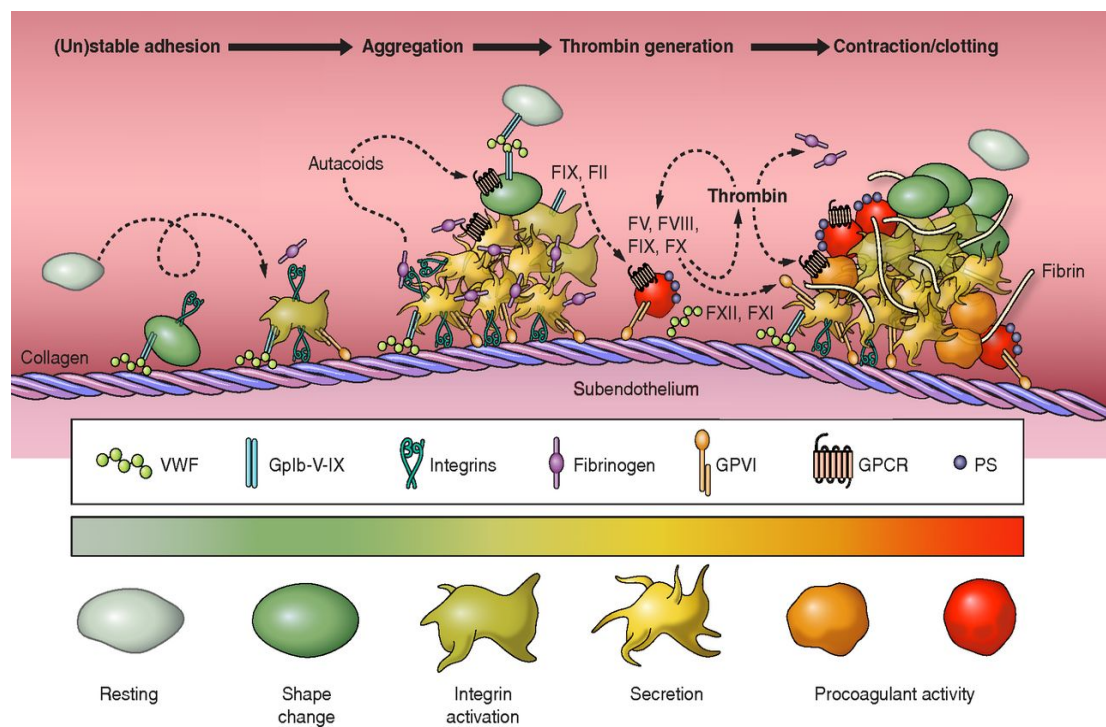


Figure 2.1: Platelet adhesion and aggregation on subendothelium to create blood clotting [19]

The process of stopping bleeding at the site of interrupted endothelium is shown in Figure 2.1. Platelets adhere firstly to a von Willebrand factor (vWF)/collagen matrix on the subendothelium. They get activated and change their shape, concurrently, they secrete their stored granular contents including ADP, serotonin, platelet-activating factor (PAF), platelet factor 4, and thromboxane A₂ (TXA₂), which, in turn, activate additional platelets. Platelets express certain receptors, some of which are used for the adhesion of platelets to collagen. When platelets are activated, they express glycoprotein receptors that interact with

2.2 Mechanisms of thrombosis formation on biomaterial surfaces

other platelets, producing aggregation and adhesion. They produce thrombin after developing a procoagulant surface, and form a contracted thrombus with fibrin [19].

2.2 Mechanisms of thrombosis formation on biomaterial surfaces

Thrombosis is a complex pathophysiological process that may be induced by a variety of potential risk factors, such as physiological, biochemical, genetic and hemodynamic factors. The main triggers of thrombus formation on a biomaterial are platelet adhesion, activation and aggregation. Natural blood vessels have a host of structural properties, which combined with endothelial cells, to prevent the triggering of platelet adhesion and clotting cascade [20]. Although platelets show no interaction with the intact inner surface of normal blood vessels, they are extremely sensitive when they come into contact with any thrombogenic surface such as injured endothelium, subendothelium and artificial surfaces. [8].

When a biomaterial comes into contact with blood, after a short time (less than 1 second) the luminal surface of the graft becomes coated with plasma proteins, primarily fibrinogen and *von Willebrand Factor (vWF)* [21],[22],[23],[24]. They are the two most important proteins mediating thrombus formation. In a time frame which lasts somewhere between a few seconds to a minute, a monolayer of protein can be observed on the biomaterial surfaces. Protein absorption on the surface is the biological foundation for the next interaction between cells and a synthetic surfaces.

Due to the blood flow, platelets move with quite high velocity. Immobilized von Willebrand factor is the protein that can catch fast moving platelets (Fig. 2.2) [26],[27]. It is mediated by the interaction between GPIb integrin receptors on platelet membranes with absorbed vWF proteins on the graft surface. The adhesion of platelets to vWF occurs rapidly but is reversible. There are attachments and detachments between GPIb receptors and vWF, and consequently, the velocity of platelets is slowed down and platelets roll on the graft surface. The slowed-down platelets will then interact with absorbed fibrinogen on the graft

2.2 Mechanisms of thrombosis formation on biomaterialial surfaces

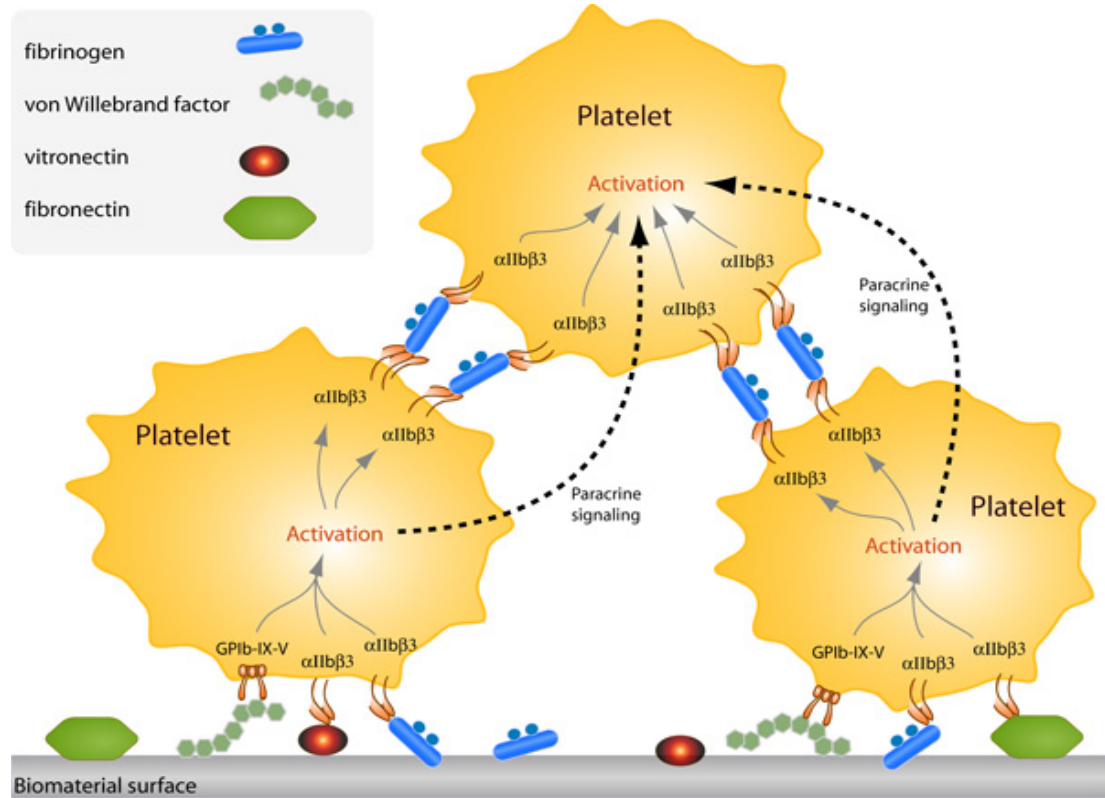


Figure 2.2: Schematic representation of platelet adhesion to an artificial surface under flow conditions through interaction with surface adsorbed adhesion molecules like fibrinogen, von Willebrand factor, vitronectin and fibronectin [25]

surface, mediated by platelet glycoprotein IIb/IIIa (integrin $\alpha IIb\beta 3$). In addition, the platelet receptor GPVI also interacts with adsorbed fibrinogen and this leads to firm platelet adhesion on the graft surface [28],[29]. The adhered platelets will be activated and can change their biological activity. They can release active compounds, recruit other cells, aggregate, replicate and die. The activation of a platelet is accompanied by internal contraction and extrusion of the storage granule contents into an extracellular environment. Secreted platelet products such as ADP stimulate other platelets, leading to irreversible platelet aggregation and the formation of a fused platelet-fibrin aggregate [30].

When the synthetic vascular graft is implanted, this platelet-fibrin layer develops over time to create a pseudointima [8]. When endothelial cells of the natural blood vessels cover this layer simulating the inner layer of a native blood vessel

2.3 Effect of hemodynamic factors on thrombosis formation

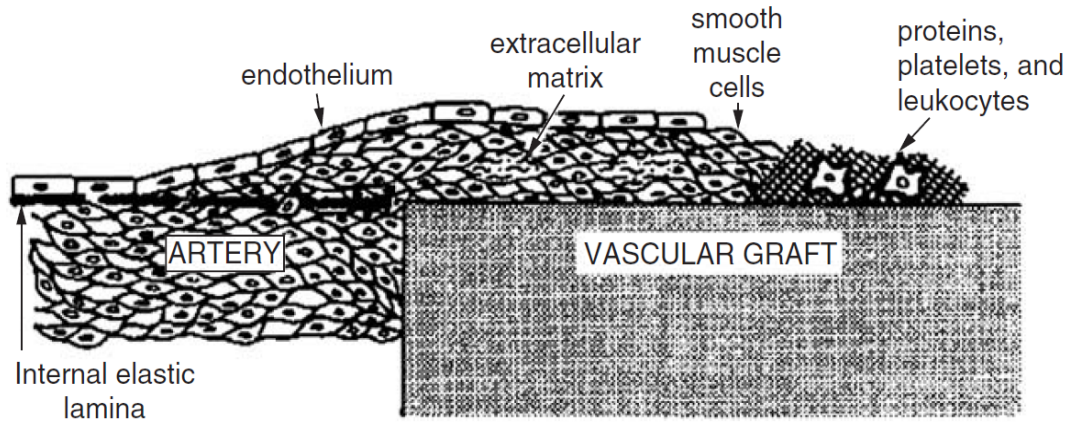


Figure 2.3: Schematic diagram of a vascular graft connected with a natural artery. Smooth muscle cells migrate from the media to the intima of the adjacent artery and extend over and proliferate on the graft surface. This smooth muscle cell layer is covered by endothelial cells [8]

and serving as a nonthrombogenic surface, it is called a neointima [8]. Unfortunately, humans have a very limited ability to endothelialize synthetic vascular grafts to develop a true neointima. The endothelial cells only cover a 10 to 15 *mm* pseudointima zone adjacent to the anastomosis [8]. The remaining areas of the synthetic vascular graft that are not covered by endothelial cells will act as adhesion points for protein adsorption and blood components (Fig. 2.3)[8]. Platelets can adhere to graft surface areas which are not covered by endothelial cells to initiate thrombus formation [8]. Therefore incomplete endothelial cell coverage is a significant reason in the failure of synthetic vascular grafts.

2.3 Effect of hemodynamic factors on thrombosis formation

Hemodynamic factors are considered one of the most important factors which affect thrombus formation or platelet adhesion. Many studies have investigated the formation of platelet deposition under different hemodynamic conditions [31],[32]. Two important definitions in hemodynamics are shear stress and shear rate. They

2.3 Effect of hemodynamic factors on thrombosis formation

have different effects on cellular adhesive interaction. Shear rate is the rate of change of velocity at which one layer of fluid passes over an adjacent layer [33]. The shear rate is directly related to blood velocity and high shear rate limits the time of contact between platelets and the vessel wall. This means a higher shear rate condition will decrease the contact between platelet membrane receptors and immobilized protein on the vessel wall. Consequently, cell recruitment onto the surface decreases with increasing shear rate. Shear stress is defined as the component of stress coplanar with a material cross section. Shear stress influences the lifetime of an adhesive bond once formed, and the consequence is decreased efficiency caused by detachment of adherent cells with increasing shear stress [33].

In natural arteries, hemodynamic factors play an important role not only in regulating arterial blood pressure and oxygen supply in the tissue but also in vascular diseases, such as atherosclerosis, aneurysm and thrombus formation [34]. One example is the carotid bifurcation where the blood flow disorders in the direction. This leads to stagnation of blood flow and low and oscillatory shear stress in this area. Therefore, this area is often the site where atherosclerotic plaques may develop. Investigations *in vitro* and *in vivo* have revealed the effect of low and oscillatory shear stress on endothelial cell dysfunction [34]. Under physiological shear ($> 10 \text{ dynes/cm}^2$), endothelial cells align in the direction of flow whereas they do not when exposed to low shear stress ($< 4 \text{ dynes/cm}^2$) [34]. Low and oscillatory shear stress leads to the inhibition of NO-synthase and increase in apoptosis. They contribute to endothelial cell dysfunction and consequently increase platelet activation and thrombus formation [34].

Hemodynamic factors play not only a role in arterial disease in natural blood vessels, but also major determinants in the function of synthetic vascular grafts. When a synthetic vascular graft is implanted, intimal hyperplasia develops to various degrees, especially over the the anastomosis. It is the primary cause of restenosis of the vascular grafts [35]. Thereby, the blood flow is disturbed at the anastomosis and the blood flow rate is also reduced. An important aspect of blood-material interaction is platelet activation, adhesion, and subsequent aggregation of blood platelets on the artificial surface, which are directly affected by local fluid dynamics. Low and oscillatory wall shear stress seems to be responsible for the failure of vascular grafts [36]. Flow disturbance is a principal

2.3 Effect of hemodynamic factors on thrombosis formation

driver of platelet aggregation and thrombus formation [37]. Maximum platelet deposition was observed in areas of flow recirculation and reattachment or local curved streamlines and minimum in locations of high shear stress [36].

The effect of hemodynamic factors on platelet attachment to thrombogenic surfaces is quite different in different shear stress or shear rate range. Platelet adhesion to thrombogenic surfaces under a shear rate of approximately 1000 s^{-1} appears to be absolutely dependent on the interaction between fibrinogen and the platelet GPIIb/IIIa ($\alpha\text{IIb}\beta\text{3}$) receptor [38]. In addition, the absorbed amount of fibrinogen was proved to decrease with the increasing shear rate [39]. At the shear rate from 1000 s^{-1} to 10000 s^{-1} , platelet aggregation to surface is a two-stage process. It is absolutely dependent on the platelet GPIb α receptor [38]. The necessary adhesive protein for this process is mainly plasma vWF. Platelets will be initially captured by immobilized vWF via the GPIb/V/IX, become activated and firmly attach to the thrombogenic surface through $\alpha\text{IIb}\beta\text{3}$ and GPIV receptors [38]. At an extreme high shear rate above 10000 s^{-1} , platelets can directly interact with soluble multimeric vWF in the flow to initiate platelet aggregation. This process is no longer dependent on the function of $\alpha\text{IIb}\beta\text{3}$ receptors. At this shear rate threshold and above, active A1 domains in soluble VWF multimers are exposed and allow the binding of platelet GPIb α and additional platelet recruitment without the stimulation of platelets [38]. The formed platelet aggregation is unstable, whereas shear rate above 20000 s^{-1} platelets, adhesion to immobilized VWF which are stretched into elongated structures becomes the core of aggregates that can persist on the surface for minutes [40]. In another study, platelet adhesion and aggregation is concluded to be observed in the range of shear stress approximately 1 to 200 dynes/cm^2 . Within this range, when the shear stress is higher than 30 dynes/cm^2 , platelet adhesion and aggregation depend on vWF binding to platelets GpIb/IX/V and GpIIb-IIIa [41].

3

Literature review

This chapter provides an overview of the state-of-the-art approaches to address thrombosis formation on the vascular graft inner wall. Traditional method in preventing platelet adhesion on the vascular graft is endothelialization by biofunctionalization and physical modifications of graft surfaces. Another approach to reduce platelet adhesion is coating the inner surface of vascular grafts with anti-coagulants. Recent novel approach to improve performance of vascular grafts is bioinspired surface mimicking topography of natural blood vessel surfaces which can reduce platelet adhesion.

3.1 Endothelialization approaches for the inner surface of vascular grafts

In natural blood vessels, endothelium plays a pivotal role in the control of vascular functions, especially haemostasis and thrombosis [42]. The healthy *endothelial cells (ECs)* provide a haemocompatible layer by controlling the platelet adhesion, aggregation, coagulation and fibrinolysis [42, 43, 44]. The anticoagulant and antithrombotic properties of ECs are due to the regulated secretion of antiplatelet agents including protacylin and nitric oxide [42, 43]. In the last few decades, intensive research has focused on polymer functionalization by modifying the inner wall of vascular grafts for better endothelialization to improve the biocompatibility of vascular grafts. Many strategies have been developed to establish a complete

3.1 Endothelialization approaches for the inner surface of vascular grafts

endothelium on the inner wall of vascular grafts before implantation. Investigations of in vitro endothelialization have shown that the confluent endothelium can prevent thrombosis formation and consequently improve the long term patency of vascular grafts [45, 46, 47, 48]. These strategies have been somewhat successful, but the endothelial cell layer is not completely built on the inner surface of vascular grafts. The endothelial cells cannot persist for a long time when the blood flow circulates in the vascular grafts. Consequently, endothelialization methods have not revealed better results in preventing thrombosis formation compared to bare vascular grafts. In vitro endothelialization procedures are labor intensive and require a considerable amount of time and expertise to extract and culture the cells until they become mature endothelial cells. These reasons make the in vitro endothelialization process costly and unable to be used widely [49, 50].

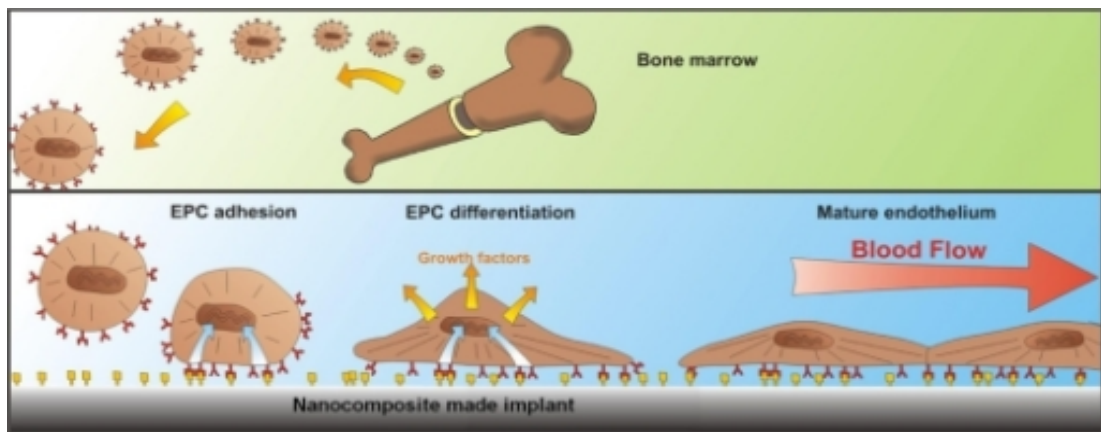


Figure 3.1: Biofunctional of the implant surface to catch EPCs from the blood flow to enhance in situ endothelialization [51].

In situ endothelialization methods have been established for endothelial cell seeding on the vascular graft inner wall using biofunctional molecules or other components (Fig. 3.1) to mobilize autologous cells within the vasculature to the graft postimplantation. Targeted cells for in situ endothelialization are in vivo circulating ECs and *endothelial progenitor cells (EPCs)*. These EPCs are derived from bone marrow and circulate in the blood flow [52, 53, 54]. EPCs also play a critical role in vascular formation and they possess the ability to differentiate into endothelial cells due to their high proliferative capacity [55, 56, 57]. Circulating

3.1 Endothelialization approaches for the inner surface of vascular grafts

EPCs have been identified as a crucial factor and a promising autologous cell source for the endothelialization process of synthetic vascular grafts after implantation which can prevent thrombosis and hyperplasia. Grafts seeded with EPCs have been demonstrated a high patency in animal models [58, 59].

3.1.1 Biofunctionalization of biomaterials for accelerated in situ endothelialization

As a living organism, cells are responsive to stimuli from their surrounding environment. In vivo cells are in contact with the *extra cellular matrix (ECM)* [60, 61, 62]. The ECM is the extracellular part of the cell structure that provides structural and biochemical support to the surrounding cells. In addition, the ECM contains a wide range of growth factors and is a local source of cell signals. Therefore, the ECM can regulate intercellular communication and a cell's dynamic behavior. One strategy to enhance endothelialization on the inner wall of vascular grafts is to mimic the features of ECM [63, 64]. In order to mimick the properties of the ECM for vascular grafts, it is important to promote desirable protein adsorption and subsequently, desirable cellular interaction. Material surfaces can therefore be modified by using growth factors, biofunctional molecules to promote desirable EPCs for in situ endothelialization.

Growth factors are protein molecules which have the ability to regulate cell growth, proliferation and differentiation. They act as signaling molecules between cells and just bind to specific receptors on the surface membrane of their target cells. It has been proven that growth factors can induce host progenitor cell mobilization and recruitment [65, 66, 67]. Synthetic vascular grafts modified with specific biofunctional molecules such as antibodies, peptides and aptamers to capture the circulating EPCs directly from the blood stream after implantation have shown better in situ endothelialization [68].

3.1 Endothelialization approaches for the inner surface of vascular grafts

3.1.2 Physical modification of inner graft surfaces for EPCs adhesion and proliferation

ECs are strongly affected by the surrounding environment and the mechanical properties or topography of the substrate. These factors can influence cell adhesion, proliferation and cell morphology. Therefore, the physical modification approach by changing mechanical properties, porosity of material or surface roughness has been widely used to improve endothelialization in vascular grafts [69, 70, 71].

Fiber alignment

Numerous studies have demonstrated that the fiber alignment in scaffolds may serve as a biomimetic tool to induce cell orientation and in situ migration [72, 73, 74]. In the last three decades, a biodegradable scaffold approach which mimicking the morphological and mechanical properties of natural blood vessels was improved to become a good blood vessel substitute in revascularization. The advantage of this approach is that the architecture of these scaffolds, in which endothelial cells are seeded, can be designed in any desirable shape using the electrospinning technique [75, 76, 77].

Nano- and microstructured surfaces

The nano- and microstructured surfaces may influence the EPCs/ECs adhesion, migration and elongation by altering the surface protein absorption [78, 79, 80]. Hence, the micro- or nano-pattern technique based on micro-contact printing has been the most widely studied approach for the design of these materials. Using this technique, spatially defined patterns of ECM proteins or other biomolecules can be prepared on biomaterial surfaces to guide the overall cell shape, the adhesion sizes and locations [81, 82].

Porosity

Porosity of biomaterial is also an important factor which affects endothelial cell coverage on surfaces. In order to generate a homogeneous cell distribution, the porosity of the surface must be small enough so that the endothelial cell can migrate across the porous structure and cover the whole surface. The endothelial cells were shown not to be able to cover pores of 80 μm or more in diameter, and they are unaffected by pores of 30 μm or less [83].

3.2 Coating with anticoagulants

Heparin is a polysaccharide anticoagulant with potent inhibitory effects on coagulation which are widely used in clinical prevention and treatment of thrombosis [84]. The anticoagulant effect of heparin lies in its ability to inhibit thrombin and activated factor which are involved in the conversion of prothrombin to thrombin, thereby reducing thrombin formation through an antithrombin mechanism [85]. Heparin is able to bind to and enhance the inhibitory activity of the plasma protein antithrombin against several serine proteases of the coagulation system through a high affinity pentasaccharide [86].

One potential strategy for reducing thrombogenicity of prosthetic materials is to incorporate heparin into the biomaterials to inhibit intrinsic thrombogenicity, leading to a better patency rates for vascular reconstructions with vascular grafts [87, 88, 89]. Heparin immobilization techniques have been widely investigated including physisorption, electrostatic deposition, and covalent bonding to surfaces. Heparin-bonded vascular grafts have shown favorable results in animal models and humans compared with untreated vascular grafts. Some of the ideal functional characteristics of a heparinized graft include uniform heparinization, retention of heparin on the graft surface, and maintenance of heparin bioactivity [90].

Heparin coating on the surface of vascular grafts by physical adsorption could maintain its bioactivity. However, the quick leaching of heparin compared to other techniques, leading to the unprotected surface areas of vascular grafts [91]. In contrast, covalent coupling technique could enhance the stability of the immobilized heparin but lower the bioactivity of heparin [91]. The use of heparin-releasing coating so that the bioactive heparin can be slowly released into the boundary layer of grafts over a period of time has been investigated to enhance the patency of vascular grafts. In this way, heparin is controlled at low-dose levels and be available at exactly where it is needed [91].

3.3 Bioinspired nano- and microstructured surface approach

3.3 Bioinspired nano- and microstructured surface approach

The definition of bioinspired materials has been well-known for some decades. It refers to synthetic materials whose desired structures, properties or functions mimic those of natural materials or living matter. The effect of natural nano- and microstructures on fluid dynamics interests more investigations nowadays. Fluid dynamic behavior in nano- and microscale systems is quite different from those in a macroscopic system. Macroscopic structures are considered to act against the fluid flow which result in a high pressure drop. In contrast, some natural nano-and microstructures have been shown to have properties of low drag, self-cleaning and low adhesion of contaminants on the surface [92],[93]. Certain plant leaves such as lotus leaves, are widely known to be superhydrophobic and self-cleaning due to the micro and nanostructures (hierarchical structure) of their surface [93],[94]. Another familiar example of biomimetics is shark skin structures which have been applied to the development of competitive (faster) swimwear due to their ability to reduce vortices flow on the surface [95],[96]. Artificial surfaces with periodic microstructures were also demonstrated to be able to reduce drag more than a smooth surface with the same material and to possess self-cleaning ability [93, 97].

Recently, several studies have investigated a new approach of bioinspired surface to improve the blood compatibility of vascular grafts. The main goal of this approach is to create a nano/microstructured surfaces mimicking the surface topography of natural blood vessels which can reduce platelet adhesion and consequently, thrombosis formation [98, 99, 100].

3.3.1 Hierarchical structure of the inner surface of a natural blood vessels

In principle, arterial walls consist of three layers. The outermost layer is the tunica adventitia which is composed of connective tissue as well as collagen and elastic fibers. The middle layer, tunica media is composed of smooth muscle and elastic fibers. The innermost layer of the arterial wall is the tunica intima which is a continuous layer of endothelial cells (Fig. 3.2).

3.3 Bioinspired nano- and microstructured surface approach

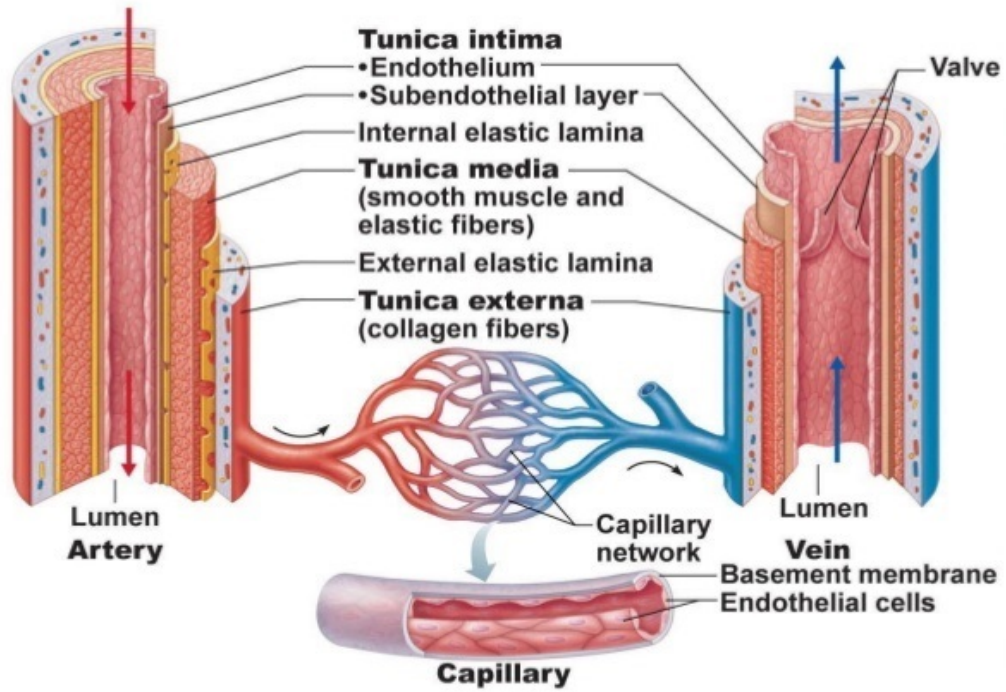


Figure 3.2: Structure of natural blood vessels [101].

A natural blood vessel is considered the 'best' material for preventing platelet adhesion and aggregation. The inner surface of natural blood vessels is not flat but rather rough at nano- or micro-scale. Over millions of years of evolution, the natural blood vessel has developed to possess an amazing hierarchical structure: micro-structure grooves parallel to the blood flow direction and micro-structures of endothelial cells which locate on these grooves and also orientate to the blood flow.

Figure 3.3 shows the structure of the natural blood vessels of domestic pigs investigated in our laboratory. The blood vessel diameter is around 2mm, and the parallel micro groove structures which elongate to the blood flow direction has a width of about 30-60 μm (Fig. 3.3). We also observed the endothelial cell layer covering the groove structure. The difference in size between grooves and the endothelial cell structures in different blood vessels is assumed to depend

3.3 Bioinspired nano- and microstructured surface approach

on animal species, blood vessel types and blood flow conditions in these blood vessels.

3.3.2 Nano- and microstructured surface mimicking inner topography of natural blood vessels

Recently, several investigations have focused on creating nano-microstructured surfaces, mimicking the structure of the inner surface of natural blood vessels to reduce platelet adhesion [98, 100, 102, 103].

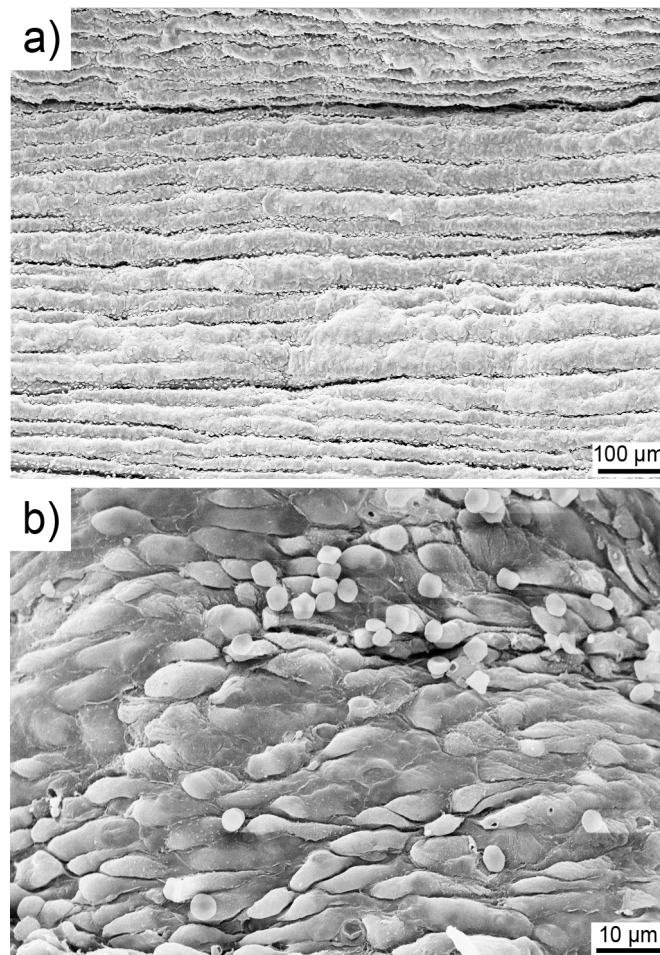


Figure 3.3: Inner layer structure of a natural blood vessel of the domestic pig: (a) SEM picture of inner surface with groove structures (magnification of 50 X) (b) SEM picture of inner surface with microstructure of endothelial cells (magnification of 500 X).

3.3 Bioinspired nano- and microstructured surface approach

Submicrometer range

Surfaces with submicrometer structures, which are smaller than platelet dimensions, for example longitudinal grooves [103], pillars [104, 105] or hierarchical structures [99] mimicking the inner surface of natural blood vessels have been reported to decrease the activation and adhesion of platelets under static and shear conditions, possibly because of superhydrophobicity leading to a low chance for contact with platelets.

Vascular grafts with submicron longitudinally aligned topography which mimicked the tunica intima of the native arterial vessels were prepared by electrospinning and investigated in vivo in the study of Liu et al [103]. A significant higher patency rate and less thrombus formation was found in vascular graft with aligned topography than vascular graft with smooth topography. It was assumed that the groove topography remodeled the boundary conditions of the blood flow, i.e. increased the velocity of the boundary layer and, thereby, decreased the collision frequencies of platelets with the surface. However, the effect of hemodynamic factors on platelet adhesion was not investigated [103].

Surfaces with submicron pillars with sub-platelet dimensions created using a soft lithography two-stage replication molding technique were shown to be able to reduce platelet adhesion under shear condition compared with the smooth surface with the same material under small shear condition [104]. The sub-platelet dimensions of the pillar microstructures resulted in a reduced contact between platelets and surfaces, and platelet adhesion was, therefore, decreased[104].

The blood compatibility of multiscale architecture comprising submicrometer ridges and nanoprotuberances, mimicking topography of natural blood vessels [99]. This multiscale structure surface is created on a *polydimethylsiloxane* (PDMS) surface by using soft lithography and physical treatment. The width of the ridges is about 500 *nm* and the height is about 100 *nm*, while the diameter of the nanoprotuberances is about 100 *nm* and the height is about 40 *nm*. Results indicated that this hierarchical structure reduced platelet adhesion in comparison to smooth surfaces by providing an optimal surface of low adhesion interaction. The multiscale structures on the surface was suggested to remodel the boundary condition of liquids, thus leading to a low collision frequency of platelets [99].

Micrometer range

3.4 Summary

The effect of surface features in the micrometer range (e.g. endothelial cells' size range), larger than the dimensions of platelets, has been controversially discussed so far. Ye et al. [100] and Li [102] found a reduced platelet adhesion on mastoid and parallel grating microstructured surfaces under static experimental condition. Both studies identified the wettability as the main underlying mechanism.

Chen et al. [106] tested the protein adsorption and its influence on platelet adhesion on microstructured polydimethylsiloxane (PDMS) surfaces under flow conditions. The amount of adsorbed protein and adherent platelets on the microstructured surface was higher than on the flat control surface [106]. In addition, platelets especially adhered in the interspaces between the microstructures where the amount of adsorbed protein was highest. Thus, the authors concluded that platelet adhesion was mainly driven by protein adsorption. However, no reduced platelet adhesion on the microstructured surface was found [106].

The bioinspired nano-microsurfaced surfaces have been demonstrated a valuable approach to improve the blood compatibility of synthetic vascular grafts. The nano-microstructured surfaces operate for a long time without using chemical modifications. However, this ideal has not yet been widely investigated to become a mature approach.

3.4 Summary

This chapter has reviewed the state-of-the-art approaches to improve the blood compatibility of vascular grafts. Endothelialization of the inner surface of vascular grafts is the traditional method used to prevent platelet adhesion and thus thrombosis formation. The aim of this method is to catch the EPCs circulating in the blood stream for the inner surface of vascular grafts by using biofunctionalization of biomaterials or physical modification. However, the method of endothelialization still does not meet the requirements of practical application. The adhesion and proliferation of endothelial cells on artificial surfaces are very complex phenomena. Endothelialization requires a considerable amount of time and complex experimental procedures which involve high costs and cannot be used widely, especially in an emergency situation. In addition, the endothelial cells also can-

3.4 Summary

not cover the whole graft surface [107, 108]. The graft areas without completed endothelial cells are potential for platelet adhesion and thrombosis formation.

Heparin-bonded grafts demonstrated a trend to improved patency, but the difference between heparin-bonded grafts and standard grafts was not statistically significant [109]. Heparin-bonded grafts had a significantly lower early thrombosis rate that was sustained only for the first 5 months of follow-up [109].

Another quite new approach to improve the performance of vascular grafts is bio-inspired nano-microstructured surfaces mimicking the topography of the natural blood vessel surface which has gained more interest recently. However, the idea of mimicking the topography of the inner surface of natural blood vessels has not yet been developed to a main research approach. Most of the investigations of bio-inspired nano-microstructured surfaces were carried out based on the individual measurements but not based on a statistical characterization of natural surface structures. In addition, many investigations revealed the important role of hemodynamic factors of nano-microstructured surfaces on platelet adhesion. However, the effect of these hemodynamic factors on platelet adhesion has not been investigated.

The next chapter, Chapter 4, the aims and objectives as well as Hypotheses of the PhD research will be presented.

4

Aims and Objectives of the PhD research

4.1 Open questions

As a unique layer in contact with blood, *endothelial cells (ECs)* have a function of preventing the triggering of platelet adhesion and clotting cascade. With the ability to release NO and other anticoagulant molecules to prevent platelet adhesion and aggregation, ECs provide an anticoagulant and antiplatelet surface [110]. In addition, ECs are strongly affected by hemodynamic factors. It was shown that ECs can adapt their shapes in response to applied shear flow to create a suitable form which supports the blood flow [111].

The changes of ECs due to hemodynamic factors has been observed for a long time ago. Significant investigations have shown that the ECs' response to shear stress occurs at both the cellular and molecular levels [112],[113]. Not only biochemical functions [114, 115] but also the morphology of endothelial cells [116] change due to *wall shear stress (WSS)* alterations or oscillatory shear stress [117],[118],[119],[120]. Consequently, the antiplatelet surface of ECs is believed to depend on not only their biological and chemical functions but also their geometrical shapes. Therefore, a potential approach for a potential less-thrombogenic surface for vascular grafts is maybe microstructured surfaces mimicking the form of endothelial cells.

This thesis focused on the approach of microstructured surface mimicking the EC morphology which is capable to reduce platelet adhesion for a better

4.2 Aims and Objectives

performance of vascular grafts. This research addressed on the micrometer range, e.g. ECs' size range.

According to the literature, the following questions have not yet been investigated:

1. Reduction of platelet adhesion on microstructured surfaces has not yet been observed under shear conditions.
2. The effect hemodynamic factors of microstructured surfaces on platelet adhesion and aggregation has not been investigated so far.
3. The quantitative characterization of the EC morphology in different blood vessels with shear stress conditions has not yet been investigated statistically.
4. Models of EC microstructures (geometrical forms and parameters) for microstructured surface approach have not yet been optimized under different shear stress conditions based on hemodynamic factors which affect platelet adhesion.

4.2 Aims and Objectives

The main aim of this thesis is to find a suitable microstructured surface which acts against platelet adhesion for a better performance of vascular grafts. The idea for such a microstructure is to mimic the form of the natural ECs. To achieve this aim, the following objectives were set:

1. to investigate the effect of hemodynamic aspects of microstructured surfaces on platelet adhesion under shear condition with both experimental and theoretical approaches

To achieve this objective, it was further divided into three subobjectives as follows:

- to fabricate microstructured surfaces using soft lithography

4.3 Hypotheses

- to investigate platelet adhesion on microstructured and unstructured control surfaces using a flow cell channel
 - to simulate the blood flow over the microstructured surface using Finite element method (FEM) to gain the distributions of shear stress on surfaces
2. to undertake quantitative characterization of EC morphologies in different blood vessels depending on blood shear stress

To achieve this objective, it was further divide into two subobjectives as follows:

- to carry out the measurements of blood flow rates and vessel diameters of different natural blood vessels to calculate shear stress in these blood vessels
 - to carry out the characterization of EC geometrical parameters (length, width, height, aspect ratio of length to with, area, perimeter) in these blood vessels
3. to optimize microstructured surfaces mimicking EC morphologies

To achieve this objective, it was further divided into three subobjectives as follows:

- to find a suitable microstructure model for vascular grafts mimicking EC form using hemodynamic simulations
- to find an optimal combination of geometrical parameters for this microstructure model which could reduce platelet adhesion using simulations with FEM

4.3 Hypotheses

In this thesis, the following hypotheses were tested:

1. Platelet adhesion is statistically significantly reduced on bioinspired microstructured surfaces compared to unstructured surfaces under shear conditions.

2. ECs in the arteries of different organs have different cell morphologies due to different shear conditions in those arteries.
3. The aspect ratio (of length to width), base area and perimeter of EC microstructure model are proportional to shear stress, whereas the height is decreased with increasing shear stress.

4.4 Contributions

There are three main contributions of this thesis as follow:

Firstly, the approach of microstructured surface mimicking EC morphology for vascular grafts is investigated in this study under shear condition with the consideration of hemodynamic factors. This study shows the first time that platelet adhesion was statistically significantly reduced (by up to 78% ; $p \leq 0.05$) on the bioinspired microstructured PDMS surfaces compared to that on the unstructured control surface under shear conditions. The study indicates that on the surfaces with the highest differences of the shear stress between the top of the microstructures and the ground areas, platelet adhesion was reduced most.

Secondly, the quantitative correlation of EC morphology and shear stress was investigated in this study for the first time for all cell geometrical parameters (length, width, height, aspect ratio, area and perimeter) to provide a reliable statistical data for further investigations of mimicking EC morphology.

Finally, this study suggests a microstructure model of EC which can be applied for vascular graft inner surfaces by FEM computational simulations. Furthermore, this study also presents an effective method to find the most suitable combination of geometrical parameters which may perform the most effective effect on reducing platelet adhesion on biomaterial surfaces.

4.5 Related publications

1. **T.T. Pham**, J. Schumacher, S. Maenz, K.D. Jandt, J. Bossert. How to optimize the inhibition of platelet adhesion on microstructured surfaces - a Finite Element Method (FEM) approach. (In preparation)

2. **T.T. Pham**, S. Wiedemeier, S. Maenz, G. Gastrock, U. Settmacher, K.D. Jandt, J. Zanow, C. Lüdecke, J. Bossert. Hemodynamic aspects of reduced platelet adhesion on bioinspired microstructured surfaces. *Colloids Surface B* 145 (2016) 502-509.
3. **T.T. Pham**, S. Maenz, C. Lüdecke, C. Schmerbauch, U. Settmacher, K.D. Jandt, J. Bossert, J. Zanow. Quantitative characterization of endothelial cell morphologies depending on shear stress in different blood vessels of domestic pigs using a focused ion beam and high resolution scanning electron microscopy (FIB-SEM). *Tissue Cell* 47 (2015) 205-212.
4. B. Garipcan, S. Maenz, S., **T. Pham**, U. Settmacher, K.D. Jandt, J. Zanow, J. Bossert. Image analysis of endothelial microstructure and endothelial cell dimensions of human arteries – A preliminary study. *Adv. Eng. Mater.* 13 (2011) B54-57.

4.6 Thesis Outline

I tried to present as in detail as possible the most highlighted aspects of the research work in the next 4 chapters.

Chapter 5 represents a practical approach for investigating the effect of micro-structured surfaces on platelet adhesion - the main cause of thrombosis under shear condition. By using a flow cell channel, it is able to investigate platelet adhesion and aggregation on microstructured and smooth surfaces. In this chapter, the result of significant reduction of platelet adhesion on the bioinspired microstructured surfaces under shear condition was discussed.

Chapter 6 describes the quantitative characterization of EC morphologies depending on shear stress for a better understanding of the effect of blood flow on EC morphology. In this chapter, the state-of-the-art methods for EC characterization is described step by step. The relationships between EC geometry parameters and blood shear stress are then statistically illustrated.

Chapter 7 focuses on finding the most suitable EC microstructure model for vascular graft surfaces. In this chapter, three 3D-models of the EC microstructure were computationally approximated as cuboid, ellipsoid and pyramid with

4.6 Thesis Outline

the same measurements (length, width, height, distance) and then simulated using FEM. The best EC model found in the previous step with varied geometrical parameters was simulated to find the optimal combination of geometrical parameters. A central composite design (CCD) was used to find the most rapid way to obtain this optimal combination.

Chapter 8 summarizes the major contributions of this thesis.

5

Hemodynamic aspects of reduced platelet adhesion on bioinspired microstructured surfaces

In this chapter, the effect of hemodynamic factors of micro-structured surface on platelet adhesion was investigated for the first time under a shear condition with both theoretical and experimental approaches. Different microstructured surfaces were designed, fabricated and tested with the whole porcine blood using a flow cell channel.

This study shows for the first time that platelet adhesion was statistically significantly reduced on the bioinspired microstructured PDMS surfaces compared to that on the unstructured control surface under shear conditions. Finite element method (FEM) simulations of blood flow revealed an important role of the micro shear gradient created by the microstructures on reducing platelet adhesion. The results indicate that on the surfaces with the highest differences of the shear stress between top and the ground of the microstructures platelet adhesion was reduced most.

5.1 Introduction

Different strategies have been introduced so far to improve the performance of artificial vascular grafts by enhancing blood compatibility i.e. reducing platelet adhesion on the inner surfaces of vascular grafts. Bioinspired nano- or microstructuring, mimicking the inner surface of natural blood vessels, achieved substantial attention in order to reduce thrombosis formation [99, 100, 102, 106]. However, this new strategy has not been widely investigated so far.

Surfaces modified with nano- or submicrostructures (nanoprotrusions, submicron longitudinally aligned topography, hierarchical structures), smaller than the dimensions of platelets, can reduce platelet adhesion compared to unstructured surfaces due to a reduced contact between platelets and the structured surfaces [98, 99, 103, 104, 105, 121]. In contrast, the effect of surface features in the micrometer range (e.g. ECs' size range), larger than the dimensions of platelets, is controversially discussed so far. Ye et al. [100] and Li [102] found a reduced platelet adhesion on mastoid and parallel grating microstructured surfaces under static experimental condition. Both studies identified the wettability as the main underlying mechanism. Chen et al. [106] tested the protein adsorption and its influence on platelet adhesion on microstructured polydimethylsiloxane (PDMS) surfaces under flow conditions. The amount of adsorbed protein and adherent platelets on the microstructured surface was higher than on the flat control surface [106]. In addition, platelets especially adhered in the interspaces between the microstructures where the amount of adsorbed protein was highest. Thus, the authors concluded that platelet adhesion was mainly driven by protein adsorption.

A further factor potentially influencing platelet adhesion is the surface resistance to flow i.e. the surface friction factor which is proportional to the pressure drop caused by the microstructured surfaces [97]. A higher resistance to flow may reduce the efficiency of the blood flow and, thus, increase platelet adhesion and vice versa. However, since platelet adhesion was mostly measured under static conditions the influence of the resistance to flow caused by microstructures on platelet adhesion was to the best of our knowledge not considered in studies so far. In addition, it was shown previously that high shear stresses in general re-

5.2 Materials and methods

duce the adhesion of blood cells on biomaterials surfaces [31, 122]. However, the influence of shear stress on platelet adhesion caused by the blood flow over the microstructured surfaces was not taken into account so far.

The aim of the present study was, therefore, to investigate platelet adhesion on bioinspired microstructured surfaces under blood flow conditions by a combined experimental and theoretical approach to deepen our understanding on the physical mechanisms of the platelet adhesion process. We tested the hypotheses i) that platelet adhesion is statistically significantly reduced on bioinspired microstructured surfaces compared to unstructured surfaces and ii) that surface microstructures increase the wall shear stress which leads to a reduced platelet adhesion. For this, PDMS model surfaces with hemispherical microstructures inspired from the natural EC layer were prepared with soft lithography. Platelet adhesion on these microstructured surfaces and unstructured control surfaces was investigated in a flow cell using porcine blood with fluorescence labelled platelets. Water contact angles and pressure drops between inlet and outlet (representative for surface resistance) were determined and correlated with platelet adhesion on these surfaces. Hemodynamic simulations of the blood flow on the microstructured surfaces and the unstructured control were carried out to investigate the influence of shear stress conditions caused by the surface structures on platelet adhesion. Our findings suggest that shear stress gradients caused by the microstructures play a major role in reducing platelet adhesion on bioinspired microstructured surfaces.

5.2 Materials and methods

5.2.1 Design and fabrication of microstructured PDMS surfaces

Based on the values of EC dimensions investigated in our previous studies [123, 124] and given in the literature [125, 126, 127], the microstructures were designed as hemispheres with different ground diameters (a), heights (h) and interspacing distances (b) arranged in regular arrays (Fig. 5.1). Three differently microstructured sample types were prepared (Table 5.1).

5.2 Materials and methods

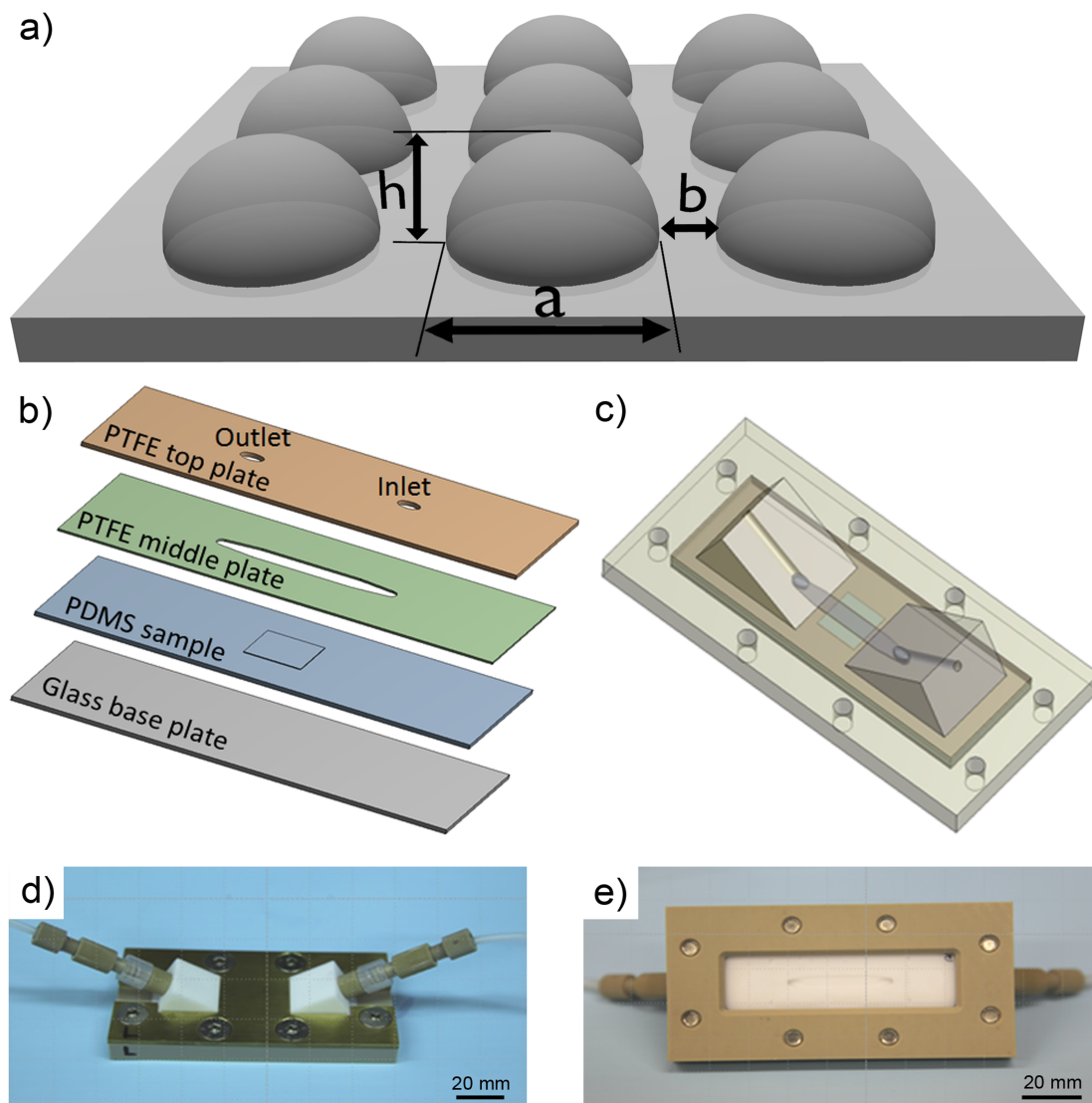


Figure 5.1: Set-up of the experimental flow cell and design of microstructured surfaces used in this study: a) schematical illustration of the microstructured surfaces with hemispherical microstructures arranged in regular arrays; b) sketch of the experimental flow cell with the multilayer plate construction: PTFE top plate with inlet and outlet, PTFE middle plate with the flow channel (height: 0.5 mm , largest width: 4 mm , length: 17.2 mm), PDMS sample containing the microstructured area ($1 \times 1\text{ cm}$) and a microscope slide as a base plate, all plates had a size of $76 \times 26\text{ mm}$; c) sketch of the flow cell with case; d) photograph of the flow cell with inlet and outlet connected to silicon tubes; e) photograph of the flow cell from the bottom-side with the flow channel visible in the middle part.

5.2 Materials and methods

The PDMS microstructured samples were prepared using laser ablation and soft lithography. Negative hemispherical microstructures were generated in the middle area (size: $1 \times 1 \text{ cm}$) of a glass microscope slide ($76 \times 26 \text{ mm}$) using a femtosecond laser following the designs in Fig. 1 (carried out at the Institute of Joining Technology and Materials Testing GmbH, Jena, Germany). A PDMS gel Sylgard 184 (Dow Corning, Midland, USA) was mixed with its curing agent in a weight ratio of 10:1, poured carefully on the negatively structured glass substrates and then cured for 5 h at 80°C . After hardening, the PDMS replicas were carefully peeled off from the glass substrates and sonicated in ethanol using an ultrasonic bath to remove non-crosslinked molecules from the PDMS surface. The surface structures of the PDMS samples were characterized using an AU-RIGA 60 CrossBeam® FIB-SEM scanning electron microscope (Carl Zeiss AG, Oberkochen, Germany).

5.2.2 Flow cell and platelet adhesion experiments

Fresh porcine blood (provided by the Institute of Laboratory Animals Science, University Hospital Jena, Jena, Germany) was obtained from a healthy pig using a sterile syringe containing anticoagulant citrate dextrose (ACD, Sigma-Aldrich) resulting in an ACD to blood volume ratio of 1:9. For fluorescence-based imaging of the platelets, 1 g 3,3-dihexyloxycarbocyanine iodide (DiOC6, Sigma-Aldrich) was added per 1 ml porcine blood and incubated for 10 min at 37°C .

A flow cell was designed as a multilayer parallel plate device (by the Institute for Bioprocessing and Analytical Measurement Techniques, HeilbadHeiligenstadt, Germany) (Fig. 5.1b). The inlet of the flow cell chamber was connected with silicon tubes to a neMESYS syringe pump system (Cetoni GmbH, Korbußen, Germany) and the outlet was connected to a waste reservoir. In addition, inlet and outlet were connected to two pressure sensors to measure the pressure drop between the inlet and outlet. Each adhesion experiment was carried out for 2.5 min. The volumetric fluid flow rate was kept constant at $9 \text{ ml}/\text{min}$. The pressure at the inlet and the outlet was measured 1000 times per second. After 2.5 min, the PDMS samples were taken out of the flow cell, rinsed very carefully to remove non-adherent cells and fixed in glutaraldehyde solution (4 % (v/v) in PBS) for 30

5.2 Materials and methods

min at room temperature and, subsequently, for 2 h at 4°C. After fixation, the PDMS samples were dried for microscopy. The platelet adhesion was investigated on 3 replicates ($n = 3$) of each structure.

PDMS samples with adherent fluorescence-labelled platelets were characterized using confocal laser scanning microscopy (CLSM; Zeiss LSM 510 Meta, Carl Zeiss Microscopy GmbH) with $n = 10$ images taken of each sample surface. CLSM images were analyzed with the Leica QWin Pro V 2.6 image analysis software (Leica Microsystems Imaging Solutions, Cambridge, UK) using a binarization algorithm to obtain the average coverage of the surfaces with platelets (%).

5.2.3 Contact angle measurement

The static water contact angle on microstructured PDMS surfaces and unstructured control samples was determined with the sessile drop method using a drop shape analysis system DSA 10 MK 2 (Krüss GmbH, Hamburg, Germany) and deionized water. For statistical analysis, five measurements were carried out for each structure type and averaged.

5.2.4 Preparation of blood and platelet labelling

Fresh whole porcine blood was drawn from a healthy pig obtained from the Institute of Laboratory Animals Science Jena, Germany using a clean syringe containing anticoagulant citrate dextrose (Product of Sigma-Aldrich) with the concentration of 1:9 (ratio of ACD volume to blood). For the fluorescent imaging of platelets on the surfaces, whole porcine blood was labelled with DiOC6 (3,3-Dihexyloxacarbocyanine iodide) (Product of Sigma-Aldrich). Before starting the platelet adhesion experiment, porcine whole blood was gently mixed with DiOC6 (1 μ g DiOC6 for 1 ml porcine blood) and incubated at 37°C for 10 minutes. The porcine blood was then mixed by inversion again carefully, prior to the experiment with the flow cell channel.

5.2.5 Simulation of blood flow

Hemodynamic simulations of the blood flow on the unstructured and microstructured surfaces were carried out using the CFX package ANSYS Workbench 13.0 (Ansys Inc., Canonsburg, USA). The geometrical model of the flow cell and a constant blood flow rate of 9 ml/min, both as in the laboratory experiment, were used as basis for the simulation. According to the literature [103], the hydraulic diameter (DH) of the rectangular flow cell was calculated as:

$$DH = \frac{2 \times W \times H}{W + H} \quad (5.1)$$

where W is the width (4 mm) and H is the height (0.5 mm) of the flow cell. The Reynolds number (Re) was calculated as:

$$Re = \frac{\rho \times V \times DH}{\mu} \quad (5.2)$$

where ρ is the density of blood, V is the velocity and μ is the blood dynamic viscosity. In this study, the Reynold number was much lower than 2000. Therefore, we considered the blood flow to be steady laminar. In addition, we considered the blood to be Newtonian fluid with a constant density of 1,050 kg/m³ and a viscosity of 3.45 × 10³ Pas.

5.2.6 Statistical analysis

All results are presented as mean standard deviations. The statistical analysis of platelet adhesion as function of the surface microstructures was carried out using SPSS software 19.0 (IBM, Armonk, USA). Statistical significance was tested using a one-way analysis of variance (ANOVA) with a 95% confidence interval ($p \leq 0.05$) and a Fisher's least significant difference (LSD) post-hoc test.

5.3 Results

5.3.1 Characterization of microstructured surfaces with microscopy

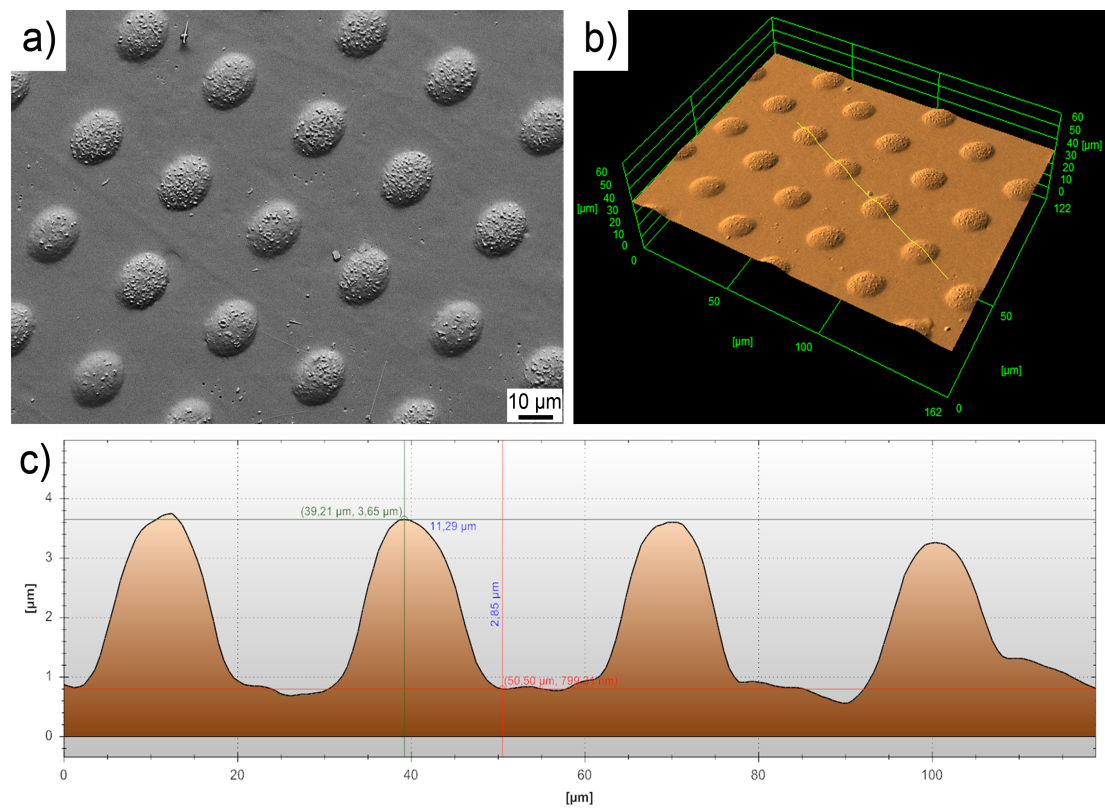


Figure 5.2: Characterization of the microstructured PDMS surfaces using SEM exemplarily illustrated for the surface structure type 1: a) SEM-2D micrograph of the hemispherical microstructured surface; b) SEM-3D image of the hemispherical microstructures acquired by using a 4 quadrant detector; c) profile of the microstructure illustrated in b) (yellow line; see for comparison also Table 5.1).

PDMS microstructured samples were prepared using laser ablation and soft lithography. SEM-2D imaging and SEM-3D imaging with a 4 quadrant detector were used to characterize the surface structures of the PDMS samples (Fig. 5.2). These images revealed well-arranged hemispherical microstructured surfaces. The sur-

face microstructures of all sample types were uniform without deformations or visible defects.

5.3.2 Platelet adhesion on the microstructured and unstructured surfaces

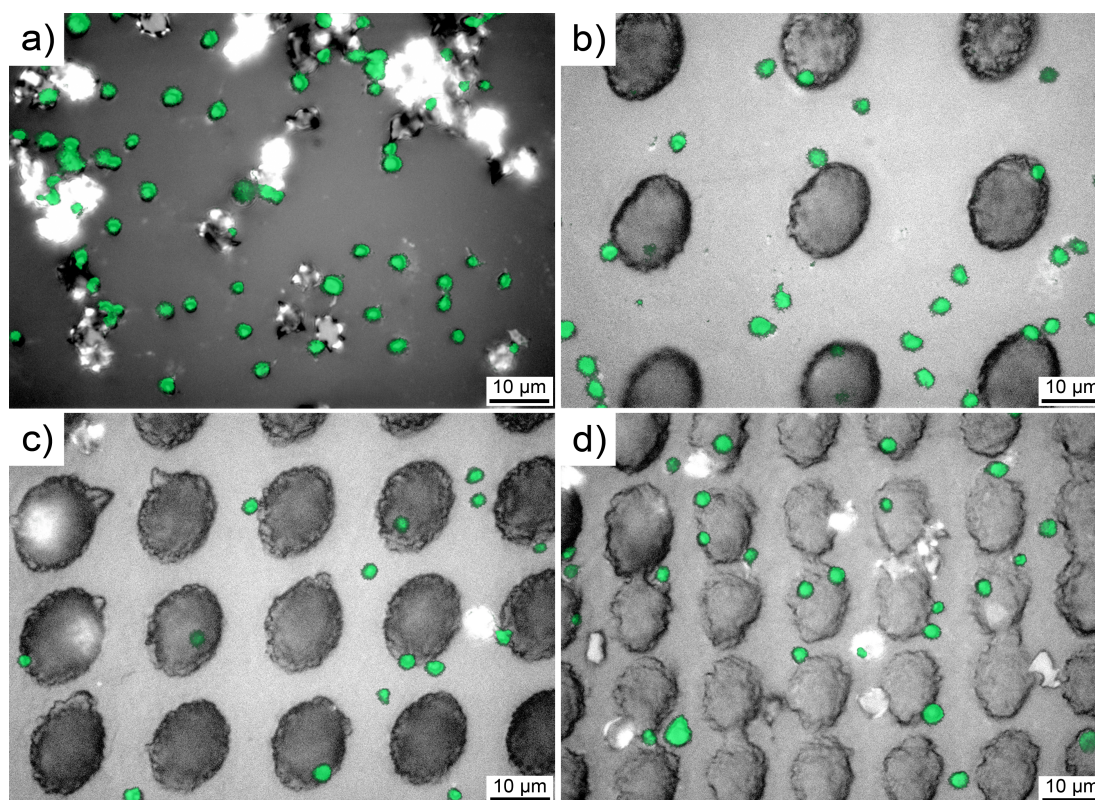


Figure 5.3: Platelet adhesion to microstructured and unstructured PDMS surfaces illustrated by overlapping of the representative fluorescence images and the corresponding light microscopy images: a) unstructured surface; b) structure type 1; c) structure type 2; d) structure type 3.

Platelet adhesion to microstructured and unstructured PDMS surfaces was tested in a flow cell under shear conditions using porcine blood labelled with DiOC6. Platelet adhesion to microstructured and unstructured PDMS surfaces is illustrated in Fig. 5.3 by overlapping of the representative fluorescence images and the

corresponding light microscopy images. On the unstructured control surface, the coverage with platelets was highest with $3.7 \pm 1.3\%$ (Fig. 5.4). All microstructured surfaces showed a statistically significantly lower surface coverage with platelets compared to the unstructured control surface. On structure type 2, platelet adhesion was reduced most with a surface coverage of only $0.8 \pm 0.4\%$ which means an overall reduction of the adhesion by 78.4% compared to the control. On the structure types 1 and 3, the platelet adhesion was reduced as well with a surface coverage of $2.2 \pm 1.1\%$ and $2.0 \pm 0.8\%$, respectively. The surface coverage on structure type 2 was statistically significantly lower compared to structure type 1 and 3. On the microstructured surfaces, platelets adhered mainly in between the hemispherical microstructures (Fig. 5.3 b-d).

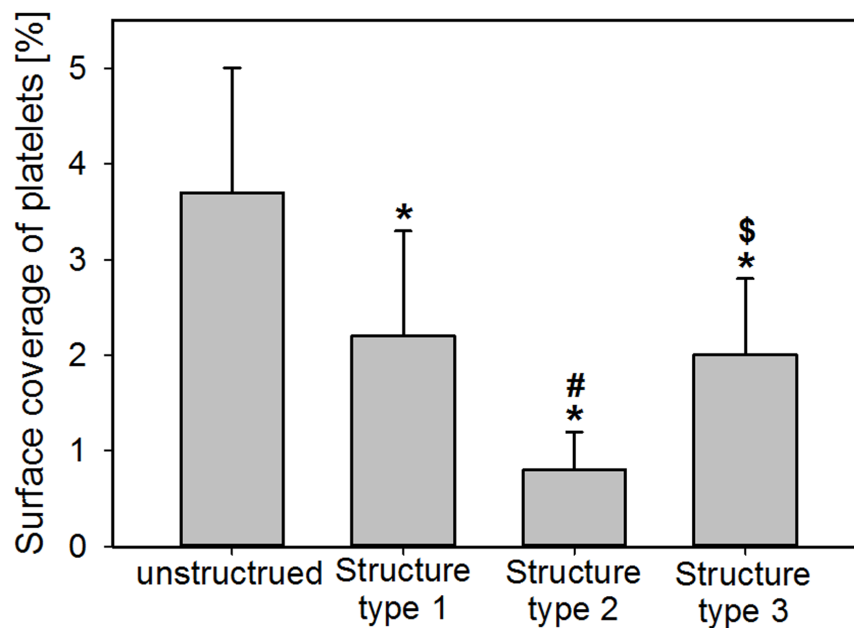


Figure 5.4: Coverage of the microstructured and unstructured PDMS surfaces with platelets. * $p \leq 0.05$ vs. unstructured surface, # $p \leq 0.05$ vs. structure type 1, \$ $p \leq 0.05$ vs. structure type 2.

5.3.3 Contact angle and pressure drop

To examine the effect of wettability on platelet adhesion, the static water contact angles of the different microstructured surfaces and the unstructured surface were

5.3 Results

Table 5.1: Dimensions, average static contact angle (mean \pm standard deviation based on $n = 5$) and pressure drop (mean \pm standard deviation based on $n = 3$) of the microstructured and unstructured surfaces.

	Control (unstructured)	Structure type 1	Structure type 2	Structure type 3
Diameter a [μm]	-	15	15	12
Interspacing b [μm]	-	15	5	3
Height h [μm]	-	2.5	2.7	0.9
Contact angle [$^\circ$]	113.5 ± 1.3	115.3 ± 0.9	127.7 ± 0.8	120.2 ± 0.4
Pressure drop [kPa]	9.9 ± 0.2	10.3 ± 0.7	9.8 ± 0.3	9.9 ± 0.3

measured (Table 5.1). All surfaces were hydrophobic. The unstructured control surface had an average water contact angle of $113.5 \pm 1.3^\circ$, whereas the water contact angles were increased on the microstructured surfaces with $115.3 \pm 0.9^\circ$ (structure type 1), $127.7 \pm 0.8^\circ$ (structure type 2) and $120.2 \pm 0.4^\circ$ (structure type 3). The results indicate a correlation between surface wettability and platelet adhesion. The lower the surface wettability is, the fewer platelets adhere to the surface.

The effect of surface resistance to flow on platelet adhesion was investigated by measuring the pressure drop caused by the microstructured surfaces or by the unstructured surface. The pressure drop during blood flow caused by structure type 2 and structure type 3 was 9.8 ± 0.3 kPa and 9.9 ± 0.3 kPa, respectively, and thus equal to the pressure drop caused by the unstructured control surface (9.9 ± 0.2 kPa). In contrast, structure type 1 caused a numerically higher pressure drop of 10.3 ± 0.7 kPa (Table 5.1). However, statistically significant differences among the pressure drop caused by the different structure types and the control surface were observed. No correlation between surface resistance to flow and platelet adhesion was obvious.

5.3.4 Hemodynamic simulation of blood flow

To gain insight into the relationship between hemodynamics and platelet adhesion, shear stress and velocity distributions were investigated by FEM simulation (Fig. 5.5). The *wall shear stress (WSS)* on the unstructured areas of all three structure types was uniform with $1.8Pa$ (Fig. 5.5 a-c). Gradients in the shear stress distribution caused by the microstructures were observed with noticeably increased shear stress values on the top of the structures and partly decreased values in the interspacing areas compared to the unstructured control regions (Fig. 5.5 a-c). Structure type 1 caused a WSS of $3.0 Pa$ on the top of the microstructure and in the interspacing regions a shear stress of $1.8 Pa$ which is approximately the same as on the unstructured control areas ($1.9 Pa$; Fig. 5.5 a). Structure type 2 showed the highest WSS with $3.1Pa$ on the top and, simultaneously, the smallest wall shear stress with $1.0 Pa$ on the ground inbetween the microstructures which was below the shear stress of the control regions (Fig. 5.5 b). Structure type 3 caused a slightly lower WSS with $2.4 Pa$ on the top of the microstructure but a wall shear stress on the ground inbetween the microstructures in the same range as that of structure 2 with $1.1 Pa$ (Fig. 5.5 c).

To gain deeper insight into the effect of hemodynamic factors on platelet adhesion on the microstructured surfaces, the velocity distribution in three different regions of structure type 2 is illustrated in Fig. 5.5 d-f. The hemodynamic simulation demonstrated that the blood velocity was increased on the top of the structure compared to that on the unstructured area (Fig. 5.5 d, e). The blood velocity vectors around $1 \mu m$ (radius of the platelet) perpendicularly away from the top of the structures had the magnitude of $1 \times 10^{-3} m/s$, while that on the unstructured area is $0.6 \times 10^{-3} m/s$ (Fig. 5.5 d, e). In addition, Fig. 5.5 f shows low blood velocity vectors on the interspacing between the structures compared to other areas. These velocity vectors have a magnitude of approximately zero (Fig. 5.5 f). These results suggest that a thin layer of blood is trapped in the interspacings between the microstructures.

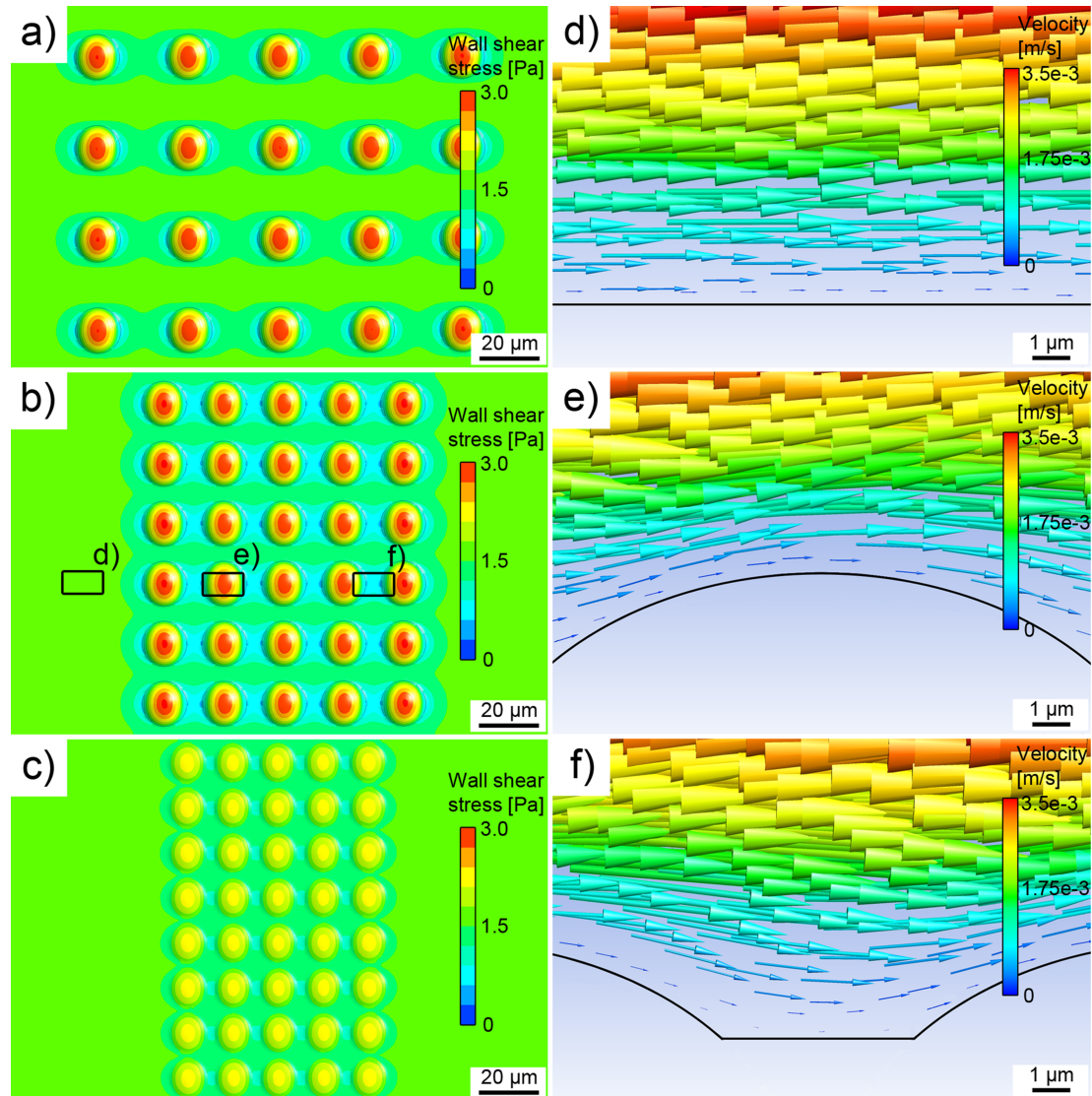


Figure 5.5: Hemodynamic simulations of blood flow on microstructured surfaces. Simulation plots showing wall shear stress distribution caused by the blood flow on the microstructured surfaces: a) structure type 1; b) structure type 2; c) structure type 3. Red indicates the highest (3.0 Pa) and blue the lowest value (0 Pa) of the wall shear stress (a-c). Simulation plots showing blood velocity close to the surface of structure type 2: d) on the unstructured area; e) on top of the microstructures; f) in between the microstructures. Red indicates the highest (0.0035 m/s) and blue the lowest value (0 m/s) of the blood velocity. The size of the arrows also demonstrates the magnitude of the velocity vectors (d-f).

5.4 Discussion

The study presented here investigated the effect of bioinspired microstructures mimicking EC morphology on platelet adhesion. Surface contact angles, surface resistance to flow and hemodynamic aspects were considered as factors possibly influencing platelet adhesion. Platelet adhesion was statistically significantly reduced by up to 78% on the bio-inspired microstructured PDMS surfaces for the first time under blood flow conditions (Fig. 5.4). Therefore, the first hypothesis can be accepted. On the control surface, platelets were partly aggregated together (Fig. 5.3 a) while on the microstructured surfaces only few separated platelets were adherent (Fig. 3 b-d). Thus, our findings indicated that bioinspired, hemispherical microstructures are able to reduce platelet adhesion under shear conditions.

5.4.1 Water contact angle

Platelet adhesion reduction on microstructured surface has been recently recognized in some previous studies under static conditions [100, 102]. The investigations of Li et al. and Ye et al. indicated a reduced platelet adhesion on the grafting and mastoid microstructured surfaces compared to the smooth surfaces due to a higher water contact angle of these surfaces [100, 102]. In our study, the hemispherically microstructured PDMS surface was shown to be more hydrophobic compared to the unstructured control PDMS surface (Table 5.1) which may, thus, be one reason for the reduced platelet adhesion on the microstructured surfaces (Fig. 5.4). An increase in contact angle, i.e. a decrease in wettability, is correlated with a decreased strength of interaction between blood, which consists to a large part of water, and the hydrophobic materials surface. This leads, in consequence, to a reduced contact between platelets and surfaces resulting in platelet adhesion reduction (similar to a self-cleaning effect of the surfaces [94, 128, 129]). However, in this current study, on the surface structure type 1 and type 3, the contact angle was only slightly increased compared to the unstructured control surface whereas platelet adhesion was significantly reduced on the control surface. Thus, the contact angle seems to play overall only a secondary role in reducing platelet adhesion, especially under shear conditions.

5.4.2 Surface resistant to flow

Since previous studies were carried out mostly under static experimental conditions, the surface resistance to flow, i.e., the pressure drop caused by the surfaces, as a parameter possibly influencing platelet adhesion was investigated in our study for the first time. Our study showed that the hemispherically microstructured surfaces did not create a statistically significantly higher surface resistance to flow compared to the unstructured surface (Table 5.1). Thus, a correlation between pressure drop and platelet adhesion is not obvious. Our findings indicate that at least under the specific experimental conditions used in the current study the endothelial cell-like hemispherical microstructures do not obstruct the blood flow compared to the unstructured surface.

5.4.3 Shear stress

Previous studies showed that high shear stresses in general reduce the adhesion of blood cells on biomaterials surfaces [31, 122]. The highest overall WSS was found on the top of our bioinspired microstructures. In particular, on the top of the microstructure type 2, the WSS was highest (3.1 Pa), followed by the top of microstructure type 1 (3.0 Pa) and type 3 (2.4 Pa). The lowest WSS was found on the unstructured control (1.9 Pa). However, the platelet adhesion was not as much reduced on surface type 1 compared to that on surface type 2 (Fig. 5.4) although both surfaces had nearly the same shear stress value measured on top of the structures (Fig. 5.5 a, b). Therefore, no direct correlation between the maximum shear stress and platelet adhesion was obvious. Our second hypothesis, that surface microstructures increase the wall-shear stress which leads, in consequence, to a reduced platelet adhesion was, thus, only partially accepted.

Our experimental and simulation results revealed that the local WSS difference between the top of the microstructures and the ground inbetween seems to be more important for the reduction of platelet adhesion. The highest WSS difference between top and ground with 2.1 Pa and simultaneously the lowest platelet adhesion of $0.8 \pm 0.4\%$ (Fig. 5.4, Fig. 5.5) was found for structure type 2. The structure type 1 and 3 with the WSS difference of 1.2 Pa and 1.3 Pa, respectively, had nearly the same platelet adhesion coverage of $2.2 \pm 1.1\%$ and

$2.0 \pm 0.8\%$, respectively.

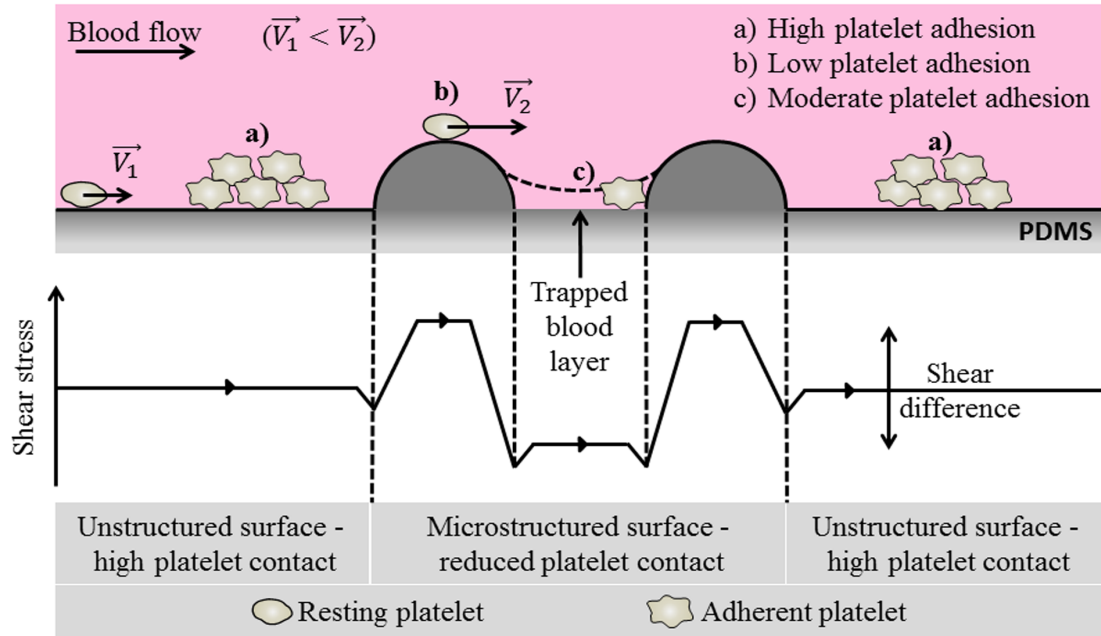


Figure 5.6: Proposed model of reduced platelet adhesion on microstructured surfaces.

A blood velocity of approximately zero inbetween the microstructures (Fig. 5.5 f) indicates a kind of trapped blood layer in the interspacing after whole-blood perfusion through the flow cell that hardly moves out of the interspacing. A high shear difference between top and ground means an increase of the blood velocity on the top of the microstructures and a decrease of the velocity due to the trapped blood layer on the ground of the interspacing. This leads to an overall fast moving upper blood layer compared to the trapped blood layer, which results in two phenomena causing a reduced platelet adhesion on the microstructured surfaces: i) on top of the microstructures, platelets move with the highest velocity resulting in low contact time between platelets and material surface and ii) the interaction between the trapped blood layer and the fast moving upper blood layer is reduced, if the shear stress difference is high, which leads to a reduced transfer of platelets from the upper layer to the trapped layer (Fig. 5.6). On the unstructured surface, platelets have a lower velocity compared to that on the top of microstructures

5.4 Discussion

and, in consequence, an increased contact time with the surface, leading to a high platelet adhesion (Fig. 5.6).

The magnitude of the WSS difference (between top of the microstructures and ground inbetween) was affected by the height of the microstructures and the distance inbetween the single hemispherical structures on each sample type. In our study, the sample type 2 with the distance of 5 μm and the height of 2.7 μm resulted in the highest shear difference of 2.1 Pa, leading to the lowest platelet adhesion. On sample type 1, with the highest distance of 15 μm inbetween the microstructures, the shear stress was on the ground area with 1.8 Pa almost the same as on the unstructured control surface with 1.9 Pa (Fig. 5.5 a). In summary, the magnitude of the WSS difference increased with increasing height of the microstructures and decreasing distance between the single hemispherical structures. The WSS difference is proportional to the aspect ratio R of the height of the microstructures to the interspacing between the microstructures. The aspect ratio R can, thus, be expressed as follows:

$$R = \frac{a + b}{h} \quad (5.3)$$

with a (diameter), b (interspacing), h (height) as the structure dimensions, as shown in Fig. 5.1. Our findings suggest that the microstructure aspect ratio R should be lower than that of the structure type 1 with $R = 12$ (under the specific flow condition used in the current study with a shear stress of 1.8 Pa, i.e. shear rate of 480 1/s) to achieve a significant effect of platelet adhesion reduction. This finding agrees well with the results of Koh et al., who investigated the effect of interspacing and aspect ratios of sub-micrometer structures on platelet adhesion under static conditions [105].

Chen et al. [106] investigated the adsorption of fibrinogen and its influence on platelet adhesion on microstructured PDMS surfaces under flow conditions (shear rate of 300 1/s) with similar structures. They demonstrated that the amount of adsorbed protein on the microstructured surfaces was statistically significantly higher compared to the flat surface. In addition, platelets in particular adhered in the interspaces between the microstructures where the amount of adsorbed

5.5 Conclusion

protein was high. Chen et al., therefore, concluded that platelet adhesion is mainly driven by protein adsorption most probably by binding of glycoprotein IIb/IIIa receptor of the platelet to the fibrinogen [105]. Interestingly, in the current study, a significant reduction of platelet adhesion was observed on the microstructured surfaces compared to the unstructured control surfaces (under shear stress of 1.8 Pa or approximately shear rate of 480 1/s) despite a higher amount of adsorbed proteins as expected from the results of Chen et al. [106]. The different results of our present study compared to the study of Chen et al. may be due to the different experimental shear conditions in both studies. Therefore, our results suggest that the effect of shear condition may overcome the effect of protein adsorption at a certain point.

Our study reveals for the first time that an intelligent design of surface microstructures affects local shear stress regimes near the biomaterial surface potentially reducing platelet adhesion. As a next step, platelet adhesion should be investigated on microstructured materials relevant for artificial vascular grafts preferred under pulsatile flow. Since platelet adhesion is a self-reinforcing process, the investigation of the platelet adhesion as function of time, i.e. kinetics, might be useful to gain further insight into the processes and involved parameters.

5.5 Conclusion

Platelet adhesion on the bioinspired microstructured surfaces was investigated under shear condition using a combined experimental and theoretical approach to give new insight into the involved physical processes. This study reveals a reduction of platelet adhesion (up to 78%) on bioinspired microstructured surfaces compared to unstructured surface. Microstructures cause a local shear stress gradient with the highest shear stress value on the top and lowest shear stress value on the ground which is affected by interspacing and height of the microstructures. On surfaces with the highest differences of the shear stress between the top of the microstructures and the ground areas, platelet adhesion was reduced most. This new knowledge lays the basis for the development of innovative next-generation vascular grafts with a reduced risk of thrombosis formation.

6

Quantitative characterization of endothelial cell morphologies depending on shear stresses in different blood vessels of domestic pigs

This chapter describes the quantitative characterization of endothelial cell morphologies for all cell geometrical parameters (length, width, height, aspect ratio, area and perimeter) depending on shear stress for a better understanding of the effect of blood flow on endothelial cell morphology. In this chapter, the state-of-the-art methods for endothelial cell characterization is described step by step.

This results show that the ECs in the arteries of different organs have different cell morphologies due to different shear conditions in those arteries. In our study, the exponential correlation between endothelial cell parameters and shear stress was shown the first time. This study provides a reliable statistical data for further investigations of mimicking EC morphology

6.1 Introduction

Recently, a new approach using micro- and nanostructures mimicking the morphology of the inner surface of natural blood vessels gained interest to improve

6.2 Materials and Methods

the blood compatibility of vascular grafts [98, 99, 100, 102]. To further develop this bioinspired approach, the exact endothelial cell morphology has to be reproduced on the artificial vascular graft surfaces. However, depending on the type of the blood vessel, the location and the specific blood flow, the ECs differ in their morphology [125, 130, 131, 132]. This is assumed to be due to different shear stress conditions in these vessels, because it was shown that the ECs adapt their shapes in response to the applied shear flow to create a suitable morphology which supports the blood flow [111]. However, the quantitative relationship between EC geometrical forms and shear stress has still not been investigated in detail. To achieve an optimized microstructured surface mimicking the shape of the ECs for vascular grafts under specific different shear conditions in different blood vessels, it is indispensable to understand how the EC shape changes under shear conditions. The aim of this study was, therefore, to investigate the quantitative correlation of the form and dimension of EC and shear stress.

To achieve this aim, four different types of blood vessels (carotid, renal, hepatic and iliac arteries) from three domestic pigs were investigated. The blood flow rates in these vessels were measured first in vivo for the calculations of shear stress. These blood vessel samples were then removed and fixed to keep the original morphology of the ECs. The EC morphologies in these blood vessels and vessel diameters were quantitatively characterized using a state-of-the-art Focused Ion Beam (FIB) - Scanning Electron Microscope (SEM). The geometrical parameters of ECs were statistically analyzed and quantitatively correlated with the calculated shear stresses.

6.2 Materials and Methods

6.2.1 Blood flow measurement

Three healthy domestic pigs of around 3 months of age and nearly the same weight (27.3 kg, 28.8 kg and 29 kg respectively, obtained from the Institute of Laboratory Animals Science Jena, Germany) were anesthetized with 2 ml propofol, 2 ml pancuronium and 1.5 ml fentanyl (The experiment with the pigs was permitted with ethical approval number 02-132/10).

6.2 Materials and Methods

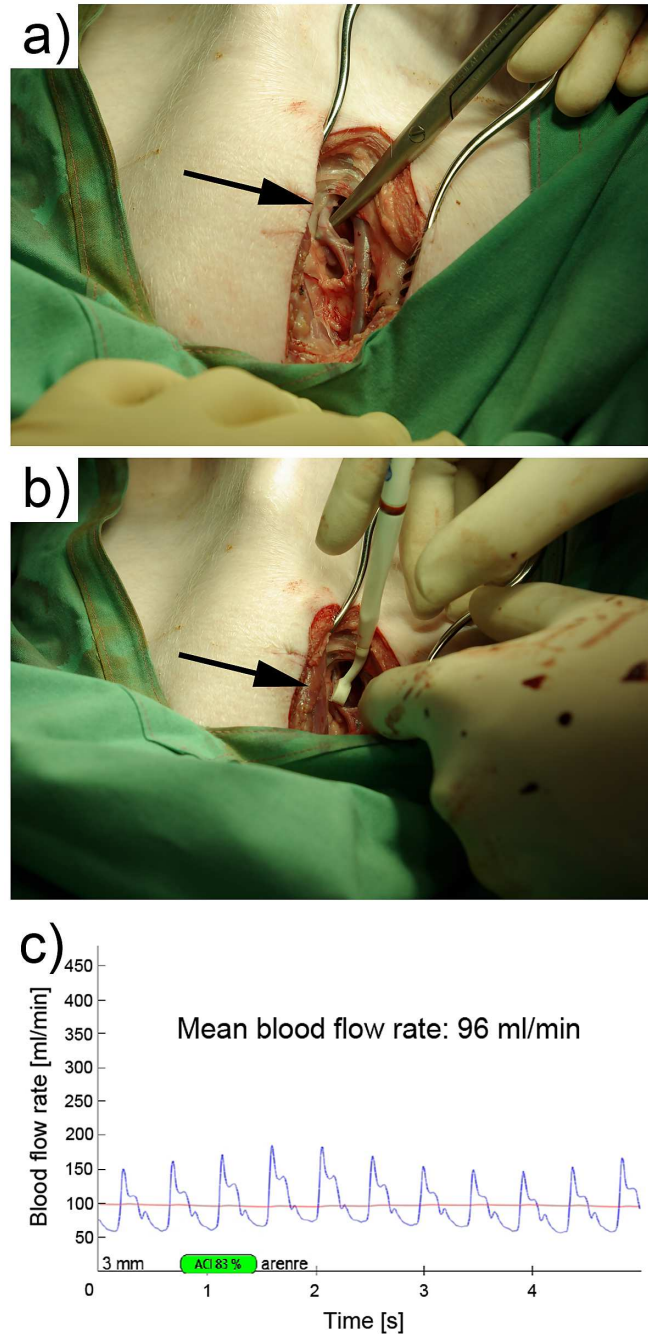


Figure 6.1: Operation to measure blood flow rates in different blood vessels of three domestic pigs: (a) Exposed blood vessel of a domestic pig; (b) blood flow measurement carried out with QuickFit sensor and VeriQ system; (c) pulsatile blood flow measured by VeriQ.

6.2 Materials and Methods

These pigs were first operated at the neck area to expose the common carotid artery and afterwards at the belly area to expose the hepatic, renal and iliac arteries (Fig. 6.1 a). VeriQ Flowmeter System and PeriVascular transit time probes (Medistim ASA, Norway) were used to measure the blood flow rates in these blood vessels. For this, the transit time method utilizing two piezoelectric crystals transmitting ultrasound through the blood vessel toward a reflector on the other side of the vessel is used. The volume blood flow rate is calculated by measuring the difference between transit times upstream and downstream in the blood vessel. The PeriVascular probes were placed over each exposed artery to measure the pulsatile blood flow (Fig. 6.1 b). For each pig, the volume blood flow rates in seven different blood vessels were measured: common carotid arteries (left and right), hepatic artery, renal arteries (left and right) and iliac arteries (left and right). The monitor of the VeriQ displayed the diagram of the blood flow rate with mean value (Fig. 6.1 c). Blood flow measurements were carried out at the middle of the exposed vessels. After finishing the blood flow measurements, specimens of the arteries were removed (around 2 cm long) and kept in the organ preservation solution, custodiol, for the next step. All removed vessel segments were healthy and had a cylindrical shape. There was no sign of atherosclerosis or EC dysfunction on the inner surfaces.

6.2.2 Fixation of pigs' blood vessels

As described in the literature [124], fresh artery specimens were rinsed with phosphate buffer saline (PBS) and then fixed in 4% glutaraldehydesolution (in PBS) for 30 minutes at room temperature and afterwards for 2 hours at 4°C. The fixed samples were dehydrated using ethanol solution with deionized water (10, 30, 50, 70, 80, 90, two times 100% (v/v) ethanol) with 24 hours for each step. These samples were then dried using a Critical Point Drying (CPD, Emitech K850, East Sussex, UK) system.

6.2 Materials and Methods

6.2.3 Measurements of the blood vessel diameter, EC length, width, aspect ratio, area and perimeter

After drying, a thin slice was cut-off from all blood vessel samples to image their cross sections for blood vessel perimeter measurements (Fig. 6.2 a). The rest of the samples were cut into pieces of approximately 10 mm in length and opened along their longitudinal axis to achieve the visibility of the inner wall of the blood vessel samples with the endothelium layers. All samples were then coated with a thin layer of gold and imaged using SEM (Leica S440i, Cambridge, UK) (Fig. 6.2 a, 6.2 c).

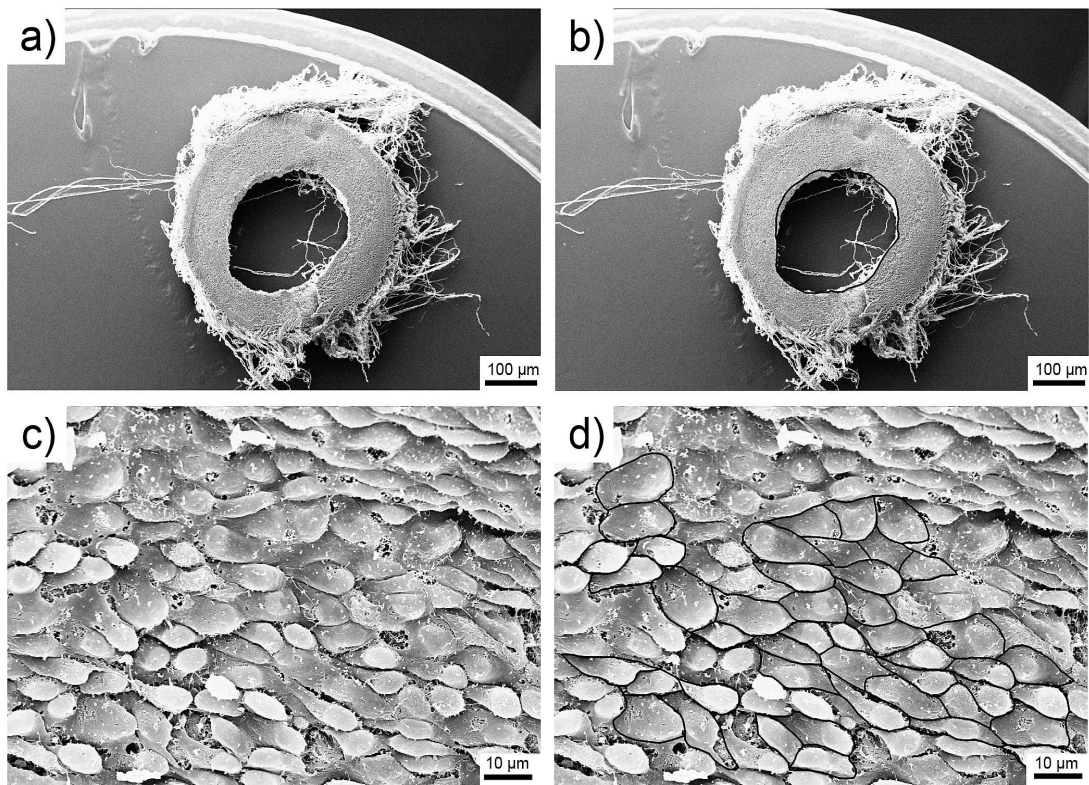


Figure 6.2: Characterization of endothelial cell dimensions and blood vessel diameter: (a) SEM picture of common carotid artery cross section; (b) lumen perimeter of common carotid artery marked with GIMP; (c) endothelium of common carotid artery with a magnification of 500x; (d) perimeters of endothelial cells marked with GIMP.

6.2 Materials and Methods

For the determination of the blood vessel diameters, the perimeters of the blood vessel lumen were drawn on the background of the SEM picture using GIMP software (GNU Image Manipulation Programme, GIMP V 2.6.6, free online version) (Fig. 6.2 b). The same method was applied to measure the EC perimeters. The ECs with clearly visible boundaries were chosen for cell characterization (Fig. 6.2 c, 6.2 d). Pixel calibration for SEM pictures was carried out using the Axio Vision software (Rel. 4.8, Carl Zeiss Microimaging GmbH, Jena, Germany). The SEM pictures with the blood vessel lumen perimeter and EC boundaries from GIMP were then characterized with Leica QWin image analysis software (Leica QWin Pro V 2.6, Leica Micro systems Imaging Solutions, Cambridge, UK) using a binarization algorithm as described in the literature [124]. After characterization, the results of the blood vessel lumen perimeters as well as mean length, width, area, perimeter and aspect ratio (of length to width) of the ECs were obtained. The blood vessel diameters were then calculated based on the blood vessel lumen perimeters.

6.2.4 Characterization of EC height

To measure the height of the ECs, the state-of-the-art dual beam FIB-SEM Auriga 60 (Carl Zeiss Microscopy, Jena, Germany) was used. In this method, the focused ion beam (FIB) is always perpendicular to the sample surface. Material of the sample surface at a chosen area was cut and removed precisely to reveal the cross section of the sample using a focused Gallium ion beam. The electron beam was adjusted to an angle of 54° in relation to the sample surface for imaging. The ECs with clearly visible boundaries were chosen (Fig. 6.3 a), and sectioned at the highest point by FIB to reveal the cell cross section at this point (Fig. 6.3 b). The cross section of the EC at the highest point was then imaged by SEM to estimate the height of the ECs (Fig. 6.3 b).

6.2.5 Calculation of wall shear stress

Porcine blood was proved to have haematocrit percentage of about 30%-40% [133]. Blood viscosity of this haematocrit percentage at high shear rate can be found in the literature [134].

6.2 Materials and Methods

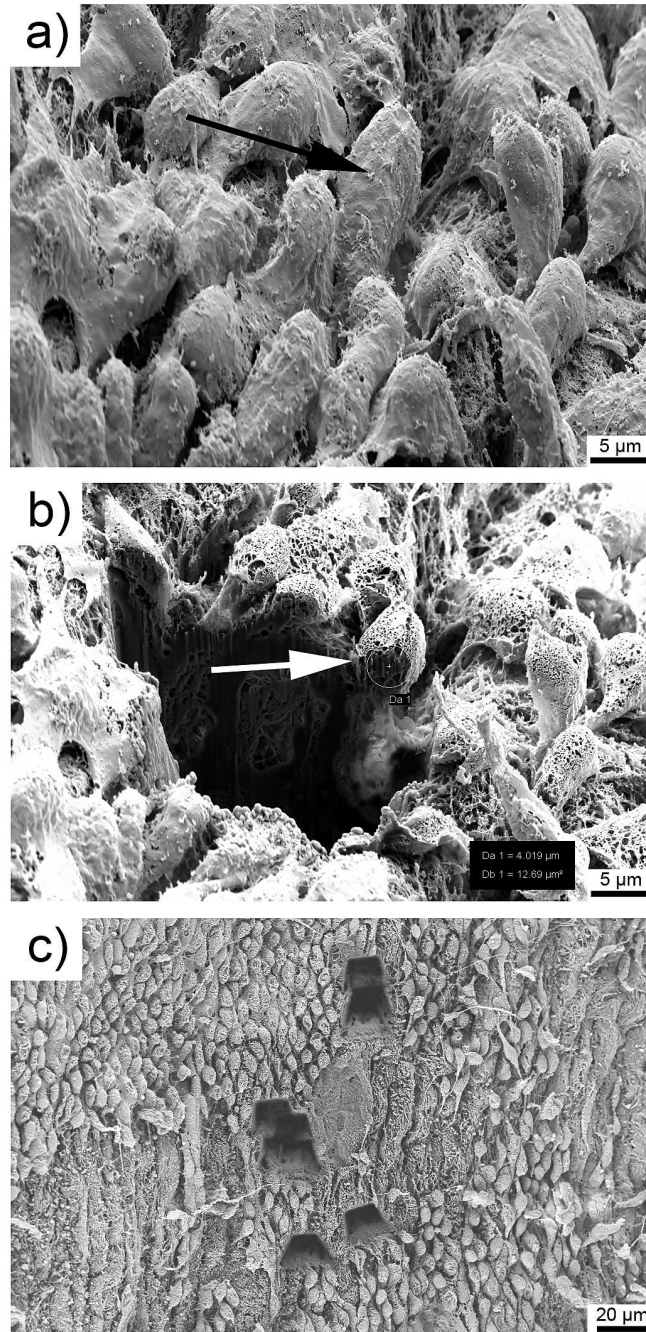


Figure 6.3: FIB-SEM images of endothelial cell layer in common carotid artery: (a) Endothelial cell (indicated with the arrow) before cross sectioning at a view angle of 54° to the surface; (b) endothelial cell (arrow) after cross sectioning at its highest point for determination of the cell height; (c) endothelial cell layer sectioned at different points to measure the cell heights (view direction perpendicular to the surface).

The blood WSS (τ) in these arteries was determined due to volume blood flow rate (Q), vessel diameter (d) and assumed blood viscosity of 3.5 cP [134] using following equation:

$$\tau = \frac{32 \times \mu \times Q}{\pi \times d^3} \quad (6.1)$$

6.2.6 Statistical analysis

Statistical analysis was performed using the SPSS software version 19.0 (SPSS, Inc., IBM Company). Statistical significance was evaluated using an one-way analysis of variance (ANOVA) at a 0.05 significance level and means were compared by the LSD post-hoc test.

6.3 Results

EC morphologies in different blood vessels are shown in Figure 6.4. In general, the ECs in renal and hepatic arteries were visibly longer and narrower compared to those in iliac and carotid arteries (Fig. 6.4). SEM images of the ECs revealed that the EC layers of blood vessel samples were still present (Fig. 6.2 and 6.4). The ECs connected to each other to form a continuous layer and the boundaries of the ECs were clearly visible for cell characterizations. However, there were some areas in which the cells were damaged during the preparation process (Fig. 6.3 c). In general, there was enough area with continuous layers of ECs available for cell characterizations.

The results from the quantitative characterization of ECs are given in Table 6.1. The average values of cell area, cell length, cell width, cell height, cell aspect ratio and cell perimeter were determined for each artery type. The ECs had statistically significantly different cell lengths (ANOVA, $P < 0.0001$) and significantly different cell widths (ANOVA, $P < 0.05$) in the different blood vessel types. The EC aspect ratio was consequently indicated to be significantly different (ANOVA, $P < 0.0001$) in different vessel types as well. The highest aspect ratio of the ECs was measured in the hepatic arteries, followed by renal arteries, while in iliac and carotid arteries, the aspect ratio was smallest. However, the highest WSS

6.3 Results

was found in the hepatic artery and the second highest was in the renal artery (Table 6.1). The WSS in iliac and carotid arteries was nearly the same (Table 6.1). The ECs also had statistically significantly different heights in different blood vessel types (ANOVA, $P < 0.01$). The hepatic artery had the smallest EC height (Table 6.1). In contrast to the hepatic artery, the ECs in the carotid and iliac arteries were highest (Table 6.1).

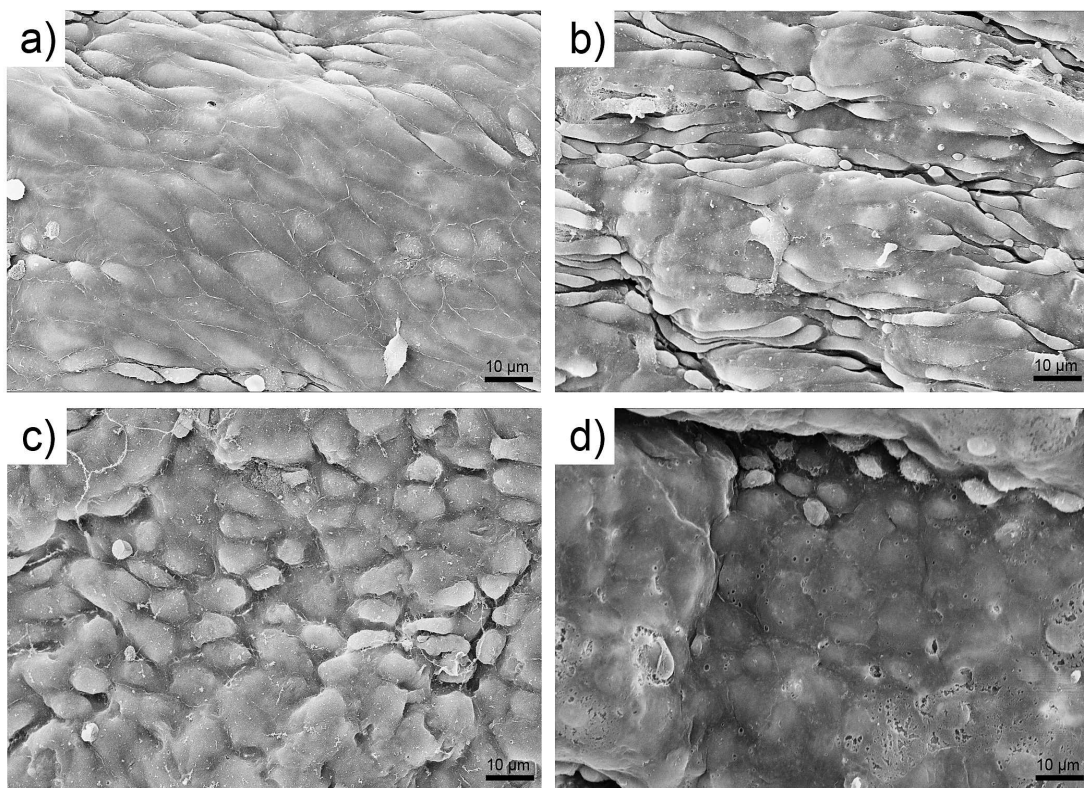


Figure 6.4: SEM images of endothelial cell layers obtained from four different blood vessels of pigs with a magnification 500x: (a) hepatic artery; (b) renal artery; (c) iliac artery; (d) carotid artery. The endothelial cells in hepatic and renal arteries had a longer and narrower shape compared to those in carotid and iliac arteries.

To investigate the effect of WSS on the EC forms, the cell dimensional parameters in each artery segment of three pigs were quantitatively correlated with the WSS. The quantitative correlation between cell aspect ratio and shear stress is illustrated in Figure 6.5 a.

6.3 Results

Table 6.1: Endothelial cells characterization of four natural blood vessel types using FIB-SEM images. The average values of all endothelial cell geometry parameters were obtained together with blood vessel diameters and blood flow rates in those arteries. The average wall shear stress in each blood vessel type was then calculated based on vessel diameter and blood flow rate.

Artery	Carotid	Renal	Hepatic	Iliac
Cell area [μm^2]	48.62 ± 11.65	44.71 ± 15.58	55.17 ± 18.78	58.08 ± 18.59
Cell length [μm]	12.46 ± 2.06	15.62 ± 2.67	18.68 ± 3.08	14.36 ± 2.6
Cell width [μm]	5.79 ± 1.14	4.53 ± 0.94	4.78 ± 0.84	6.08 ± 1.42
Cell height [μm]	4.43 ± 0.3	3.17 ± 0.39	2.74 ± 0.36	3.82 ± 0.56
Cell perimeter [μm]	30.99 ± 4.11	35.83 ± 6.01	43.46 ± 7.21	35.22 ± 5.57
Aspect ratio	2.24 ± 0.57	3.52 ± 0.59	3.98 ± 0.68	2.47 ± 0.65
Number of cells evaluated	362	428	204	686
Blood flow rate [ml/sec]	0.61 ± 0.15	1.7 ± 0.51	2.28 ± 0.91	1.63 ± 0.78
Vessel diameter [mm]	1.29 ± 0.13	1.35 ± 0.2	1.0 ± 0.07	2.06 ± 0.58
Wall shear stress [Pa]	10.15 ± 1.9	25.11 ± 7.54	89.16 ± 56.32	7.21 ± 3.1

The correlation between the cell aspect ratio and the shear stress can be described with the following exponential fit function:

$$y = a \times \exp\left(-\frac{x}{b}\right) + y_0 \quad (6.2)$$

6.3 Results

where x is the WSS and y is the EC aspect ratio. The fit parameters were $a = -2.95$; $b = 18.18$ and $y_0 = 4.15$ for this case. The coefficient of determination (R^2) was 0.74 for this exponential fit. The cell aspect ratio increased with increasing WSS (Fig. 6.5 a).

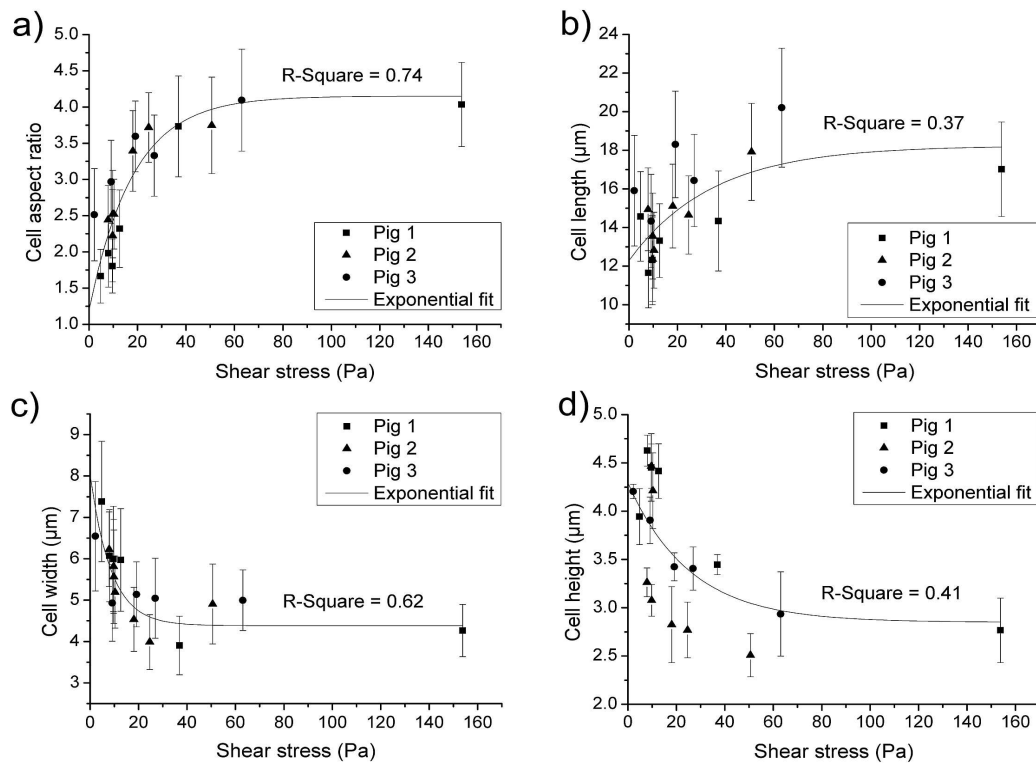


Figure 6.5: Correlations of endothelial cell geometry parameters with shear stress fitted with an exponential function of Equation 6.2. The data are shown as mean values and according standard deviation (for each type of blood vessel of each pig). (a) Correlation of endothelial cell aspect ratio with shear stress, $a = -2.95$; $b = 18.18$ and $y_0 = 4.15$. (b) Correlation of endothelial cell length with shear stress, $a = -5.95$; $b = 34.53$ and $y_0 = 18.24$. (c) Correlation of endothelial cell width with shear stress, $a = 3.64$; $b = 8.64$ and $y_0 = 4.38$. (d) Correlation of endothelial cell height with shear stress, $a = 1.44$; $b = 25.47$ and $y_0 = 2.85$.

The exponential fit showed that in the case of a shear stress of zero, the cell aspect ratio would be around 1.2. This means that the ECs have an almost

round shape under static conditions. The cell aspect ratio increased strongly with increasing WSS in the range of 0 to 60 Pa. For higher WSS, the cell aspect ratio then increased more slowly up to a threshold value of around 4.2.

A similar exponential correlation was found between the cell length, width and height and the WSS. Figure 6.5 b represents the change of the cell length due to the blood WSS. The length of the ECs strongly increased with increasing WSS in the range of 0 to 60 Pa. The threshold value of the cell length under high shear stress is approximately 18 μm . The pig ECs are assumed to have a length of 12 μm under static conditions (no shear stress).

The correlation between the cell width and the WSS is illustrated in Figure 6.5 c. In contrast to the cell aspect ratio and the cell length, the width of the ECs decreased with increasing WSS (Fig. 6.5 c). The cell width markedly decreased in the WSS range between 0 and 60 Pa and reaches a threshold value of around 4.2 μm . The highest cell width is assumed to be approximately 8.0 μm under static conditions according to the exponential fit function (Fig. 6.5 c). The EC height also decreased rapidly with increasing WSS, especially in the range between 0 and 60 Pa (Fig. 6.5 d). Due to the exponential fit function, it is assumed that the ECs have an average height of 4.3 μm under static conditions. The threshold value of the EC height is assumed to be 2.7 μm under higher WSS conditions.

6.4 Discussion

Mimicking the morphology of ECs has been reported recently as a promising novel approach to reduce platelet adhesion on artificial surfaces [98, 99, 100]. However, it is known that ECs adapt their shape to different shear conditions [135]. In consequence, it is indispensable to specifically adapt the biomimetic surface structure of artificial vascular grafts to their field of application to optimize their anti-blood coagulation properties. Thus, a statistic description of EC geometrical parameters as function of shear stress is required to enhance the blood compatibility of vascular grafts by surface structures mimicking the form of ECs. In this study, therefore, the EC morphologies in different blood vessels exposed to different shear stress conditions were quantitatively investigated.

The characterization of the EC shapes in their native state in natural blood

vessels has been performed in previous studies. The existence of EC morphological difference between different blood vessels or different parts of the same blood vessel as well as in different physiological states was already observed [124, 125, 130, 131, 136]. Kibria et al. described the difference in EC dimensions between inferior vena cava, pulmonary vein, pulmonary trunk and aorta [125]. The aorta was shown to have the highest cell aspect ratio (length to width) in comparison to the other blood vessels [125]. Helliwellet al. characterized the EC forms in carotid, pulmonary and aorta arteries [125]. They found that the ECs have different shapes, such as spindle, polygon or gigantic forms. The ability of ECs to adapt their shapes and functions in response to applied shear stress of the fluid flow was demonstrated in many in vivo and in vitro studies [112, 113, 137, 138]. In order to specifically mimic the microstructure of ECs for vascular grafts under different shear conditions, a quantitative relationship between EC morphology and shear stress is required. In this study, we quantitatively analyzed for the first time, how the EC dimensions change due to different shear stress conditions. The characterization procedure represented in this current study used glutaraldehyde, critical point drying and FIB-SEM for investigation of a high amount of ECs in different blood vessels. SEM images showed that the ECs were still connected and formed a continuous layer and most of the ECs maintain their boundaries and forms (Fig. 6.2,6.4). However, we cannot completely avoid the possibility of preparation artefacts (e.g. shrinkage during drying or contracting due to absence of tension). The statistical analyses indicated that the ECs in different artery types had significantly different cell length, cell width, aspect ratio and cell height.

SEM imaging of the EC shapes (Fig. 6.4) revealed that the ECs had different dimensions in different blood vessels of domestic pigs. In renal and hepatic arteries, the ECs clearly were longer and narrower compared to iliac and carotid arteries (Fig. 6.4). This is assumed to be due to the different WSS conditions in those arteries. WSS in the hepatic artery was highest in comparison to the other arteries (Table 6.1). The second highest shear stress was measured in the renal artery, followed by the iliac and carotid artery, which had nearly the same WSS condition. The ECs in the hepatic artery had the highest aspect ratio and, accordingly, the largest length and the smallest width (Table 6.1). Furthermore,

6.4 Discussion

the ECs height in the hepatic artery was smallest (Table 6.1). It is assumed to be due to the highest WSS in the hepatic artery. In contrast, the ECs in the iliac and carotid artery had the smallest aspect ratio and the highest height assumed to be due to the smallest WSS. This observation can be explained by the effect of blood flow shear force on the EC membrane. The higher the WSS, the more blood shear force applies to the EC membrane. This leads to a change of the EC cytoskeleton [135]. In consequence, the ECs elongate their shape with increasing length and decreasing width and height due to higher shear stress. This confirms the resulted already published in other studies [135, 139].

The correlation between WSS and the EC form was also analyzed quantitatively (Fig. 6.5). The exponential fit suggests that the cell aspect ratio increases with increasing WSS (Fig. 6.5 a). In addition, it can be predicted that the cell aspect ratio is around 1.2 when there is no applied shear stress. This means that ECs have an almost round shape under static conditions. This finding is in a good agreement with data published for single cell investigations [127, 139, 140, 141]. Barbee et al. showed that bovine ECs had an almost round shape with cell length and width of approximately 30 μm under static conditions [127]. Under shear stress condition of 1.2 Pa, the ECs adapted their shape to the flow and the ECs became longer and narrower, whereas the ECs length and width changed to 60 μm and 20 μm , respectively [127].

The exponential fit in Figure 6.5 a also gives information about the maximal expected aspect ratio of the ECs. Under high WSS, the cells may reach a maximal aspect ratio of approximately 4.2 (threshold for high WSS). It seems reasonable, that the EC length cannot infinitely increase with increasing shear stress; rather, there is a threshold value of cell aspect ratio, somehow limited by the size of the cell nucleus and a finite volume of the cell.

The length of the ECs is also revealed to increase with increasing WSS (Fig. 6.5 b). The threshold value of cell length is expected from exponential fit to reach a value of around 18 μm when the WSS increases. The ECs of pig are suggested to have a length of 12 μm under static conditions. In contrast to the cell length, the cell width was assumed to decrease quantitatively with increasing WSS (Fig. 6.5 c). The cell width decreased rapidly in the shear stress range of 0 to 60 Pa and then reaches a threshold value from exponential fit of around 4.2 μm . The highest

6.4 Discussion

cell width is assumed to be approximately $8 \mu\text{m}$ in static conditions, according to the exponential fit function (Fig. 6.5 c).

The EC height was proven to decrease with increasing WSS (Fig. 6.5 d). In this current study, the exponential function suggests that under static conditions the EC height could reach the highest value of approximately $4.3 \mu\text{m}$. Figure 6.5 d also shows that the expected minimum EC height from exponential fit is approximately $2.7 \mu\text{m}$ under higher WSS conditions. These results agree with the invitro investigation by Barbee et al. [127]. Under static conditions, bovine EC height was around $5 \mu\text{m}$ [127]. Under a flow condition with a WSS of 1.2 Pa , the EC height decreased and reached a value of a $2.5 \mu\text{m}$ [127]. The expected minimal height of $2.7 \mu\text{m}$ can be assumed to be the minimal size of the cell nucleus under maximal deformation due to flow conditions. The nucleus deformation appears to be in direct and immediate response to alterations of the cell adhesion area under flow conditions [142]. It was demonstrated that the cytoskeletal fibers could also reliably transmit the flow shear force to the nucleus in the order of seconds [143]. Additionally, a theoretical analysis of ECs exposed to fluid flow has suggested that the cells adapt to the flow by minimizing the magnitude of force acting on the nucleus ([144]. It was also found that the minimal total force applied results from a lower cell height ([144]. The nucleus was assumed to be a stiff structure for a long time. The elastic modulus of nuclei in round and spread cells was found to be around 5000 N/m^2 , on average 10 times more rigid than the cytoplasm [141, 145]. It can be briefly summarized that, under flow conditions, the ECs attempt to minimize the applied shear force on their bodies by reducing the cell height and width. When flow shear force is applied on ECs, there is a deformation of cytoplasm. The cytoskeletal fibers can also transfer the flow shear force to the nucleus in the order of seconds. Therefore, the cell height and width decrease rapidly at the beginning because the cytoplasm has a lower stiffness than the cell nucleus. The deformation then occurs more slowly because of the high stiffness of the cell nucleus. The nuclear stretch was also proven to decrease over time [145].

The EC height under the shear condition seems to be limited due to the cell nucleus. This study agrees with previous studies of the cell nucleus mechanical properties in the literature. Cailleet al. investigated the mechanical properties of

ECs and their nuclei [141]. Compression tests of the round and spread cell as well as of isolated nuclei were carried out until the cell height went down to 30% of the original cell height [141]. However, the threshold value of the compression was not given. For example, if an EC has a height of 5 μm , it would be theoretically possible to compress the cell perpendicular to the cell base until the cell height is 1.5 μm . In reality, under shear conditions, the height of the compressed nucleus cannot reach this value since the blood shear force is applied parallel but not perpendicular to the cell base. The exponential fit in Figure 6.5 d suggests that this limited cell height is around 2.7 μm .

This study provides the quantitative correlation of EC geometrical parameters and shear stress which are indispensable data to further optimize the mimicking of ECs morphologies in vascular grafts to enhance their blood compatibility. Due to the fit functions, suitable geometrical parameters of microstructures mimicking ECs can be derived for each shear condition.

6.5 Conclusion

The current study addressed the quantitative correlation of EC geometrical parameters with shear stress. The relationships between most geometrical parameters and shear stress were found to be exponential. The results show that the ECs under higher shear stress conditions have longer and narrower shapes but smaller height than in static conditions. According to the obtained quantitative relationships between EC shapes and shear stress it can be assumed that the ECs are nearly round under static conditions. Furthermore, the limited width and height of ECs under very high shear stress conditions can also be predicted. These new data are urgently needed to develop, microstructures for vascular grafts mimicking EC morphologies and, in consequence, enhancing blood compatibility of the artificial blood vessels.

The next chapter, Chapter 7, optimized the inhibition of platelet adhesion on bioinspired microstructured surfaces using FEM simulations. The aim of this chapter is to find a suitable endothelial cell model with an optimal combination of geometrical parameters, distance and pattern for vascular grafts which could reduce platelet adhesion - the main cause of thrombosis.

7

Optimizing the inhibition of platelet adhesion on bioinspired microstructured surfaces - a Finite Element Method (FEM) approach

This chapter describes how to optimize the shape and geometrical dimensions of the microstructures depending on the blood flow conditions for synthetic vascular grafts using Finite Element Method (FEM) approach. The Central Composite Design (CCD) method is also introduced as an effective method to reduce the required number of simulations to find an optimal value for a certain parameter.

In this chapter, suitable EC microstructure models with optimal geometrical parameters for vascular grafts under two different shear conditions were suggested. For the first time we found that the physical effect of the endothelial cell morphology also contributes to antithrombotic property of ECs. Under a certain shear condition, ECs adapt their form to the blood flow to create a most suitable shape which induces the highest WSS difference for reducing platelet adhesion.

7.1 Introduction

Recently, a further approach gained substantial attention in order to reduce platelet adhesion: mimicking the inner surface topography of natural blood vessels, i.e. the EC morphology [98, 99, 100]. However, the investigations of bioinspired microstructured surfaces were carried out based on the individual measurements but not based on a statistical characterization of natural surface structures [98, 99, 100]. The optimal microstructure form as well as geometrical parameters under different shear conditions have not been investigated so far [98, 99, 100].

In chapter 5, a reduction of platelet adhesion on such bioinspired microstructured surfaces was obtained by up to 78 % compared to unstructured surfaces [146]. The microstructures caused a local shear stress gradient with the highest shear stress value on the top and lowest shear stress value on the ground. The higher the wall shear stress (WSS) difference between the top and the ground areas of the microstructures is, the fewer platelets adhered to the microstructured surfaces. Disturbed flow with low and oscillating WSS, i.e. high oscillatory shear index (OSI), is also a decisive factor in cell dysfunctions which also promotes platelet adhesion and aggregation [147, 148, 149]. However, the influence of bioinspired microstructures on these factors has not been taken into account so far.

It is well known, that ECs are strongly affected by hemodynamic factors [114, 150, 151] and respond to shear stress at cellular and molecular levels [152, 153]. ECs optimize their shapes under applied shear flow to create a suitable form which supports the blood flow [123, 124, 135, 154, 155]. Thus, it seems probable that the optimal microstructure mimicking ECs depends also on the local shear conditions.

The aim of the current study was, therefore, to find a suitable microstructure form for vascular graft surfaces with optimal geometrical parameters based on geometrical parameters of the natural ECs under two different shear conditions in the common carotid and iliac arteries. We tested the hypothesis that the aspect ratio (of length to width), base area and perimeter of EC microstructure model are proportional to the shear stress, whereas the height is decreased with increasing shear condition. For this, three computational models (cuboid, ellipsoid

and pyramid) were created with the same geometrical parameters (length, width, height and distance) based on the real geometrical parameters of the natural ECs in the common carotid artery. These models were simulated using the Finite Element Method (FEM) to investigate their effects on the WSS difference and *oscillatory shear index (OSI)* considered as factors influencing platelet adhesion. The best EC microstructure form found in the previous step with varied geometrical parameters (area, height, aspect ratio of length to width) and distance was investigated using the Central Composite Design (CCD) method to reduce the number of required simulations under two different shear conditions. Our findings revealed that the suggested optimal geometrical parameters of EC model inducing the highest WSS difference are similar to the geometrical parameters of the natural ECs.

7.2 Materials and methods

7.2.1 Blood flow measurement and endothelial cell characterization

In chapter 6, three healthy domestic pigs were utilized for endothelial cell characterization [123] of four different blood vessel types (common carotid, hepatic, renal and iliac arteries) following the method described in the literature [124]. In this current study, these parameters of the common carotid artery (CCA) and the iliac artery (IA) were used.

7.2.2 Wall shear stress and oscillatory shear index

Time-averaged WSS was calculated as follows [156]:

$$WSS = \frac{1}{T} \int_0^T |\vec{\tau}| dt \quad (7.1)$$

where τ is the WSS at a certain time step and T is the total time of one cardiac cycle.

7.2 Materials and methods

The OSI was chosen as a quantitative indicator for the angular change of the shear force during the cardiac cycle [156],[157]. It is calculated as follows:

$$OSI = \frac{1}{2} \left(1 - \frac{|\int_0^T |\vec{t}| dt|}{\int_0^T |\vec{t}| dt} \right) \quad (7.2)$$

OSI number ranges from 0 to 0.5. A high OSI number represents unidirectional WSS, i.e. disturbed flow, which leads to higher risk of platelet adhesion and aggregation.

7.2.3 Simulation of blood flow

Hemodynamic simulations of the blood flow were carried out using the CFX package ANSYS Workbench 13.0 (Ansys Inc., Canonsburg, USA) based on FEM. The EC models were computationally approximated as cuboid, ellipsoid and pyramid. These EC computational models were created with the same height, length and width (based on the statistical measurements of the natural ECs in CCA found in previous step in chapter 6) listed in Table 7.1 and the same distance of $5 \mu\text{m}$ to compare the effect of these models on shear stress and OSI distributions which directly affects platelet adhesion.

The blood flow was considered as a pulsatile flow (Fig. 7.1) based on the blood flow measurements of pigs in chapter 6 [123]. The Reynolds number (Re) was calculated as:

$$Re = \frac{\rho \times v \times DH}{\mu} \quad (7.3)$$

where, ρ is the density of blood, V is velocity, DH is the hydraulic diameter of the pipe and μ is the blood dynamic viscosity. In addition, we considered the blood to be Newtonian fluid with a constant density of 1050 kg/m^3 and a viscosity of $3.45 \times 10^{-3} \text{ Pa s}$. In this study, the Reynolds number was much lower than 2000. Therefore, we considered the blood flow to be steady laminar. The results of time average WSS and OSI for the whole cardiac cycle were displayed with Tecplot (Tecplot Inc., USA).

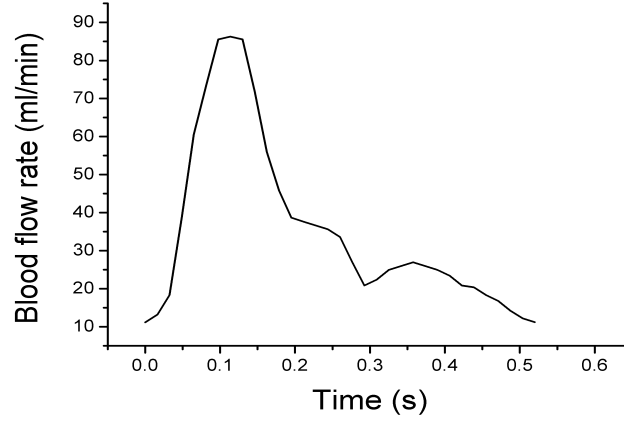


Figure 7.1: Rebuilt diagram of pulsatile blood flow in one cardiac cycle (0.52 s) in a natural porcine common carotid artery measured by VeriQ Flowmeter system (Medistim ASA, Norway) with average blood flow rate of 36.5 ml/min, i.e. average blood velocity of 0.46 m/s.

7.2.4 Finding the optimal geometrical parameters, distance and pattern for vascular grafts

The most suitable EC model found in the previous step inducing the highest WSS difference and the lowest OSI value was simulated with varied geometrical parameters (area, aspect ratio and height) and varied distance to find optimal combinations of these parameters for the common carotid artery and iliac artery which lead to the highest WSS difference under shear condition. Since an exhaustive grid search to identify the best combination of the four geometrical parameters (area, aspect ratio of length to width, height and distance) was not feasible, we applied the statistical response surface methodology (Box and Draper 2007) to reduce the number of simulations needed as described in the literature [158]. To this end the unknown response surface is locally approximated by a quadratic surface and the direction of steepest ascent on this approximating quadratic surface defines the direction of further search. We used the popular *Central Composite Design (CCD)* consisting of the corners of a cube supplemented by additional design points forming a “star” (Fig. 7.2) to enable the quadratic approximation of the response surface based on a minimum number of design points. For $d = 4$

dimensions the CCD consists of 26 design points. After simulating the response for an initial CCD, further simulations were done along the line of steepest ascent until a ridge of the response surface was reached (i.e., response values start to decrease again). At the ridge a new CCD was set up, resulting in a new quadratic approximation of the response surface. This process was continued until an optimum was found. All calculations were done using the package `rsm` (Lenth 2010) of the statistical software system R (R Development Coe Team 2014) [159].

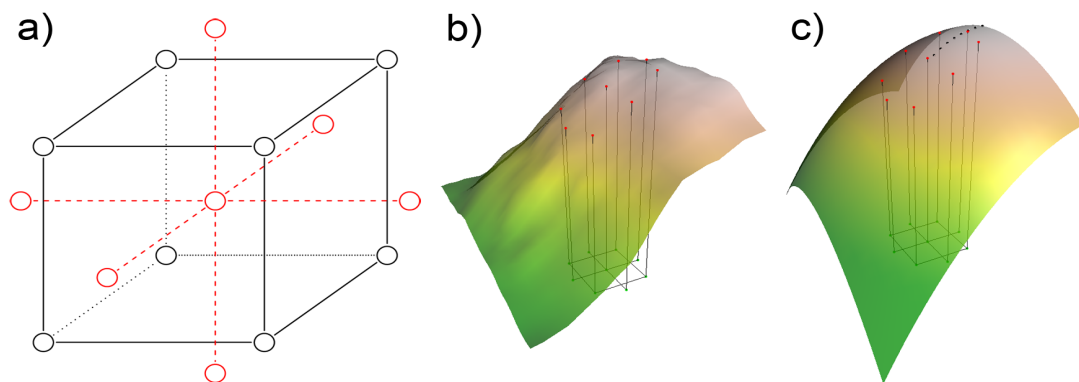


Figure 7.2: Illustration of the Central Composite Design (CCD) and the search strategy: a) three-dimensional CCD consisting of the corners of a cube (black) complemented by star design points (red); b) the response variable is simulated at the points of an initial Central Composite Design; c) based on these values the unknown response surface is approximated by a quadratic surface. The direction of steepest ascent (black dots) suggests points for further simulations.

7.3 Results

7.3.1 Hemodynamic simulations of three EC models

Time-averaged WSS and WSS difference distribution

To gain insight into the effect of different microstructure models on platelet adhesion, the time-averaged WSS distribution (Fig. 7.3 a-c) and WSS difference between top and ground area of the microstructures (Fig. 7.4) in one cardiac cycle of 0.52 s was investigated.

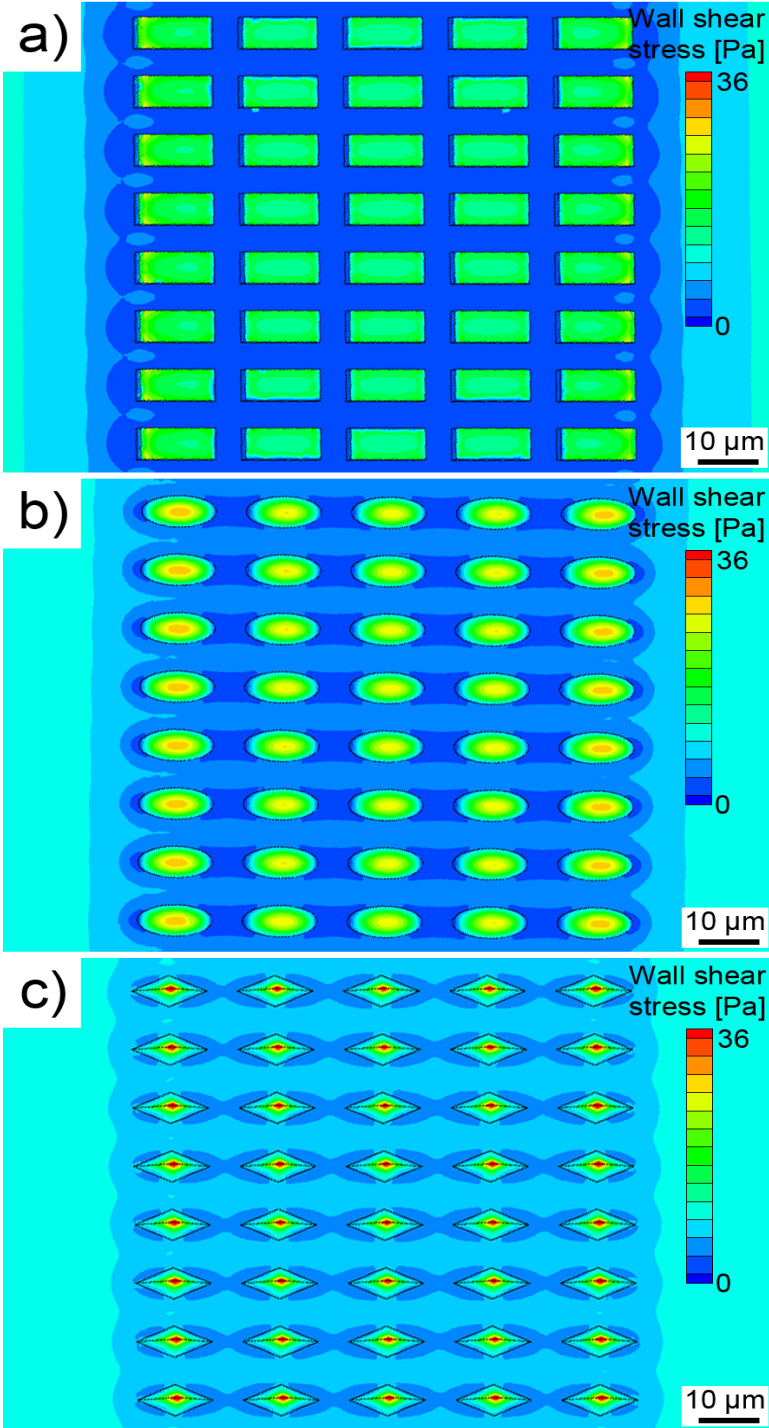


Figure 7.3: Simulation plots show the time-averaged WSS distributions on the three models during one cardiac cycle: a) cuboid; b) ellipsoid; c) pyramid, with red being the highest value (36 Pa) and blue being the lowest value of WSS (0 Pa).

The WSS on the unstructured areas of all three microstructure models was uniform with 9.3 Pa (Fig. 7.3 a-c). The microstructures caused a shear gradient with noticeably increased shear stress values on the top of the structures and partly decreased values in the interspacing areas compared to the unstructured regions (Fig. 7.3 a-c).

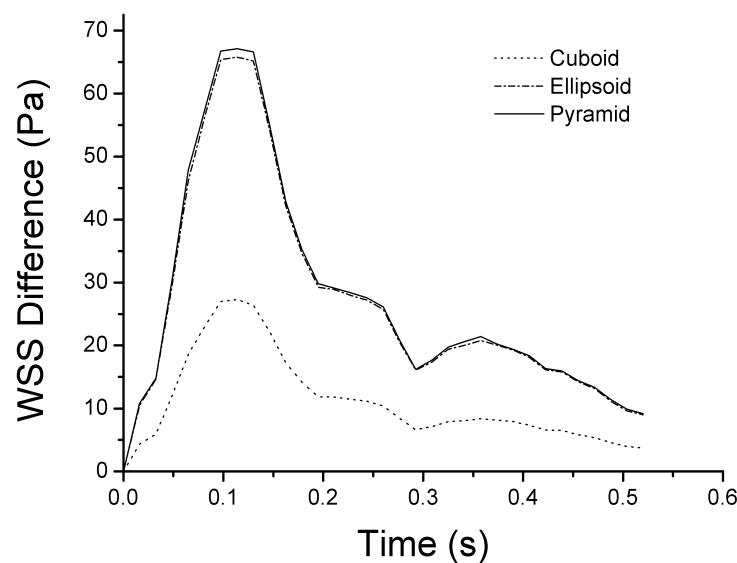


Figure 7.4: The WSS difference between top and ground areas of the microstructures for the whole cardiac cycle of 0.52 s of three models: cuboid, ellipsoid and pyramid.

The cuboid model caused a time-averaged WSS of 12.4 Pa on top of the structures and in the interspacing regions a time-averaged WSS of 1.2 Pa which resulted in the lowest WSS difference between top and ground of 11.2 Pa (Fig. 7.3 a, Fig. 7.4). The ellipsoid model induced a significantly higher time-averaged WSS of 28.3 Pa on top of the structure compared to the cuboid model, while that on the interspacing was lower (0.9 Pa), leading to a WSS difference of 27.4 Pa (Fig. 7.3 b, Fig. 7.4). The pyramid model showed the highest time-averaged WSS of 33.8 Pa on top of the structures and, simultaneously, the highest time-averaged WSS of 5.8 Pa on the ground inbetween microstructures which led, to the highest WSS difference of 28 Pa (Fig. 7.3 c, Fig. 7.4). According to this

point, the cuboid model seems less favorable in order to reduce platelet adhesion and aggregation compared to other microstructure models.

Velocity vector and OSI distributions

The velocity vector and OSI distributions on the three models are illustrated (Fig. 7.5). The velocity vectors of the cuboid model show a turbulent region inbetween two neighboring structures (Fig. 7.5 a). The blood flow in this area is disturbed and circled (Fig. 7.5 a). In consequence, the WSS in this region is very small (Fig. 7.3 a) and oscillatory (Fig. 7.5 a). The oscillatory WSS was further quantified by the OSI ranged from 0 (non-disturbed flow, i.e. lowest risk of platelet adhesion) to 0.5 (for the most disturbed flow, i.e. the highest risk of platelet adhesion and aggregation). The OSI was calculated for the whole cardiac cycle and the whole surface. The cuboid model showed the highest mean OSI ($5e^{-4}$) compared to the other models. The highest OSI values appeared in the interspacing between microstructures. In the ellipsoid model, the regions with high OSI values were observed close to the edges of the ellipsoids (Fig. 7.5 e), where velocity vectors (i.e. the shear vectors) changed their direction (Fig. 7.5 b). The lowest values of OSI were found in the pyramid model (Fig. 7.5 f) resulting from a laminar blood flow over the pyramid microstructured surface. Therefore, the pyramid model seems most favorable in order to reduce platelet adhesion and aggregation compared to the other microstructure models.

7.3.2 Optimal geometrical parameters and distance

The geometrical parameters (area, aspect ratio, height) and the distance between adjacent microstructures were optimized in order to achieve the highest WSS difference (between top and ground of the microstructures). Therefore, the statistical response surface methodology using Central Composite Design (CCD) was used in order to reduce the number of needed simulations. Analysis of simulation results due to the final CCD revealed the contour plots for the approximated response surface of time-averaged WSS difference between top and ground of the microstructures in relationship to the geometrical parameters of EC pyramid model under each shear condition, e.g. for the CCA (Fig. 7.6).

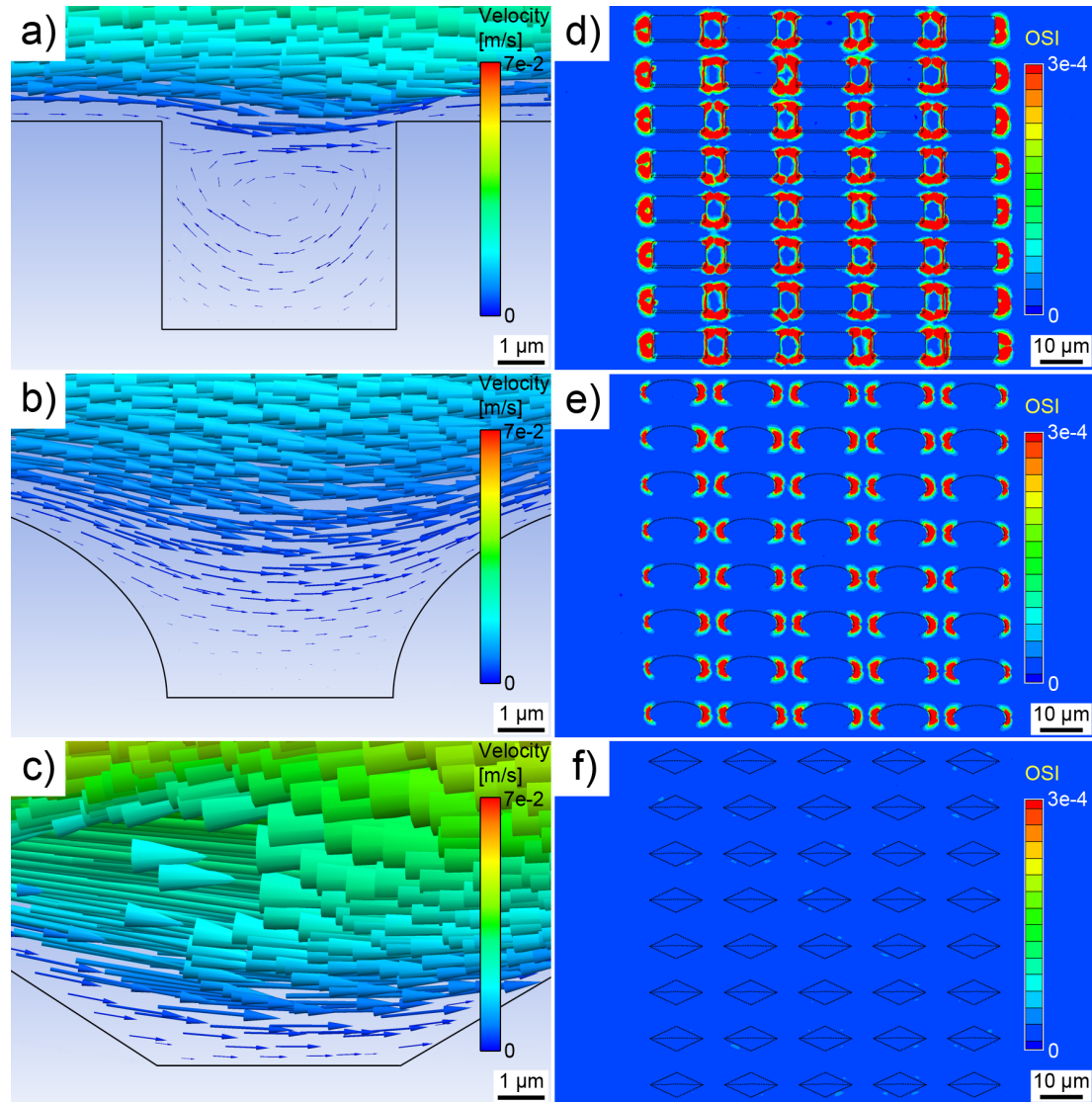


Figure 7.5: Velocity vectors and OSI distribution in three different models. Simulation plots showing velocity vectors at the chosen time step $t = 0.114$ s: a) cuboid model; b) ellipsoid model; c) pyramid model. The size and color of vectors in all the images show the magnitude of velocity, with red being the highest value (0.07 m/s) and blue being the lowest value (0 m/s). Simulation plots showing OSI values for one cardiac cycle in three models: d) cuboid model; e) ellipsoid model; f) pyramid model with red being the highest OSI value (5×10^{-4}) and blue being the lowest value of WSS (0).

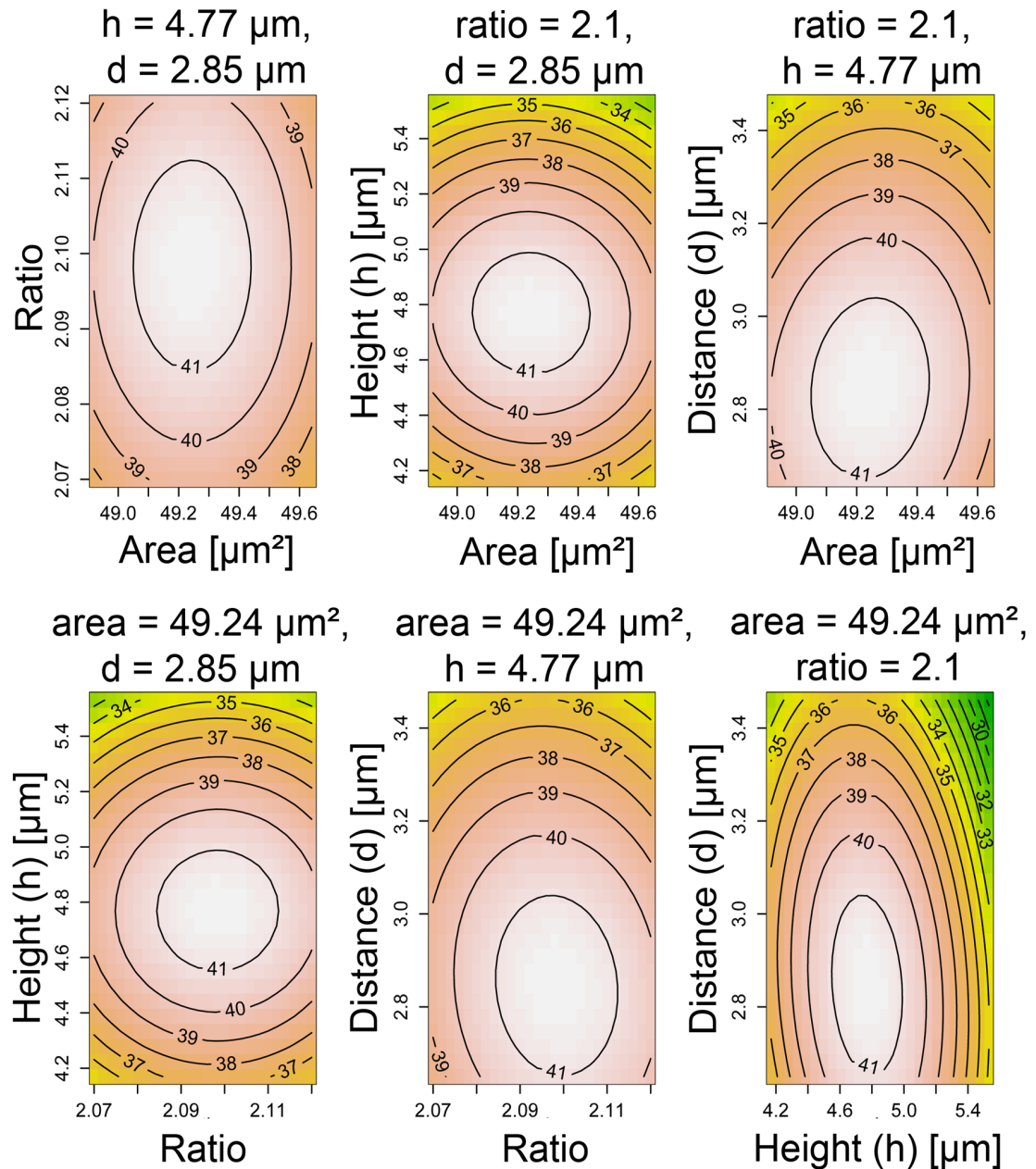


Figure 7.6: Contour plots for the approximated response surface for shear difference (between top and ground of the microstructures) in the common carotid artery resulting from the final Central Composite Design (CCD).

7.3 Results

Table 7.1: Results of the best combination of geometrical parameters and distance for the endothelial cell pyramid model in two different patterns for the carotid and iliac artery. (*The parameters were calculated based on the blood flow rate and vessel diameter investigated in chapter 6 [123]. **The information was investigated in chapter 6 [123].)

Artery	Carotid		Iliac	
	Simulation	Natural EC**	Simulation	Natural EC**
Blood velocity* [m/s]	0.46	0.46	0.49	0.49
WSS condition [Pa]	9.26	-	10.56	-
Cell length [μm]	14.38	12.46 ± 2.06	17.47	14.36 ± 2.6
Cell width [μm]	6.85	5.79 ± 1.14	6.24	6.08 ± 1.42
Cell height [μm]	4.77	4.43 ± 0.3	4.05	3.82 ± 0.56
Aspect ratio	2.1	2.24 ± 0.57	2.75	2.47 ± 0.65
Cell area [μm^2]	49.24	48.62 ± 11.65	54.5	58.08 ± 18.59
Cell perimeter [μm]	31.85	30.99 ± 4.11	37.1	35.22 ± 5.57
Distance [μm]	2.85	-	4.75	-
Highest WSS difference [Pa]	41.55	-	35.98	-
WSS on top [Pa]	47.02	-	46.17	-

The analysis results were divided into six plots showing the relationship between every two parameters (area, aspect ratio, height and distance) and the time-averaged WSS difference (Fig. 7.6). The contour plots (Fig. 7.6) also sug-

gest the highest value of WSS difference and the corresponding parameters of area, aspect ratio, height and distance for the common carotid and iliac arteries listed in Table 7.1. Based on the results of area and aspect ratio, the length, width and perimeter were calculated (Table 7.1).

The optimal geometrical parameters of the EC pyramid models are different in the common carotid and iliac arteries due to different shear conditions. To examine the correlation between the optimal geometrical parameters and shear condition, the time-averaged WSS values in these arteries were calculated (with smooth surfaces, i.e. without microstructures) using simulations with FEM. The simulation results revealed a shear condition of 10.56 Pa in the iliac artery, whereas that was lower in the common carotid artery with 9.26 Pa (Table 7.1). The CCD results showed a higher aspect ratio (length to with) for the EC model in the iliac artery (2.1) compared to that of the common carotid artery (2.75) (Table 7.1). This resulted in an EC model with longer length and a narrower width in the iliac artery (Table 7.1). The height of the EC pyramid model for the iliac artery and the common carotid artery was $4.77 \mu\text{m}$ and $4.05 \mu\text{m}$, respectively (Table 7.1). In contrast to the height, the area and perimeter of the EC model in the iliac artery were higher compared to that of the common carotid artery (Table 7.1). These results indicate a correlation between geometrical parameters of EC model and the WSS condition. Under high shear condition, the EC model exhibits a reduced height and becomes longer and narrower (i.e. increased aspect ratio) with the increased area of the base and increased perimeter compared to that under lower shear condition. These optimal values of the geometrical parameters of the EC pyramid model as well as their relationships to shear stress conditions agree well with that of the natural ECs in each artery. Interestingly, the WSS on the top of the pyramid microstructure are nearly the same in the iliac (46.17 Pa) and carotid (47.02 Pa) arteries (Table 7.1).

7.4 Discussion

The study presented here investigated the effect of different computational models (cuboid, ellipsoid and pyramid) mimicking ECs and the effect of varied geometrical parameters on shear stress difference which directly affects platelet adhesion.

By using hemodynamic simulations with FEM, we found that the pyramid model induced the highest shear difference between top and ground of the microstructures with the lowest oscillatory shear index (OSI) compared to other models which is assumed to have the best effect on reducing platelet adhesion. By utilizing CCD to reduce the number of necessary simulations of the pyramid model with varied geometrical parameters and distance, we found that the optimal combination of these parameters which induce the highest shear differences for each artery type agrees well with the geometrical parameters of the natural ECs in the respective artery.

7.4.1 Hemodynamic simulations of three EC models

It has long been known that high shear stresses in general reduce platelet adhesion on biomaterials surfaces [31, 122]. Our previous study investigated the effect of bioinspired microstructured surface on reducing platelet adhesion. The results indicated that the WSS difference between top and ground of the microstructures directly affects the platelet adhesion [146]. The higher the WSS difference between the top and ground of the microstructures, the fewer platelets adhere to the microstructured surface [146]. High WSS difference lead to less interaction between the upper blood layer on top of the microstructures and the trapped blood layer on the ground inbetween the microstructures, leading to a reduced transfer of platelets from the upper layer to the trapped layer and, consequently, to reduced platelet adhesion to the biomaterial surface [146]. In this current study, the pyramid and ellipsoid models had a higher time-averaged WSS difference of 27.4 Pa and 28 Pa, respectively, compared to the cuboid model of 11.2 Pa (Fig. 7.3). Hence, our findings show that the cuboid model is less favorable in reducing platelet adhesion compared to the other models.

The effect of flow disturbance on platelet adhesion and aggregation has been widely investigated [148, 149, 160]. A disturbed flow resulting from a reduction in the vessel lumen diameter is the main cause of platelet adhesion, activation and aggregation in both natural and artificial blood vessels [148, 149, 160]. In addition, the development of thrombi through the progressive stabilization of discoid platelets aggregates normally happens in low and oscillatory shear zones [32]. In

this current study, the hemodynamic simulation results of vector fields revealed the most disturbed flow on the interspacing between the cuboid microstructures. The shear stress vectors in this area were, consequently, oscillated and circled which resulted in the highest OSI value (Fig. 7.5 a, d). The pyramid model induced no disturbed flow with the smallest OSI number compared to the other models, which means that the shear stress vectors did not change their direction. Therefore, the pyramid model may have the highest impact on reducing platelet adhesion compared to the other models.

In brief, microstructured surfaces causing high WSS difference and low OSI reduce the adherence of platelets to the surface, leading to a low risk of thrombosis. Overall, our findings indicate that the cuboid is the least suitable model, whereas the pyramid model is most favorable for decreasing platelet adhesion and aggregation because of the highest WSS difference and the lowest OSI values. Thus, the pyramid model was used for optimizing the geometrical parameters by CCD method.

7.4.2 Optimal geometrical parameters and distance

Although the adaption of the natural ECs form under shear stress conditions has long been recognized [114, 151, 161], research on bioinspired microstructures mimicking ECs for vascular grafts depending on shear stress has not been carried out in detail. Our study suggested the best combinations of geometrical parameters of the EC pyramid model inducing the highest WSS difference under the two different shear conditions that occur within the common carotid and iliac arteries.

Hemodynamic simulations of the blood flow indicated higher shear stress of 10.56 Pa in the iliac artery compared to that in the common carotid artery with 9.26 Pa (Table 7.1). In our previous study [123], the characterization of the natural EC shapes in their native state revealed a cell height of $3.82 \pm 0.56 \mu\text{m}$ and $4.43 \pm 0.30 \mu\text{m}$ in the iliac and common carotid arteries, respectively (Table 7.1). In contrast to the cell height, the cell aspect ratio of the natural ECs was increased with increasing shear stress. The cell aspect ratio of the natural ECs in the carotid and iliac arteries were $2.24 \pm 0.57 \mu\text{m}$ and $2.47 \pm 0.65 \mu\text{m}$, respectively. In ad-

dition, the cell area and perimeter increased under higher shear stress conditions (Table 7.1). In general, under high shear conditions, the native ECs reduce their height and become longer and narrower (i.e. higher cell aspect ratio), whereas the area of the base and the cell perimeter are increased compared to that under lower shear condition. In the current study, the suggested EC pyramid model for the iliac artery inducing the highest shear difference also shows lower height but higher aspect ratio, area and perimeter compared to that of the common carotid artery (Table 7.1). The geometrical parameters of the EC pyramid model have the same relationship to shear stress conditions as that of the natural ECs. Our hypothesis, that the aspect ratio (of length to width), base area and perimeter of the EC microstructure model are proportional to the shear stress, whereas the height is decreased with increasing shear condition was, therefore, accepted. In addition, the suggested optimal values of geometrical parameter inducing the highest WSS difference in each artery are quite similar to the geometrical parameters of the natural ECs (Table 7.1). Therefore, our findings indicate that the natural ECs exhibit the best effect on enhancing WSS difference, i.e. reducing platelet adhesion. Our investigations of a pyramid model mimicking ECs on WSS difference help to gain better insight into the reorganization mechanism of the natural ECs under shear conditions. Applied shear stress is considered as a primary triggering signal for cellular remodeling of ECs when exposed to blood flow [162]. The distributions of WSS on the EC surface are not uniform with the highest shear stress on the top and the smallest shear stress on the ground of the cell [162]. This non-uniformity distribution of WSS on the EC surface plays a crucial role in the mechanism of cell activation, cell modification of cytoskeleton and distributions of adhesion molecules, etc. leading to cell shape change [162]. This stress is transmitted from the luminal surface to focal adhesion contacts through the endothelial cytoskeleton including microtubule and microfilament networks [135]. Our study indicates that, under higher shear condition, the reorganization of the cytoskeleton leads to a new steady state of the EC configuration with longer, narrower shape, increased area and cell perimeter but decreased cell height. This new shape induces the possible highest WSS difference leading to the best effect on reducing platelet adhesion.

As a unique layer in contact with blood, the ECs play a pivotal role in the

control of haemostasis and thrombosis. They are the primary source of many of the major haemostatic regulatory molecules. Healthy ECs are anticoagulant and antithrombotic. With the ability to release antiplatelet agents, including prostacyclin and nitric oxide to prevent platelet adhesion and aggregation, ECs provide an antiplatelet surface [163]. Our study figured out that, the form of ECs also plays an important role in preventing platelet adhesion. Under a certain shear condition, ECs adapt their form to the blood flow to create a most suitable shape which induces the highest WSS difference to reduce platelet adhesion. Our findings help change the paradigm about the antithrombotic property of endothelial cells that, beside the biological functions, the physical function of the EC morphology also contribute to prevent platelet adhesion.

Our study investigated for the first time the microstructure form mimicking the natural ECs for vascular graft surfaces with optimal geometrical parameters depending on shear stresses. As a next step, the effect of these models should be experimentally investigated under different shear conditions.

7.5 Conclusion

Our results indicate that the pyramid shape is the most suitable model for the microstructure mimicking ECs because of the induced highest WSS difference and the lowest OSI value compared to other models. In addition, an optimized combination of geometrical parameters for the pyramid microstructure model under each shear condition of carotid and iliac arteries was suggested. Our findings may lay a basis for the development of the-next-generation of vascular grafts with bioinspired microstructured surface. We found that the natural ECs possess the optimal form to prevent platelet adhesion. Under shear stress, the ECs change themselves into the most suitable shape which induces the highest WSS difference to reduce platelet adhesion.

8

Summary

Thrombosis is one of the major failures of synthetic vascular grafts, especially for those with a small diameter ($< 6mm$). The main trigger of thrombosis is platelet adhesion, activation and aggregation. A natural blood vessel with an endothelial cell layer is believed to be the best material to prevent the triggering of platelet adhesion and aggregation. The traditional approach to enhance the blood compatibility of vascular grafts is endothelialization for the inner wall of grafts. However, endothelialization procedures are labor intensive, costly and require a considerable amount of time. The endothelial cell sheet is somewhat neither complete nor stable. A new recently investigated approach to improve the blood compatibility of vascular grafts is to create micro- and nanostructures mimicking the morphology of the inner surface of natural blood vessels, i.e. the EC morphology.

The aim of the PhD research project was to design a bioinspired microstructured surface for synthetic vascular grafts by mimicking the EC morphology that inhibits the platelet adhesion and aggregation, thereby decreases the activation of thrombogenic pathways. The research goal was achieved by using both computer simulations and experimental studies of haemodynamics.

Hemodynamic aspects of reduced platelet adhesion on bioinspired microstructured surfaces

The first objective of this PhD research was to investigate the hemodynamic aspects of platelet adhesion, the main cause of thrombosis, on bioinspired mi-

crostructured surfaces. The hypothesis that platelet adhesion is statistically significantly reduced on bioinspired microstructured surfaces compared to unstructured surfaces under shear condition was tested.

For this, platelet adhesion as a function of the microstructure dimensions was investigated under flow conditions on polydimethylsiloxane (PDMS) surfaces by a combined experimental and theoretical approach. PDMS surfaces were modified with hemispherical microstructures arranged in regular arrays. The fabrication of these microstructured surfaces was realized by using laser ablation and soft-lithography. The effect of microstructures on platelet adhesion was investigated in a flow cell channel with multilayer parallel plates using porcine blood labelled with DiOC6. The platelet adhesion on surfaces was observed and analyzed by confocal laser scanning microscopy. In addition, water contact angle and surface resistance to flow characterized by pressure drop of both PDMS microstructured and smooth surfaces were measured to study the effect of these factors on platelet adhesion.

Platelet adhesion was statistically significantly reduced (by up to 78 %; $p \leq 0.05$) on the microstructured PDMS surfaces compared to that on the unstructured control surface. FEM simulations of blood flow dynamic revealed a micro shear gradient on the microstructure surfaces which plays a pivotal role in reducing platelet adhesion. On the surfaces with the highest differences of the WSS between the top of the microstructures and the ground areas, platelet adhesion was reduced most. In addition, the microstructures help to reduce the interaction strength between fluid and surfaces, resulting in a larger water contact angle but no higher resistance to flow compared to the unstructured surfaces.

Quantitative characterization of endothelial cell morphologies depending on shear stress

In the natural blood vessel, the ECs are able to change their shapes depending on different shear conditions. In order to mimic the EC morphology for microstructured surfaces, it is necessary to understand the change of the EC morphology under shear conditions. However, the quantitative correlation between EC morphology and shear stress has not yet been investigated statistically. Therefore, second objective of the PhD research was to investigate the quantitative correlation between EC forms in different blood vessels and shear stress.

For this, the EC morphologies in four types of natural blood vessels (carotid, renal, hepatic and iliac arteries) from domestic pigs were quantitatively characterized ex vivo by imaging with high resolution scanning electron microscopy (SEM) and cross-sectioning of the cells using a state-of-the-art Focused Ion Beam (FIB). The blood flow rates and blood vessel diameters were also measured to calculate the shear stress in these blood vessels.

The relationships between EC geometrical parameters (length, width, aspect ratio of length to width and height) and shear stress were statistically analyzed and found to be exponential. ECs in the blood vessels of different organs have different cell morphologies due to different shear conditions in those vessels. ECs under high shear stress conditions had a longer length and narrower width, i.e. a higher aspect ratio, while the cell height was smaller compared to low shear conditions.

Optimize the inhibition of platelet adhesion on microstructured using FEM simulations

After successful characterization of the EC morphology, the third objective of this research was to find a suitable microstructure form mimicking the natural ECs for vascular graft surfaces with optimal geometrical parameters depending on shear stresses.

By using FEM simulations of the blood flow over different EC computational models (cuboid, ellipsoid and pyramid) based on the geometrical characterization of the natural ECs, we found that the pyramid microstructure model induced the highest WSS difference between top and ground of the microstructures with the lowest OSI compared to the other models which is assumed to have the best effect on reducing platelet adhesion. By utilizing CCD to reduce the required simulation number of the pyramid model with varied geometrical parameters (aspect ratio of length to width, base area and height) and distance, we suggest optimal combinations of these parameters which induce the highest shear differences under two different shear conditions of the common carotid and iliac arteries. In addition, we found that the physical effect of the EC morphology also contributes to antithrombotic property of ECs. The natural ECs have an optimal form to prevent platelet adhesion. Under a certain shear condition, endothelial cells adapt their form to the blood flow to create a most suitable shape which induces the

highest WSS difference for reducing platelet adhesion.

These findings provide new insight into the fundamental mechanisms of reducing platelet adhesion on microstructured bioinspired surfaces and may lay the basis for the development of innovative next generation artificial vascular grafts with reduced risk of thrombosis.

References

- [1] L.A. Hidalgo-Bastida, J.J.A. Barry, N.M. Everitt, F.R.A.J. Rose, L.D. Buttery, I.P. Hall, W.C. Claycomb, and K.M. Shakesheff. Cell adhesion and mechanical properties of a flexible scaffold for cardiac tissue engineering. *Acta biomaterialia*, 3(4):457–462, 2007. 1
- [2] S. Nikeghbalian, S.M.V Hosseini, A.M. Bananzadeh, A. Monabati, M.H. Bagheri, T. Razmi, and S.A. Malek-Hosseini. Using inverted autogenous veins to substitute arteries in a canine model. *Journal of Emergencies, Trauma and Shock*, 3(3):238, 2010. 1
- [3] J.A. DeWeese, H.B. Barner, E.B. Mahoney, and C.G. Rob. Autogenous venous bypass grafts and thromboendarterectomies for atherosclerotic lesions of the femoropopliteal arteries. *Annals of surgery*, 163(2):205, 1966. 1
- [4] R.J. Manson, J.M. Unger, A. Ali, S.M. Gage, and J.H. Lawson. Tissue-engineered vascular grafts: autologous off-the-shelf vascular access? In *Seminars in nephrology*, volume 32, pages 582–591. Elsevier, 2012. 1
- [5] M.T.G. López, A.S. Dorgham, F.C. Rosas, and J.G. de Loma. Aneurysmal degeneration of a saphenous vein graft following the repair of a popliteal aneurysm: case report and literature review. *Vascular*, 20(5):294–298, 2012. 1, 2
- [6] S. Wan, .S.J. George, C. Berry, and A.H. Baker. Vein graft failure: current clinical practice and potential for gene therapeutics. *Gene therapy*, 19(6):630–636, 2012. 1
- [7] S.P. Hoerstrup, I. Cummings, M. Lachat, F.J. Schoen, R. Jenni, S. Leschka, S. Neuenschwander, D. Schmidt, A. Mol, C. Günter, et al. Functional growth in tissue-engineered living, vascular grafts follow-up at 100 weeks in a large animal model. *Circulation*, 114(1 suppl):I–159, 2006. 1
- [8] B.D. Ratner, A.S. Hoffman, F.J. Schoen, and J.E. Lemons. *Biomaterials*

REFERENCES

- Science: An Introduction to Materials in Medicine*. Elsevier Science, 2012. x, 2, 3, 4, 5, 6, 7
- [9] K.H. Yow, J. Ingram, S.A. Korossis, E. Ingham, and S. Homer-Vanniasinkam. Tissue engineering of vascular conduits. *British journal of surgery*, 93(6):652–661, 2006. 2
- [10] M.R. Hoenig, G.R. Campbell, B.E. Rolfe, and J.H. Campbell. Tissue-engineered blood vessels alternative to autologous grafts? *Arteriosclerosis, thrombosis, and vascular biology*, 25(6):1128–1134, 2005. 2
- [11] J.D. Kakisis, C.D. Liapis, C. Breuer, and B.E. Sumpio. Artificial blood vessel: the holy grail of peripheral vascular surgery. *Journal of vascular surgery*, 41(2):349–354, 2005. 2
- [12] S. Ravi and E.L. Chaikof. Biomaterials for vascular tissue engineering. *Regenerative medicine*, 5(1):107–120, 2010. 2
- [13] J. Stitzel, J. Liu, S.J. Lee, M. Komura, J. Berry, S. Soker, G. Lim, M. Van Dyke, R. Czerw, J.J. Yoo, et al. Controlled fabrication of a biological vascular substitute. *Biomaterials*, 27(7):1088–1094, 2006. 2
- [14] M.S. Conte. The ideal small arterial substitute: a search for the holy grail? *The FASEB journal*, 12(1):43–45, 1998. 2
- [15] H.P. Greisler. Interactions at the blood/material interface. *Annals of vascular surgery*, 4(1):98–103, 1990. 2
- [16] D. Motlagh, J. Yang, K.Y. Lui, A.R. Webb, and G.A. Ameer. Hemocompatibility evaluation of poly (glycerol-sebacate) in vitro for vascular tissue engineering. *Biomaterials*, 27(24):4315–4324, 2006. 2
- [17] L. Berardinelli. Grafts and graft materials as vascular substitutes for haemodialysis access construction. *European journal of vascular and endovascular surgery*, 32(2):203–211, 2006. 2

REFERENCES

- [18] Z. Yang, J. Tao, J.M. Wang, C. Tu, M.G. Xu, Y. Wang, and S.R. Pan. Shear stress contributes to t-pa mrna expression in human endothelial progenitor cells and nonthrombogenic potential of small diameter artificial vessels. *Biochemical and biophysical research communications*, 342(2):577–584, 2006. 2
- [19] H.H. Versteeg, J.W.M. Heemskerk, M. Levi, and P.H. Reitsma. New fundamentals in hemostasis. *Physiological reviews*, 93(1):327–358, 2013. x, 4, 5
- [20] S. Sarkar, K.M. Sales, G. Hamilton, and A.M. Seifalian. Addressing thrombogenicity in vascular graft construction. *Journal of Biomedical Materials Research Part B: Applied Biomaterials*, 82(1):100–108, 2007. 5
- [21] K.J. Clemetson and J.M. Clemetson. Platelet collagen receptors. *Thrombosis and haemostasis*, 86(1):189–197, 2001. 5
- [22] R.W. Colman. *Hemostasis and thrombosis: basic principles and clinical practice*. Lippincott Williams & Wilkins, 2006. 5
- [23] S.L. Cranmer, P. Ulsemer, B.M. Cooke, H.H. Salem, C. De La Salle, F. Lanza, and S.P. Jackson. Glycoprotein (gp) ib-ix-transfected cells roll on a von willebrand factor matrix under flow importance of the gpib/actin-binding protein (abp-280) interaction in maintaining adhesion under high shear. *Journal of Biological Chemistry*, 274(10):6097–6106, 1999. 5
- [24] B. Savage, S.J. Shattil, and Z.M. Ruggeri. Modulation of platelet function through adhesion receptors. a dual role for glycoprotein iib-iiia (integrin alpha iib beta 3) mediated by fibrinogen and glycoprotein ib-von willebrand factor. *Journal of Biological Chemistry*, 267(16):11300–11306, 1992. 5
- [25] Biomaterial. <http://platelets.se/biomaterial/>. x, 6
- [26] T. Szántó, L. Joutsu-Korhonen, H. Deckmyn, and R. Lassila. New insights into von willebrand disease and platelet function. In *Seminars in thrombosis and hemostasis*, volume 38, page 55, 2012. 5

REFERENCES

- [27] C.A. Siediecki, B.J. Lestini, K.K. Kottke-Marchant, S.J. Eppell, D.L. Wilson, and R.E. Marchant. Shear-dependent changes in the three-dimensional structure of human von willebrand factor. *Blood*, 88(8):2939–2950, 1996. 5
- [28] Y.P. Wu, T. Vink, M. Schiphorst, G.H. van Zanten, M.J.W. IJsseldijk, P.G. de Groot, and J.J. Sixma. Platelet thrombus formation on collagen at high shear rates is mediated by von willebrand factor–glycoprotein ib interaction and inhibited by von willebrand factor–glycoprotein iib/iiia interaction. *Arteriosclerosis, thrombosis, and vascular biology*, 20(6):1661–1667, 2000. 6
- [29] M. Moroi, S.M. Jung, S. Nomura, S. Sekiguchi, A. Ordinas, and M. Diaz-Ricart. Analysis of the involvement of the von willebrand factor–glycoprotein ib interaction in platelet adhesion to a collagen-coated surface under flow conditions. *Blood*, 90(11):4413–4424, 1997. 6
- [30] M.B. Gorbet and M.V. Sefton. Biomaterial-associated thrombosis: roles of coagulation factors, complement, platelets and leukocytes. *Biomaterials*, 25(26):5681–5703, 2004. 6
- [31] J.L. Moake, N.A. Turner, N.A. Stathopoulos, L. Nolasco, and J.D. Hellums. Shear-induced platelet aggregation can be mediated by vwf released from platelets, as well as by exogenous large or unusually large vwf multimers, requires adenosine diphosphate, and is resistant to aspirin. *Blood*, 71(5):1366–1374, 1988. 7, 29, 41, 74
- [32] W.S. Nesbitt, E. Westein, F.J. Tovar-Lopez, E. Tolouei, A. Mitchell, J. Fu, J. Carberry, A. Fouras, and S.P. Jackson. A shear gradient–dependent platelet aggregation mechanism drives thrombus formation. *Nature medicine*, 15(6):665–673, 2009. 7, 74
- [33] Z.M. Ruggeri and G.L. Mendolicchio. Adhesion mechanisms in platelet function. *Circulation research*, 100(12):1673–1685, 2007. 8
- [34] N. Westerhof, N. Stergiopoulos, and M.I.M. Noble. *Snapshots of hemodynamics*. Springer, 2010. 8

REFERENCES

- [35] C. Chen, S.G. Mattar, J.D. Hughes, G.F. Pierce, J.E. Cook, D.N. Ku, S.R. Hanson, and A.B. Lumsden. Recombinant mitotoxin basic fibroblast growth factor–saporin reduces venous anastomotic intimal hyperplasia in the arteriovenous graft. *Circulation*, 94(8):1989–1995, 1996. 8
- [36] R.T. Schoepfoerster, F. Oynes, G. Nunez, M. Kapadvanjwala, and M.K. Dewanjee. Effects of local geometry and fluid dynamics on regional platelet deposition on artificial surfaces. *Arteriosclerosis, Thrombosis, and Vascular Biology*, 13(12):1806–1813, 1993. 8, 9
- [37] F.J. Tovar-Lopez, G. Rosengarten, K. Khoshmanesh, E. Westein, S.P. Jackson, W.S. Nesbitt, and A. Mitchell. Structural and hydrodynamic simulation of an acute stenosis-dependent thrombosis model in mice. *Journal of biomechanics*, 44(6):1031–1039, 2011. 9
- [38] M.J. Maxwell, E. Westein, W.S. Nesbitt, S. Giuliano, S.M. Dopheide, and S.P. Jackson. Identification of a 2-stage platelet aggregation process mediating shear-dependent thrombus formation. *Blood*, 109(2):566–576, 2007. 9
- [39] T.N. Zaidi, L.V. McIntire, D.H. Farrell, and P. Thiagarajan. Adhesion of platelets to surface-bound fibrinogen under flow. *Blood*, 88(8):2967–2972, 1996. 9
- [40] A.J. Reininger. Platelet function under high shear conditions. *Hamostaseologie*, 29(1):21–2, 2009. 9
- [41] M.H. Kroll, J.D. Hellums, L.V. McIntire, A.I. Schafer, and J.L. Moake. Platelets and shear stress. *Blood*, pages 1525–1541, 1996. 9
- [42] J.D. Pearson. Endothelial cell function and thrombosis. *Best Practice & Research Clinical Haematology*, 12(3):329–341, 1999. 10
- [43] J.D. Pearson. Normal endothelial cell function. *Lupus*, 9(3):183–188, 2000. 10
- [44] G.M. Rubanyi. The role of endothelium in cardiovascular homeostasis and diseases. *Journal of cardiovascular pharmacology*, 22:S1–hyhen, 1993. 10
-

REFERENCES

- [45] M. Boyer, L.E. Townsend, L.M. Vogel, J. Falk, D. Reitz-Vick, K.T. Trevor, M. Villalba, P.J. Bendick, and J.L. Glover. Isolation of endothelial cells and their progenitor cells from human peripheral blood. *Journal of vascular surgery*, 31(1):181–189, 2000. 11
- [46] J.G. Meinhart, M. Deutsch, T. Fischlein, N. Howanietz, A. Fröschl, and P. Zilla. Clinical autologous in vitro endothelialization of 153 infrainguinal eptfe grafts. *The Annals of thoracic surgery*, 71(5):S327–S331, 2001. 11
- [47] A.C. Thomas, G.R. Campbell, and J.H. Campbell. Advances in vascular tissue engineering. *Cardiovascular pathology*, 12(5):271–276, 2003. 11
- [48] N.B. Thébaud, D. Pierron, R. Bareille, C. Le Visage, D. Letourneur, and L. Bordenave. Human endothelial progenitor cell attachment to polysaccharide-based hydrogels: a pre-requisite for vascular tissue engineering. *Journal of Materials Science: Materials in Medicine*, 18(2):339–345, 2007. 11
- [49] R.H. Schmedlen, W.M. Elbjairami, A.S. Gobin, and J.L. West. Tissue engineered small-diameter vascular grafts. *Clinics in plastic surgery*, 30(4):507–517, 2003. 11
- [50] J.D. Berglund and Z.S. Galis. Designer blood vessels and therapeutic revascularization. *British journal of pharmacology*, 140(4):627–636, 2003. 11
- [51] H. Ghanbari, A. de Mel, and A.M. Seifalian. Cardiovascular application of polyhedral oligomeric silsesquioxane nanomaterials: a glimpse into prospective horizons. *Int J Nanomedicine*, 6:775–786, 2011. x, 11
- [52] M. Avci-Adali, G. Ziemer, and H.P. Wendel. Induction of epc homing on biofunctionalized vascular grafts for rapid in vivo self-endothelialization—a review of current strategies. *Biotechnology advances*, 28(1):119–129, 2010. 11
- [53] A. de Mel, G. Jell, M.M. Stevens, and A.M. Seifalian. Biofunctionalization of biomaterials for accelerated in situ endothelialization: a review. *Biomacromolecules*, 9(11):2969–2979, 2008. 11

REFERENCES

- [54] T. Asahara, T. Murohara, A. Sullivan, M. Silver, R. van der Zee, T. Li, B. Witzenbichler, G. Schatteman, and J.M. Isner. Isolation of putative progenitor endothelial cells for angiogenesis. *Science*, 275(5302):964–966, 1997. 11
- [55] T. Takahashi, C. Kalka, H. Masuda, D. Chen, M. Silver, M. Kearney, M. Magner, J.M. Isner, and T. Asahara. Ischemia-and cytokine-induced mobilization of bone marrow-derived endothelial progenitor cells for neo-vascularization. *Nature medicine*, 5(4):434–438, 1999. 11
- [56] S. Rafii and D. Lyden. Therapeutic stem and progenitor cell transplantation for organ vascularization and regeneration. *Nature medicine*, 9(6):702–712, 2003. 11
- [57] J.R. Crosby, W.E. Kaminski, G. Schatteman, P.J. Martin, E.W. Raines, R.A. Seifert, and D.F. Bowen-Pope. Endothelial cells of hematopoietic origin make a significant contribution to adult blood vessel formation. *Circulation research*, 87(9):728–730, 2000. 11
- [58] S. Kaushal, G.E. Amiel, K.J. Guleserian, O.M. Shapira, T. Perry, F.W. Sutherland, E. Rabkin, A.M. Moran, F.J. Schoen, A. Atala, et al. Functional small-diameter neovessels created using endothelial progenitor cells expanded ex vivo. *Nature medicine*, 7(9):1035–1040, 2001. 12
- [59] H. He, T. Shirota, H. Yasui, and T. Matsuda. Canine endothelial progenitor cell-lined hybrid vascular graft with nonthrombogenic potential. *The Journal of thoracic and cardiovascular surgery*, 126(2):455–464, 2003. 12
- [60] D.E. Discher, P. Janmey, and Y. Wang. Tissue cells feel and respond to the stiffness of their substrate. *Science*, 310(5751):1139–1143, 2005. 12
- [61] M.M. Stevens and J.H. George. Exploring and engineering the cell surface interface. *Science*, 310(5751):1135–1138, 2005. 12
- [62] J.T. Groves. Learning the chemical language of cell-surface interactions. *Science Signaling*, 2005(301):pe45–pe45, 2005. 12

REFERENCES

- [63] Y. Naito, M. Williams-Fritze, D.R. Duncan, S.N. Church, N. Hibino, J.A. Madri, J.D. Humphrey, T. Shinoka, and C.K. Breuer. Characterization of the natural history of extracellular matrix production in tissue-engineered vascular grafts during neovessel formation. *Cells Tissues Organs*, 195(1-2):60–72, 2011. 12
- [64] N. Dahan, G. Zarbiv, U. Sarig, T. Karram, A. Hoffman, and M. Machluf. Porcine small diameter arterial extracellular matrix supports endothelium formation and media remodeling forming a promising vascular engineered biograft. *Tissue Engineering Part A*, 18(3-4):411–422, 2011. 12
- [65] U. Edlund, T. Sauter, and A.C. Albertsson. Covalent vegf protein immobilization on resorbable polymeric surfaces. *Polymers for Advanced Technologies*, 22(1):166–171, 2011. 12
- [66] K.W. Lee, N.R. Johnson, J. Gao, and Y. Wang. Human progenitor cell recruitment via sdf-1 α cocervate-laden pgs vascular grafts. *Biomaterials*, 34(38):9877–9885, 2013. 12
- [67] G. De Visscher, L. Mesure, B. Meuris, A. Ivanova, and W. Flameng. Improved endothelialization and reduced thrombosis by coating a synthetic vascular graft with fibronectin and stem cell homing factor sdf-1 α . *Acta biomaterialia*, 8(3):1330–1338, 2012. 12
- [68] J. Hoffmann, A. Paul, M. Harwardt, J. Groll, T. Reeswinkel, D. Klee, M. Moeller, H. Fischer, T. Walker, T. Greiner, et al. Immobilized dna aptamers used as potent attractors for porcine endothelial precursor cells. *Journal of Biomedical Materials Research Part A*, 84(3):614–621, 2008. 12
- [69] P.B. Van Wachem, T. Beugeling, J. Feijen, A. Bantjes, J.P. Detmers, and W.G. Van Aken. Interaction of cultured human endothelial cells with polymeric surfaces of different wettabilities. *Biomaterials*, 6(6):403–408, 1985. 13
- [70] S.V. Madihally and H.W.T. Matthew. Porous chitosan scaffolds for tissue engineering. *Biomaterials*, 20(12):1133–1142, 1999. 13

REFERENCES

- [71] J.Y. Martin, Z. Schwartz, T.W. Hummert, D.M. Schraub, J. Simpson, J. Lankford, D.D. Dean, D.L. Cochran, and B.D. Boyan. Effect of titanium surface roughness on proliferation, differentiation, and protein synthesis of human osteoblast-like cells (mg63). *Journal of biomedical materials research*, 29(3):389–401, 1995. 13
- [72] C.M. Vaz, S. Van Tuijl, C.V.C. Bouten, and F.P.T. Baaijens. Design of scaffolds for blood vessel tissue engineering using a multi-layering electrospinning technique. *Acta biomaterialia*, 1(5):575–582, 2005. 13
- [73] B.M. Baker and R.L. Mauck. The effect of nanofiber alignment on the maturation of engineered meniscus constructs. *Biomaterials*, 28(11):1967–1977, 2007. 13
- [74] K.T. Kurpinski, J.T. Stephenson, R.R.R. Janairo, H. Lee, and S. Li. The effect of fiber alignment and heparin coating on cell infiltration into nanofibrous plla scaffolds. *Biomaterials*, 31(13):3536–3542, 2010. 13
- [75] H. Yoshimoto, Y.M. Shin, H. Terai, and J.P. Vacanti. A biodegradable nanofiber scaffold by electrospinning and its potential for bone tissue engineering. *Biomaterials*, 24(12):2077–2082, 2003. 13
- [76] H.J. Jin, J. Chen, V. Karageorgiou, G.H. Altman, and D.L. Kaplan. Human bone marrow stromal cell responses on electrospun silk fibroin mats. *Biomaterials*, 25(6):1039–1047, 2004. 13
- [77] R.E. Unger, M. Wolf, K. Peters, A. Motta, C. Migliaresi, and C.J. Kirkpatrick. Growth of human cells on a non-woven silk fibroin net: a potential for use in tissue engineering. *Biomaterials*, 25(6):1069–1075, 2004. 13
- [78] D.C. Miller, K.M. Haberstroh, and T.J. Webster. Plga nanometer surface features manipulate fibronectin interactions for improved vascular cell adhesion. *Journal of biomedical materials research Part A*, 81(3):678–684, 2007. 13

REFERENCES

- [79] A. Ranjan and T.J. Webster. Increased endothelial cell adhesion and elongation on micron-patterned nano-rough poly (dimethylsiloxane) films. *Nanotechnology*, 20(30):305102, 2009. 13
- [80] L.E. Dickinson, D.R. Rand, J. Tsao, W. Eberle, and S. Gerecht. Endothelial cell responses to micropillar substrates of varying dimensions and stiffness. *Journal of Biomedical Materials Research Part A*, 100(6):1457–1466, 2012. 13
- [81] V. Gauvreau and G. Laroche. Micropattern printing of adhesion, spreading, and migration peptides on poly (tetrafluoroethylene) films to promote endothelialization. *Bioconjugate chemistry*, 16(5):1088–1097, 2005. 13
- [82] M. Théry and M. Piel. Adhesive micropatterns for cells: a microcontact printing protocol. *Cold Spring Harbor Protocols*, 2009(7):pdb–prot5255, 2009. 13
- [83] A.K. Salem, R. Stevens, R.G. Pearson, M.C. Davies, S.J.B. Tendler, C.J. Roberts, P.M. Williams, and K.M. Shakesheff. Interactions of 3t3 fibroblasts and endothelial cells with defined pore features. *Journal of biomedical materials research*, 61(2):212–217, 2002. 13
- [84] J.M.M. Heyligers, H.J.M. Verhagen, J.I. Rotmans, C. Weeterings, P.G. de Groot, F.L. Moll, and T. Lisman. Heparin immobilization reduces thrombogenicity of small-caliber expanded polytetrafluoroethylene grafts. *Journal of Vascular Surgery*, 43(3):587–591, 2006. 14
- [85] P.H. Lin, C. Chen, R.L. Bush, Q. Yao, A.B. Lumsden, and S.R. Hanson. Small-caliber heparin-coated eptfe grafts reduce platelet deposition and neointimal hyperplasia in a baboon model. *Journal of Vascular Surgery*, 39(6):1322–1328, 2004. 14
- [86] E. Gray, J. Hogwood, and B. Mulloy. The anticoagulant and antithrombotic mechanisms of heparin. In *Heparin-A century of progress*, pages 43–61. Springer, 2012. 14

REFERENCES

- [87] Z. Zhou and M.E. Meyerhoff. Preparation and characterization of polymeric coatings with combined nitric oxide release and immobilized active heparin. *Biomaterials*, 26(33):6506–6517, 2005. 14
- [88] O. Larm, R. Larsson, and P. Olsson. A new non-thrombogenic surface prepared by selective covalent binding of heparin via a modified reducing terminal residue. *Biomaterials, medical devices, and artificial organs*, 11(2-3):161–173, 1983. 14
- [89] M.J.B. Wissink, R. Beernink, J.S. Pieper, A.A. Poot, G.H.M. Engbers, T. Beugeling, W.G. Van Aken, and J. Feijen. Immobilization of heparin to edc/nhs-crosslinked collagen. characterization and in vitro evaluation. *Biomaterials*, 22(2):151–163, 2001. 14
- [90] P.C. Begovac, R.C. Thomson, J.L. Fisher, A. Hughson, and A. Gällhagen. Improvements in gore-tex® vascular graft performance by carmeda® bioactive surface heparin immobilization. *European Journal of Vascular and Endovascular Surgery*, 25(5):432–437, 2003. 14
- [91] H. Wei, L. Han, J. Ren, and L. Jia. Anticoagulant surface coating using composite polysaccharides with embedded heparin-releasing mesoporous silica. *ACS applied materials & interfaces*, 5(23):12571–12578, 2013. 14
- [92] Y.C. Jung and B. Bhushan. Biomimetic structures for fluid drag reduction in laminar and turbulent flows. *Journal of Physics: Condensed Matter*, 22(3):035104, 2010. 15
- [93] J. Ou, B. Perot, and J.P. Rothstein. Laminar drag reduction in microchannels using ultrahydrophobic surfaces. *Physics of Fluids (1994-present)*, 16(12):4635–4643, 2004. 15
- [94] K. Koch, B. Bhushan, Y.C. Jung, and W Barthlott. Fabrication of artificial lotus leaves and significance of hierarchical structure for superhydrophobicity and low adhesion. *Soft Matter*, 5(7):1386–1393, 2009. 15, 40

REFERENCES

- [95] D.W. Bechert, M. Bruse, and W. Hage. Experiments with three-dimensional riblets as an idealized model of shark skin. *Experiments in fluids*, 28(5):403–412, 2000. 15
- [96] D.W. Bechert, M. Bruse, W. Hage, J.G.T. Van der Hoeven, and G. Hoppe. Experiments on drag-reducing surfaces and their optimization with an adjustable geometry. *Journal of Fluid Mechanics*, 338(5):59–87, 1997. 15
- [97] Y.C. Jung and B. Bhushan. Biomimetic structures for fluid drag reduction in laminar and turbulent flows. *Journal of Physics: Condensed Matter*, 22(3):035104, 2009. 15, 28
- [98] L. Chen, D. Han, and L. Jiang. On improving blood compatibility: from bioinspired to synthetic design and fabrication of biointerfacial topography at micro/nano scales. *Colloids and Surfaces B: Biointerfaces*, 85(1):2–7, 2011. 15, 17, 28, 46, 56, 62
- [99] H. Fan, P. Chen, R. Qi, J. Zhai, J. Wang, L. Chen, L. Chen, Q. Sun, Y. Song, D. Han, et al. Greatly improved blood compatibility by microscopic multiscale design of surface architectures. *Small*, 5(19):2144–2148, 2009. 15, 18, 28, 46, 56, 62
- [100] X. Ye, Y.L. Shao, M. Zhou, J. Li, and L. Cai. Research on micro-structure and hemo-compatibility of the artificial heart valve surface. *Applied Surface Science*, 255(13):6686–6690, 2009. 15, 17, 19, 28, 40, 46, 56, 62
- [101] Anatomy physiology lecture notes. <http://de.slideshare.net/>. x, 16
- [102] G. Li. Wettability and hemocompatibility of parallel grating microstructure surface. *Materials Research Innovations*, 2014. 17, 19, 28, 40, 46
- [103] R. Liu, Y. Qin, H. Wang, Y. Zhao, Z. Hu, and S. Wang. The in vivo blood compatibility of bio-inspired small diameter vascular graft: effect of sub-micron longitudinally aligned topography. *BMC cardiovascular disorders*, 13(1):1, 2013. 17, 18, 28, 33

REFERENCES

- [104] K.R. Milner, A.J. Snyder, and C.A. Siedlecki. Sub-micron texturing for reducing platelet adhesion to polyurethane biomaterials. *Journal of Biomedical Materials Research Part A*, 76(3):561–570, 2006. 18, 28
- [105] L.B. Koh, I. Rodriguez, and S.S. Venkatraman. The effect of topography of polymer surfaces on platelet adhesion. *Biomaterials*, 31(7):1533–1545, 2010. 18, 28, 43, 44
- [106] H. Chen, W. Song, F. Zhou, Z. Wu, H. Huang, J. Zhang, Q. Lin, and B. Yang. The effect of surface microtopography of poly (dimethylsiloxane) on protein adsorption, platelet and cell adhesion. *Colloids and Surfaces B: Biointerfaces*, 71(2):275–281, 2009. 19, 28, 43, 44
- [107] J.M.M. Heyligers, C.H.P. Arts, H.J.M. Verhagen, P.G. De Groot, and F.L. Moll. Improving small-diameter vascular grafts: From the application of an endothelial cell lining to the construction of a tissue-engineered blood vessel. *Annals of vascular surgery*, 19(3):448–456, 2005. 20
- [108] B.D. Ratner. The catastrophe revisited: blood compatibility in the 21st century. *Biomaterials*, 28(34):5144–5147, 2007. 20
- [109] D. Shemesh, I. Goldin, J. Hijazi, I. Zaghal, D. Berelowitz, A. Verstandig, and O. Olsha. A prospective randomized study of heparin-bonded graft (propaten) versus standard graft in prosthetic arteriovenous access. *Journal of vascular surgery*, 62(1):115–122, 2015. 20
- [110] D.I. Siegel-Axel and M. Gawaz. Platelets and endothelial cells. In *Seminars in thrombosis and hemostasis*, volume 33, pages 128–135. Copyright© 2007 by Thieme Medical Publishers, Inc., 333 Seventh Avenue, New York, NY 10001, USA., 2007. 21
- [111] A.M. Malek and S. Izumo. Mechanism of endothelial cell shape change and cytoskeletal remodeling in response to fluid shear stress. *Journal of Cell Science*, 109(4):713–726, 1996. 21, 46
- [112] S.R. Bussolari, C.F. Dewey Jr, and M.A. Gimbrone Jr. Apparatus for

REFERENCES

- subjecting living cells to fluid shear stress. *Review of Scientific Instruments*, 53(12):1851–1854, 1982. 21, 57
- [113] N.A. Stathopoulos and J.D. Hellums. Shear stress effects on human embryonic kidney cells in vitro. *Biotechnology and bioengineering*, 27(7):1021–1026, 1985. 21, 57
- [114] P.H. Stone, A.U. Coskun, S. Kinlay, J.J. Popma, M. Sonka, A. Wahle, Y. Yeghiazarians, C. Maynard, R.E. Kuntz, and C.L. Feldman. Regions of low endothelial shear stress are the sites where coronary plaque progresses and vascular remodelling occurs in humans: an in vivo serial study. *European heart journal*, 2007. 21, 62, 75
- [115] Y.S. Chatzizisis, A.U. Coskun, M. Jonas, E.R. Edelman, C.L. Feldman, and P.H. Stone. Role of endothelial shear stress in the natural history of coronary atherosclerosis and vascular remodeling: molecular, cellular, and vascular behavior. *Journal of the American College of Cardiology*, 49(25):2379–2393, 2007. 21
- [116] J. Ando, K. Yamamoto, et al. Vascular mechanobiology: endothelial cell responses to fluid shear stress. *Circulation journal: official journal of the Japanese Circulation Society*, 73(11):1983, 2009. 21
- [117] D.C. Chappell, S.E. Varner, R.M. Nerem, R.M. Medford, and R.W. Alexander. Oscillatory shear stress stimulates adhesion molecule expression in cultured human endothelium. *Circulation Research*, 82(5):532–539, 1998. 21
- [118] Z. Ding, K. Wang, J. Li, and X. Cong. Flow field and oscillatory shear stress in a tuning-fork-shaped model of the average human carotid bifurcation. *Journal of Biomechanics*, 34(12):1555–1562, 2001. 21
- [119] J. Hwang, M.H. Ing, A. Salazar, B. Lassègue, K. Griendling, M. Navab, A. Sevanian, and T.K. Hsiai. Pulsatile versus oscillatory shear stress regulates nadph oxidase subunit expression implication for native ldl oxidation. *Circulation research*, 93(12):1225–1232, 2003. 21

REFERENCES

- [120] D.N. Ku, D.P. Giddens, C.K. Zarins, and S. Glagov. Pulsatile flow and atherosclerosis in the human carotid bifurcation. positive correlation between plaque location and low oscillating shear stress. *Arteriosclerosis, Thrombosis, and Vascular Biology*, 5(3):293–302, 1985. 21
- [121] T. Sun, H. Tan, D. Han, Q. Fu, and L. Jiang. No platelet can adhere—largely improved blood compatibility on nanostructured superhydrophobic surfaces. *Small*, 1(10):959–963, 2005. 28
- [122] M.H.D. Wu, Y. Kouchi, Y. Onuki, Q. Shi, H. Yoshida, S. Kaplan, R.F. Viggers, R. Ghali, and L.R. Sauvage. Effect of differential shear stress on platelet aggregation, surface thrombosis, and endothelialization of bilateral carotid-femoral grafts in the dog. *Journal of Vascular Surgery*, 22(4):382–392, 1995. 29, 41, 74
- [123] T.T. Pham, S. Maenz, C. Lüdecke, C. Schmerbauch, U. Settmacher, K.D. Jandt, J. Bossert, and J. Zanow. Quantitative characterization of endothelial cell morphologies depending on shear stress in different blood vessels of domestic pigs using a focused ion beam and high resolution scanning electron microscopy (fib-sem). *Tissue and Cell*, 47(2):205–212, 2015. xv, 29, 62, 63, 64, 72, 75
- [124] B. Garipcan, S. Maenz, T. Pham, U. Settmacher, K.D. Jandt, J. Zanow, and J. Bossert. Image analysis of endothelial microstructure and endothelial cell dimensions of human arteries—a preliminary study. *Advanced Engineering Materials*, 13(1-2):B54–B57, 2011. 29, 48, 50, 57, 62, 63
- [125] G. Kibria, D. Heath, P. Smith, and R. Biggar. Pulmonary endothelial pavement patterns. *Thorax*, 35(3):186–191, 1980. 29, 46, 57
- [126] T. Reichlin, A. Wild, M. Dürrenberger, A.U. Daniels, U. Aebi, P.R. Hunziker, and M. Stolz. Investigating native coronary artery endothelium in situ and in cell culture by scanning force microscopy. *Journal of structural biology*, 152(1):52–63, 2005. 29
- [127] K.A. Barbee, P.F. Davies, and R. Lal. Shear stress-induced reorganization

REFERENCES

- of the surface topography of living endothelial cells imaged by atomic force microscopy. *Circulation Research*, 74(1):163–171, 1994. 29, 58, 59
- [128] B. Bhushan, Y.C. Jung, and K. Koch. Micro-, nano-and hierarchical structures for superhydrophobicity, self-cleaning and low adhesion. *Philosophical Transactions of the Royal Society A: Mathematical, Physical and Engineering Sciences*, 367(1894):1631–1672, 2009. 40
- [129] W. Barthlott and C. Neinhuis. Purity of the sacred lotus, or escape from contamination in biological surfaces. *Planta*, 202(1):1–8, 1997. 40
- [130] J.F. Cornhill, M.J. Levesque, E.E. Herderick, R.M. Nerem, J.W. Kilman, and J.S. Vasko. Quantitative study of the rabbit aortic endothelium using vascular casts. *Atherosclerosis*, 35(3):321–337, 1980. 46, 57
- [131] J.B. Silkworth and W.E. Stehbens. The shape of endothelial cells in en face preparations of rabbit blood vessels. *Angiology*, 26(6), 1975. 46, 57
- [132] T. Helliwell, P. Smith, and D. Heath. Endothelial pavement patterns in human arteries. *The Journal of pathology*, 136(3):227–240, 1982. 46
- [133] U. Windberger, A. Bartholovitsch, R. Plasenzotti, K.J. Korak, and G. Heinze. Whole blood viscosity, plasma viscosity and erythrocyte aggregation in nine mammalian species: reference values and comparison of data. *Experimental physiology*, 88(3):431–440, 2003. 50
- [134] M. Castellini, O. Baskurt, J.M. Castellini, and H.J. Meiselman. Blood rheology in marine mammals. *Frontiers in physiology*, 1:146, 2010. 50, 52
- [135] A.M. Malek and S. Izumo. Mechanism of endothelial cell shape change and cytoskeletal remodeling in response to fluid shear stress. *J Cell Sci*, 109(4):713–726, April 1996. 56, 58, 62, 76
- [136] T. Helliwell, P. Smith, and D. Heath. Endothelial pavement patterns in human arteries. *The Journal of Pathology*, 136(3):227–240, 1982. 57
- [137] S.L. Langille, B.L. and Adamson. Relationship between blood flow direction and endothelial cell orientation at arterial branch sites in rabbits and mice. *Circulation Research*, 48(4):481–488, 1981. 57
-

REFERENCES

- [138] S.K. Williams, J.F. Gillis, R.C. Wagnert, M.W. Bitensky, et al. Isolation and characterization of brain endothelial cells: morphology and enzyme activity. *Journal of neurochemistry*, 35(2):374–381, 1980. 57
- [139] R.L. Steward, C.M. Cheng, D.L. Wang, and P.R. LeDuc. Probing cell structure responses through a shear and stretching mechanical stimulation technique. *Cell Biochemistry and Biophysics*, 56(2-3):115–124, 2010. 58
- [140] K.A. Barbee. Role of subcellular shear–stress distributions in endothelial cell mechanotransduction. *Annals of biomedical engineering*, 30(4):472–482, 2002. 58
- [141] N. Caille, O. Thoumine, Y. Tardy, and J.J. Meister. Contribution of the nucleus to the mechanical properties of endothelial cells. *Journal of Biomechanics*, 35(2):177 – 187, 2002. 58, 59, 60
- [142] R.P. Jean, D.S. Gray, A.A. Spector, and C.S. Chen. Characterization of the nuclear deformation caused by changes in endothelial cell shape. *Journal of biomechanical engineering*, 126(5):552–558, 2004. 59
- [143] Y. Shafrir and G. Forgacs. Mechanotransduction through the cytoskeleton. *American Journal of Physiology-Cell Physiology*, 282(3):C479–C486, 2002. 59
- [144] A.L. Hazel and T.J. Pedley. Vascular endothelial cells minimize the total force on their nuclei. *Biophysical Journal*, 78(1):47–54, 2000. 59
- [145] R.P. Jean, D.S. Gray, A.A. Spector, and C.S. Chen. Characterization of the nuclear deformation caused by changes in endothelial cell shape. *J Biomech Eng*, 126(5):552–8, 2004. 59
- [146] T.T. Pham, S. Wiedemeier, S. Maenz, G. Gastrock, U. Settmacher, K.D. Jandt, J. Zanol, C. Lüdecke, and J. Bossert. Hemodynamic aspects of reduced platelet adhesion on bioinspired microstructured surfaces. *Colloids and Surfaces B: Biointerfaces*, 145:502–509, 2016. 62, 74

REFERENCES

- [147] C.G. Caro and K.H. Parker. The effect of haemodynamic factors on the arterial wall. *Atherosclerosis, Edinburgh, Churchill Livingstone*, pages 100–110, 1987. 62
- [148] S. Glagov, C. Zarins, D.P. Giddens, and D.N. Ku. Hemodynamics and atherosclerosis. insights and perspectives gained from studies of human arteries. *Archives of pathology & laboratory medicine*, 112(10):1018–1031, 1988. 62, 74
- [149] D.N. Ku, D.P. Giddens, C.K. Zarins, and S. Glagov. Pulsatile flow and atherosclerosis in the human carotid bifurcation. positive correlation between plaque location and low oscillating shear stress. *Arteriosclerosis, thrombosis, and vascular biology*, 5(3):293–302, 1985. 62, 74
- [150] A. Kamiya. Endothelial cell responses to fluid shear stress. *Biocybernetics and Biomedical Engineering*, 20(3):21–33, 2000. 62
- [151] H. Nomura, C. Ishikawa, T. Komatsuda, J. Ando, and A. Kamiya. A disk-type apparatus for applying fluid shear stress on cultured endothelial cell. *Biorheology*, 25(3):461–470, 1987. 62, 75
- [152] Peter F Davies. Hemodynamic shear stress and the endothelium in cardiovascular pathophysiology. *Nature Clinical Practice Cardiovascular Medicine*, 6(1):16–26, 2008. 62
- [153] M. Toda, K. Yamamoto, N. Shimizu, S. Obi, S. Kumagaya, T. Igarashi, A. Kamiya, and J. Ando. Differential gene responses in endothelial cells exposed to a combination of shear stress and cyclic stretch. *Journal of biotechnology*, 133(2):239–244, 2008. 62
- [154] D.C. Chappell, S.E. Varner, R.M. Nerem, R.M. Medford, and R.W. Alexander. Oscillatory shear stress stimulates adhesion molecule expression in cultured human endothelium. *Circulation research*, 82(5):532–539, 1998. 62
- [155] J. Hwang, A. Saha, Y.C. Boo, G.P. Sorescu, J.S. McNally, S.M. Holland, S. Dikalov, D.P. Giddens, K.K. Griendling, D.G. Harrison, et al. Oscillatory

REFERENCES

- shear stress stimulates endothelial production of from p47phox-dependent nad (p) h oxidases, leading to monocyte adhesion. *Journal of Biological Chemistry*, 278(47):47291–47298, 2003. 62
- [156] B.K. Lee, H.M. Kwon, T.H. Kim, H.W. Roh, and C.Y. Kim. Fluid dynamics and atherosclerotic risk burden according as coronary bifurcation angle. In *Biomedical Robotics and Biomechanics (BioRob), 2010 3rd IEEE RAS and EMBS International Conference on*, pages 693–697. IEEE, 2010. 63, 64
- [157] H. Nordgaard, A. Swillens, D. Nordhaug, I. Kirkeby-Garstad, D. Van Loo, N. Vitale, P. Segers, R. Haaverstad, and L. Lovstakken. Impact of competitive flow on wall shear stress in coronary surgery: computational fluid dynamics of a lima-lad model. *Cardiovascular research*, 88(3):512–519, 2010. 64
- [158] R.V. Lenth et al. Response-surface methods in r, using rsm. *Journal of Statistical Software*, 32(7):1–17, 2009. 65
- [159] R.C. Team et al. R: A language and environment for statistical computing. 2013. 66
- [160] C.G. Caro and K.H. Parker. The effect of hemodynamic factors on the arterial wall. In *Atherosclerosis-Biology and Clinical Science*, Churchill Livingstone, Edinburgh, pages 183–195, 1987. 74
- [161] P.F. Davies. Hemodynamic shear stress and the endothelium in cardiovascular pathophysiology. *Nature clinical practice Cardiovascular medicine*, 6(1):16–26, 2009. 75
- [162] X. Liu, P. Waché, X. Wang, and H. Chen. Simulation of the deformation of the endothelial cell under a shear flow. *Journal of biomedical engineering*, 19(4):541–546, 2002. 76
- [163] D.I. Siegel-Axel and M. Gawaz. Platelets and endothelial cells. In *Seminars in thrombosis and hemostasis*, volume 33, pages 128–135. Copyright© 2007

REFERENCES

by Thieme Medical Publishers, Inc., 333 Seventh Avenue, New York, NY
10001, USA., 2007. 77

Personal information

Name	Tam Thanh Pham
Address	Ernst-Bloch-Ring, 07743 Jena
Date of Birth	23 April 1982
Place of Birth	Vung Tau, Vietnam
Nationality	Vietnamese
Email	tam.pham@uni-jena.de

Education

09/1996 - 06/1999	Le Qui Don Specialized High School Natural Science Section
09/1999 - 08/2003	HoChiMinh University of Education Bachelor of Physics
09/2003 - 09/2006	HoChiMinh University of Technology Master of Engineering

Professional activities

03/2005 - 05/2007	Research assistant in HoChiMinh University of Technology
05/2007 - 09/2008	Researcher in Otto Schott Institute of Materials Research (OSIM), Jena
10/2008 - 03/2012	PhD student granted by DAAD in OSIM, Jena
04/2012 - 06/2016	Researcher in Otto Schott Institute of Materials Research (OSIM), Jena

Publications

T.T. Pham, J. Schumacher, S. Maenz, K.D. Jandt, J. Bossert. How to optimize the inhibition of platelet adhesion on microstructured surfaces - a Finite Element Method (FEM) approach. (In preparation)

T.T. Pham, S. Wiedemeier, S. Maenz, G. Gastrock, U. Settmacher, K.D. Jandt, J. Zanow, C. Lüdecke, J. Bossert. Hemodynamic aspects of reduced platelet adhesion on bioinspired microstructured surfaces. *Colloids Surface B* 145 (2016) 502-509.

T.T. Pham, S. Maenz, C. Lüdecke, C. Schmerbauch, U. Settmacher, K.D. Jandt, J. Bossert, J. Zanow. Quantitative characterization of endothelial cell morphologies depending on shear stress in different blood vessels of domestic pigs using a focused ion beam and high resolution scanning electron microscopy (FIB-SEM). *Tissue Cell* 47 (2015) 205-212.

T.F. Keller, J. Reichert, **T. Pham**, R. Adjiski, L. Spiess, L. Berzina-Cimdina, K.D. Jandt, J. Bossert. Facets of Protein Assembly on Nanostructured Titanium Oxide Surfaces. *ACTA BIOMATERIALIA* 9 (2013) 5810-5820.

B. Garipcan, S. Maenz, S., **T. Pham**, U. Settmacher, K.D. Jandt, J. Zanow, J. Bossert. Image analysis of endothelial microstructure and endothelial cell dimensions of human arteries – A preliminary study. *Adv. Eng. Mater.* 13 (2011) B54-57.

List of presentations

T. T. Pham, S. Wiedermeier, G. Gastrock, S. Maenz, C. Lüdecke, U. Settmacher, K. D. Jandt, J. Zanow, J. Bossert. Reduced platelet adhesion on micro-structured PDMS surfaces under shear condition. Euro BioMat, Weimar, Germany 21. – 22. April (2015).

T. T. Pham, S. Maenz, C. Lüdecke, U. Settmacher, K. D. Jandt, J. Zanow, J. Bossert. Quantitative characterization of endothelial cell morphologies depending on shear stress in different blood vessels of domestic pigs. Euro BioMat, Weimar, Germany 21. – 22. April (2015).

T. T. Pham, S. Wiedermeier, G. Gastrock, S. Maenz, C. Lüdecke, U. Settmacher,

CURRICULUM VITAE

K. D. Jandt, J. Zanow, J. Bossert. Reduced platelet adhesion on micro-structured surfaces under shear condition. Thüringer Werkstofftag, Weimar 11. March (2015).

T. T. Pham, G. Gastrock, U. Settmacher, K. D. Jandt, J. Zanow, J. Bossert. Effect of microstructured surface on nanoparticle adhesion. Thüringer Werkstofftag, Jena 19. January (2014).

T. F. Keller, J. Reichert, **T. Pham Thanh**, R. Adjiski, L. Spiess, L. Berzina-Cimdina, K. D. Jandt. Protein Assembly on Surfaces of Thermally Etched Titania. Materials Science and Engineering (MSE) Conference, Darmstadt, Germany August 24.-26. (2012).

T. T. Pham, S. Maenz, Sigrid Lang, K. D. Jandt, J. Bossert. Investigation of endothelial cell morphology on blood flow behaviour using finite element simulation. The 6th international symposium on biomechanics in vascular biology and Cardiovascular disease, Rotterdam, Netherland 14-15 April (2011).